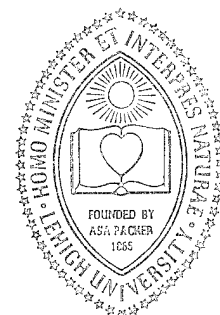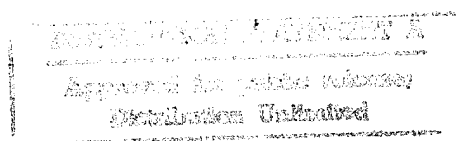LEHIGH UNIVERSITY

EXPLORATORY DEVELOPMENT OF FRACTURE
MECHANICS OF COMPOSITE SYSTEMS

By

G. C. Sih
P. D. Hilton
R. Badaliance
G. Villarreal

TECHNICAL REPORT AFML-TR-70-112
PART III

JANUARY 1973

19960320 020

AIR FORCE MATERIALS LABORATORY
AIR FORCE SYSTEMS COMMAND
WRIGHT-PATTERSON AIR FORCE BASE, OHIO 45433

NOTICE

AFML-TR-70-112

Part III

EXPLORATORY DEVELOPMENT OF FRACTURE

MECHANICS OF COMPOSITE SYSTEMS

G. C. Sih

P. D. Hilton

R. Badaliance

G. Villarreal

LEHIGH UNIVERSITY

TECHNICAL REPORT AFML-TR-70-112 Part III

January 1973

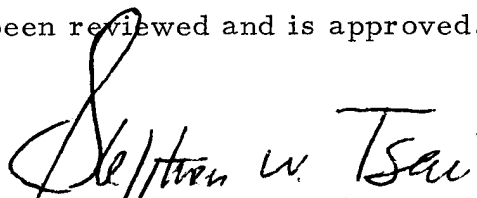Approved for public release; distribution unlimited.

FOREWORD

This is the third annual report of a four-year research program concerning the application of fracture mechanics to composite systems. The report is prepared by G. C. Sih, P. D. Hilton, R. Badaliance and G. Villarreal of the Institute of Fracture and Solid Mechanics, Lehigh University, Bethlehem, Pennsylvania, under Air Force Contract F33615-71-C-1429, entitled "Exploratory Development of Fracture Mechanics of Composite Systems", for the period of July 1971 to June 1972. The work was initiated under Project No. 7340, "Nonmetallic and Composite Materials", Task No. 734003, "Structural Plastics and Composites". The principal investigator for this project is G. C. Sih, Director of the Institute of Fracture and Solid Mechanics. N. J. Pagano (AFML) served as contract monitor and directed the project for the Air Force Materials Laboratory, Wright-Patterson Air Force Base, Ohio.

The authors are grateful to the Materials Evaluation Laboratory of the University of Dayton for making the laminate test specimens. The effort of J. A. Bunderla is also acknowledged with regard to the experimental work on fracture testing.

This technical report has been reviewed and is approved.

STEPHEN W. TSAI, Acting Branch Chief
Mechanics & Surface Interactions Branch
Nonmetallic Materials Division
Air Force Materials Laboratory

ii

ABSTRACT

Analyses for laminar plates are reviewed in this report.
It is observed that while approximate global stress analyses
have been performed for laminates, little has been accom-
plished in the area of strength analysis. The work presented
here is concentrated in that area, i.e., mathematical models
to consider the influence of flaws on failure loads asso-
ciated with crack propagation and/or delamination. In par-
ticular, an approximate three-dimensional formulation for
laminates based on the variational principle of minimum com-
plementary potential energy is presented and applied to the
problem of a three layer composite plate containing a through
crack. This model is employed to study the influences of
the geometric and material characteristics of the composite
on the local stress field in the vicinity of the flaw.

Results of an experimental program to determine the in-
fluence of plate thickness on critical load for a centrally
cracked tensile specimen are reported. Extension of the ex-
perimental program to consideration of laminated specimens is
currently in progress.

A stress analysis has been carried out for another prob-
lem of particular interest in the study of failure for com-
posite systems. The effect of voids in adhesive layers on
the behavior of multi-layer fibrous composites is modeled by
the problem of a penny shaped flaw contained in an isotropic

layer joining two orthotropic half spaces. Stresses in the vicinity of the crack edge are calculated in terms of the loading and the properties of the components for this composite system.

Blank Pages

TABLE OF CONTENTS

LIST OF FIGURES

Figure 5.6   Normalized Stress Intensity Factor as a
                    Function of Relative Layer Height

SECTION I

INTRODUCTION

A research effort primarily concerned with the understanding and prediction of failure for laminar composites is reported here. The current interest in fibrous laminates for structural application is associated with the high strength-to-weight ratio which can be developed in laminates. These laminates are generally composed of layers which have been reinforced by embedding unidirectional fibers. The layers are adhered to each other such that the fiber direction varies from one layer to the next in a previously determined manner. The freedom of choice for fiber orientation in the layers of the composite system enables the development of laminates with special preferential directional properties for particular applications. Because of this characteristic of fibrous composites, the employment of these systems rather than equivalent homogeneous members will be clearly advantageous in many applications.

The drawback of using laminates is that they are sensitive to a number of manufacturing imperfections specific to composite systems, i.e., fiber misalignment, loading imperfections between the fibers and matrix material within an individual layer, and imperfect adhesion of these layers. Composites thus exhibit additional modes of failure associated with phase separations.

-1-

Because of the complicated internal structure of compos-
ite systems, both the problems of stress analysis and failure
prediction are much more difficult than for equivalent single-
phase specimens. A review of some of the analyses which have
been performed in connection with composite systems is con-
tained in Section II of this report. One fact which immerges
very clearly from that work is that the stress field in all
composites is truly three-dimensional in character. Thus,
even the stress field in a symmetric laminate subjected to in-
plane loading, a system to be considered in this report, can-
not be accurately modeled by standard two-dimensional methods
of analysis. The review of previous work in this area further
indicates that relatively little work has been carried out
with regard to fracture analysis of laminates. This fact is
clearly associated with the difficulties of extending fracture
mechanics to composite structures.

In particular, the extension of fracture mechanics to
laminates requires consideration of both three-dimensional
effects and material interactions. Hartranft and Sih [1]
have developed an approximate three-dimensional theory for
a single material plate containing a through crack in a re-
mote tensile field. The approach to fracture of laminates
developed here, see Section III, is based on an extension of
this approximate theory to laminates and its application to
the problem of a through crack in a laminar plate subjected
to in-plane loading. This crack represents a preliminary

-2-

effort to model the failure of composite plates. Further work is clearly required; however, the relatively crude crack model developed here already gives some relevant information concerning the dependence of the stress field near the leading crack edge on the geometric and material properties of the composite plate.

The three-dimensional character of the stress field in single material plates containing cracks, which has been studied by Hartranft and Sih [1], is clearly relevant to understanding the effects of flaws on the behavior of laminates. Thus, an experimental study of these three-dimensional effects on the ability of the approximate solution [1] to model them has been carried out and is discussed in Section IV. This work constitutes a necessary background to both the application of approximate theories of this type to laminates and experimental programs for studying failure of laminates.

In Section V, a self-contained boundary value problem is presented which has particular application to the delamination process in layered composites. The effect of imperfect adhesion between layers of a fibrous composite is studied by considering a penny-shaped flaw in the adhesive layer connecting two anisotropic half-spaces. The results of the analysis suggest that less load is transferred to the adhesive (thus, decreasing the likelihood of delamination) as the relative stiffness of the fibrous layers is increased. This

effect is amplified when the relative thickness of the adhesive layer is decreased.

For future work, the stress solutions for the laminated plate presented in Section III will be further analyzed and used to develop a criterion of fracture. Preliminary experiments have indicated that an internal crack in a sandwiched layer of the laminate can propagate with and without delamination depending upon the geometry and loading conditions. A study on the stress variations near the free surface or interface will be made since they will play an important role on the failure of the laminate composite weakened by flaws.

SECTION II

MODELING OF LAMINATED PLATES

Structural composites can be classified as laminated and multiphase. Multiphase materials can be further divided into continuous fiber reinforced materials and particulate composites. Examples of fiber reinforced composites are glass fiber reinforced plastics and boron fiber reinforced plastics while an example for a particulate composite would be whisker reinforced metals. Laminated composites consist of layers of multiphase or homogeneous materials bonded together. The general potential of laminates lies in the fact that the plies (layers) of the laminate can be oriented to meet both the load and direction requirements allowing for maximum structural efficiency. An important laminated composite in use today is made of layers of unidirectional continuous fiber reinforced material. Generally there are two types of these laminated plates: cross-ply and angle-ply. Cross-ply laminates are those in which the orthotropic axes of symmetry in each ply are alternately oriented at angles of 0 and 90 degrees to the plate axes, while in angle-ply laminates the orthotropic axes of symmetry in each ply are alternately oriented at arbitrary angles of $+\theta$ and $-\theta$ to the plate axes.

The analysis involved for composite systems can be subdivided into two major categories: analytical determination of the mechanical properties of composite materials, and analysis of structures such as laminated plates. In this section

-5-

the theories predicting the elastic behavior of laminated plates are reviewed in detail, while a brief discussion of the methods evaluating material constants is provided.

2.1 ELASTIC PROPERTIES OF COMPOSITE MATERIALS

Many investigators have been involved in developing analytical methods by which the lamina elastic constants can be predicted in terms of the constituent material properties and phase geometry, i.e., the shape and arrangement of the filaments and volume ratios of the fibers and matrix. For example, the stiffness matrix of a particular lamina can be considered as a function of the above parameters, such that

$$C_{ij} = C_{ij}(E_f, \nu_f, v_f, E_m, \nu_m, v_m)$$

where E, ν and v are the modulus of elasticity, Poisson's ratio, and volume fraction of the filament and matrix materials, designated by the subscripts f and m, respectively.

The various theories which have been proposed are: (1) netting analysis, (2) strength of materials method, (3) self-consistent model, (4) variational method, (5) exact method (elasticity), (6) statistical methods, (7) finite element technique, and (8) semi-empirical method. There are several basic assumptions common to these theories, namely:

(1) The fibers are linearly elastic and generally homogeneous.

-6-

(2)   The matrix is linearly elastic and homogeneous.

(3)   Fibers and matrix are free of voids.

(4)   There is perfect bond at the interface of the fibers and matrix.

(5)   The ply is initially in a stress free state.

(6)   The fibers are regularly spaced and aligned.

Furthermore, it can be assumed that the ply or lamina is macroscopically homogeneous, linearly elastic and generally orthotropic or transversely isotropic.

These basic assumptions lead to an over-simplified model of the actual ply. The following are some of the reasons: (1) the filament arrangement within the ply is generally random and the filaments could be misaligned, (2) a transition region between constituents exists, e.g., lack of complete bond and constituents interaction, (3) presence of initial stresses.

A concise description and evaluation of these theories along with a comprehensive list of references is given by C. C. Chamis and G. P. Sendeckyj [2]. For a unidirectional fiber reinforced lamina an important point to note is that in general the exact theories contribute a very small correction to E_1 calculated by the rule of mixture, i.e.,

$$E_1 = E_f \cdot v_f + E_m \cdot v_m$$

-7-

where E_1 is the modulus of elasticity of the composite in the direction of the fiber axis. However, moduli E_2 and G_{12} are rather sensitive to the geometry and constituent properties.

2.2 COMPOSITE PLATES

In general, composite plates can be classified into two major categories: (1) sandwich plates, (2) anisotropic homogeneous or heterogeneous, single or multi-layered plates. Due to the vastness of the field, a very brief discussion of sandwich plates will be given, while the attention will be concentrated on the discussion of laminated plates.

2.2.1 SANDWICH PLATES

These composite structures may contain any number of distinct homogeneous layers separated by isotropic layers. The layers may have different thicknesses and made of different materials. Consider a simple sandwich plate consisting of a core layer of thickness h and two face layers of thickness t. It is assumed that the facings are relatively thin, i.e., t<<h and for most practical purposes they can be treated as membranes, while the core material is considered to have negligible flexural rigidity. Reissner [3] considered the bending of such a plate, where, based upon the above assumptions, he formulated the problem such that the transverse shears are predominantly carried by the core plate, while the bending stresses are primarily taken by the face plates. It is also assumed that the stresses in the face plates are uni-

form across the thickness, while no in-plane stresses σ_x, σ_y, τ_{xy} are acting through the core material. Hence from the equations of equilibrium it can be seen that the transverse shear stresses remain constant across the thickness of the core. Thus the strain energy of the sandwich plate can be written as

$$\Pi_s = \frac{t}{E_f} \iint [\sigma_{x,f}^2 + \sigma_{y,f}^2 - 2\nu\sigma_{x,f} \cdot \sigma_{y,f}$$

$$+ 2(1+\nu)\tau_{xy,f}^2]dxdy + \frac{1}{2G_c} \iiint_{-h/2}^{h/2} \times$$

$$\times [\tau_{xz,c}^2 + \tau_{yz,c}^2]dzdxdy \qquad (2.2.1.1)$$

where the subscripts f and c refer to the face layers and core regions respectively. The relations between stresses and couples are

$$\sigma_{x,f} = \pm \frac{M_x}{t(h+t)}, \quad \sigma_{y,f} = \pm \frac{M_y}{t(h+t)}, \quad \tau_{xy,f} = \pm \frac{M_{xy}}{t(h+t)}$$

$$\tau_{xz,c} = \frac{V_x}{h} \quad , \quad \tau_{yz,c} = \frac{V_y}{h} \qquad (2.2.1.2)$$

Substitution of the above into the strain energy relation results in

$$\Pi_s = \iint \left\{ \frac{1}{t(h+t)^2 E_f} [M_x^2 + M_y^2 - 2\nu M_x M_y + 2(1+\nu)M_{xy}^2] \right.$$

$$\left. + \frac{1}{2G_c h} [Q_x^2 + Q_y^2] \right\} dxdy \qquad (2.2.1.3)$$

-9-

Note that if $G_c h \to \infty$, then the formulation is that of the classical plate theory, where $\frac{12}{Eh^3}$ is replaced by $\frac{1}{t(h+t)^2 E_f}$. Hence, it can be seen that the results predicted by the classical plate theory are more conservative, since it is assumed that the plate has infinite shear rigidity, which can result in an unrealistic solution when the core layer's shear modulus is small.

2.2.2 LAMINATED COMPOSITE PLATES

In this section, we consider plates which are made of two or more unidirectional fiber reinforced plies that are bonded together to form a laminated plate. If the axes of orthotropy of all layers are oriented in the same direction, then the plate can be considered as a unidirectional anisotropic structure. If the orthotropic axes of symmetry in each layer are oriented in a particular direction, then such a configuration is an angle-ply laminate. A special case of angle-ply is the cross-ply laminate, where the orthotropic axes of symmetry in each ply are alternately oriented at angles of 0° and 90° to the plate axes.

One of the most widely used theorems in formulation of various mathematical models of laminated plates is the classical plate theory, where it is assumed, (1) the plane sections normal to the middle plane of the plate remain normal, (2) the state of stress in each layer is that of generalized plane stress or plane stress, (3) the strains in the

z-direction are negligible.

The most elementary formulation is that of unidirectional plane anisotropic plate given by Calcote [4], where it is assumed that the small deformation theory is applicable. Using x,y,z cartesian coordinate system, and assuming linear strain distribution through the thickness

$$u = - z \frac{\partial w}{\partial x}, \ v = - z \frac{\partial w}{\partial y}, \ w = w(x,y) \qquad (2.2.2.1)$$

then

$$\varepsilon_x = - z \frac{\partial^2 w}{\partial x^2}, \ \varepsilon_y = - z \frac{\partial^2 w}{\partial y^2}, \ \gamma_{xy} = - 2z \frac{\partial^2 w}{\partial x \partial y} \qquad (2.2.2.2)$$

considering the general case where the principal material directions do not correspond with the x and y directions of the plate, then the stress-strain relationship can be written as

$$\{\sigma\} = [C]\{\varepsilon\} \qquad (2.2.2.3)$$

where [C] is a full 3×3 matrix, because the coordinate planes xz and yz are not the planes of elastic symmetry of the laminate. Defining stress couples in the usual way

$$M_x = \int_{-h/2}^{h/2} \sigma_x \cdot z \, dz = - [D_{11}w_{,xx} + D_{12}w_{,yy} + 2D_{16}w_{,xy}]$$

$$M_y = \int_{-h/2}^{h/2} \sigma_y \cdot z \, dz = - [D_{12}w_{,xx} + D_{22}w_{,yy} + 2D_{26}w_{,xy}]$$

$$M_{xy} = M_y = \int_{-h/2}^{h/2} \tau_{xy} \cdot z\,dz$$

$$= - [D_{16}w_{,xx} + D_{26}w_{,yy} + 2D_{66}w_{,xy}]$$

where

$$D_{ij} = \frac{C_{ij}h^3}{12}, \quad i,j = 1,2,6$$

along with the equilibrium equations

$$M_{x,x} + M_{xy,y} = Q_x$$

$$M_{xy,x} + M_{y,y} = Q_y$$

$$Q_{x,x} + Q_{y,y} = - p$$

we obtain the governing differential equation for the plate

$$D_{11}w_{,xxxx} + 4D_{16}w_{,xxxy} + 2(D_{12}+2D_{66})w_{,xxyy}$$

$$+ 4D_{26}w_{,xyyy} + D_{22}w_{,yyyy} = p \qquad (2.2.2.4)$$

If the orthotropic axes of the material are coincident with the plate axes, then $\bar{C}_{16} = \bar{C}_{26} = 0$ implies $D_{16} = D_{26} = 0$; hence equation (2.2.2.4) reduces to

$$D_{11}w_{,xxxx} + 2(D_{12}+2D_{66})w_{,xxyy}$$

$$+ D_{22}w_{,yyyy} = p \qquad\qquad (2.2.2.5)$$

which is given in [5] as the equation for a plane orthotropic plate. Further, if the laminate is homogeneous and isotropic, then $D_{11} = D_{22} = (D_{12}+2D_{66}) = D = \frac{Eh^3}{12(1-\nu^2)}$; hence equation (2.2.2.5) is reduced to

$$\nabla^4 w(x,y) = \frac{p}{D} \qquad\qquad (2.2.2.6)$$

which is the classical plate equation.

Now let us consider a laminate made of two layers (angle-ply), where two orthotropic layers of equal thickness are laminated in such a way that the axes of elastic symmetry form an angle $+\theta$ with the x,y-axes in one layer and an angle $-\theta$ in the other layer. Smith [6] formulated this problem, assuming a linear strain distribution through the thickness as given in equations (2.2.2.1) and (2.2.2.2), and a state of generalized plane stress. His formulation provided a constitutive relation exactly as equation (2.2.2.5), where he concluded that the laminate behaves as a homogeneous orthotropic plate.

Reissner and Stavsky [7] pointed out this misconception by reformulating the problem, where they considered the effect of in-plane stretching. This was done by defining

-13-

the strain-displacement relations as

$$\varepsilon_x = \varepsilon_x^o + z\chi_x, \quad \varepsilon_y = \varepsilon_y^o + z\chi_y, \quad \varepsilon_{xy} = \varepsilon_{xy}^o$$

$$+ z\chi_{xy} \qquad\qquad (2.2.2.7)$$

$$\varepsilon_x^o = u_{,x}, \quad \varepsilon_y^o = v_{,y}, \quad \varepsilon_{xy}^o = u_{,y} + v_{,x} \qquad (2.2.2.8)$$

$$\chi_x = -w_{,xx}, \quad \chi_y = -w_{,yy}, \quad \chi_{xy} = -2w_{,xy} \qquad (2.2.2.9)$$

where the mid-surface strains, and bending curvatures are those of the classical plate theory. The equilibrium relations are

$$N_{x,x} + N_{xy,y} + p_x = 0, \quad N_{xy,x} + N_{y,y} + P_y = 0 \qquad (2.2.2.10)$$

$$M_{x,x} + M_{xy,y} - Q_x = 0, \quad M_{xy,x} + M_{y,y} - Q_y = 0 \qquad (2.2.2.11)$$

$$Q_{x,x} + Q_{y,y} + P = 0 \qquad\qquad (2.2.2.12)$$

where the stress resultants are

$$(N_x, N_y, N_{xy}) = \int_{-h/2}^{h/2} (\sigma_x, \sigma_y, \tau_{xy})\,dz \qquad (2.2.2.13)$$

and the stress couples are

$$(M_x, M_y, M_{xy}) = \int_{-h/2}^{h/2} (\sigma_x, \sigma_y, \tau_{xy})\,z\,dz \qquad (2.2.2.14)$$

-14-

The stress-strain relationship is

$$\{\sigma\} = [C]\{\varepsilon\} \qquad\qquad (2.2.2.15)$$

Substitution of equation (2.2.2.7) into equation (2.2.2.15) and the results into equations (2.2.2.13) and (2.2.2.14) leads to

$$\begin{bmatrix} N \\ \\ M \end{bmatrix} = \begin{bmatrix} A & B \\ \\ B & D \end{bmatrix} \begin{bmatrix} \varepsilon^{0} \\ \\ \chi \end{bmatrix} \qquad\qquad (2.2.2.16)$$

where A, B and D are given by

$$(A_{ij}, B_{ij}, D_{ij}) = \int_{-h/2}^{h/2} (1, z, z^{2}).C_{ij}dz,$$
$$(i,j = 1,2,6) \qquad (2.2.2.17)$$

Partial inversion of (2.2.2.16) results in

$$\begin{bmatrix} \varepsilon^{0} \\ \\ M \end{bmatrix} = \begin{bmatrix} A^{*} & B^{*} \\ \\ C^{*} & D^{*} \end{bmatrix} \begin{bmatrix} N \\ \\ \chi \end{bmatrix} \qquad\qquad (2.2.2.18)$$

where $A^{*} = A^{-1}$, $B^{*} = A^{-1}.B$, $C^{*} = B.A^{-1}$, $D^{*} = D - B.A^{-1}.B$.

In order to obtain the governing equations of equilibrium and compatibility, introduce the Airy stress

function $\phi(x,y)$ such that in the absence of body forces the stress resultants can be written as

$$N_x = \phi_{,yy}, \quad N_y = \phi_{,xx}, \quad N_{xy} = -\phi_{,xy} \qquad (2.2.2.19)$$

substituting (2.2.2.19) and (2.2.2.9) into (2.2.2.18) and the results into the following equilibrium and compatibility equations

$$M_{x,xx} + 2M_{xy,xy} + M_{y,yy} + p = 0 \qquad (2.2.2.20)$$

$$\epsilon^o_{x,yy} + \epsilon^o_{y,xx} = \epsilon^o_{xy,xy} \qquad (2.2.2.21)$$

yields the following system of simultaneous fourth-order equations

$$L_1 w - L_3 \phi = p \qquad (2.2.2.22)$$

$$L_2 \phi + L_3 w = 0 \qquad (2.2.2.23)$$

where the operators L_j are given in [7].

Note that equations (2.2.2.22) and (2.2.2.23) are coupled through the operator L_3. The coupling of w and ϕ enters into the boundary conditions as well, i.e., in a problem of transverse loading, if one has prescribed values of M_x and $R_x = Q_x + M_{xy,y}$ at an edge x = constant, at the same

-16-

time he must formulate conditions pertaining to N_x and N_{xy} or u and v. Reissner and Stavsky [7] also pointed out this cross-elasticity effect for stresses, by writing the stress-strain relationship in terms of in-plane strains and bending curvature as

$$\{\sigma\} = [C]\{\varepsilon^O\} + z[C]\{\chi\} \qquad (2.2.2.24)$$

Now invert equation (2.2.2.16)

$$\begin{bmatrix} \varepsilon^O \\ \\ \chi \end{bmatrix} = \begin{bmatrix} a & b \\ \\ c & d \end{bmatrix} \begin{bmatrix} N \\ \\ M \end{bmatrix} \qquad (2.2.2.25)$$

and substitute (2.2.2.25) into (2.2.2.24) to get

$$\{\sigma\} = [C][([a] + z[c])\{N\} + ([b] + z[d])\{M\}] \qquad (2.2.2.26)$$

Thus it can be seen that in general σ_x depends not only on N_x and M_x but also on N_y, M_y, N_{xy}, M_{xy} and an analogous cross elasticity effect is encountered in the expressions for σ_y and τ_{xy}.

2.2.3 N-LAYER LAMINATES

Dong, Pister and Taylor [8] extended the above formulation for multi-layered anisotropic plates. The as-

sumptions of the classical plate theory were used along with the strain-displacement relations given in equation (2.2.2.7). Each layer and also the laminate as a whole are assumed to be in a state of generalized plane stress. Calcote [4] has given complete formulation of this problem. The stress-strain relationship for the kth layer can be written as

$$[\sigma^k] = [C^k][\varepsilon]$$
(2.2.3.1)

where $[\varepsilon]$ is given in equation (2.2.2.7), and the symmetric matrix $[C_{ij}^{(k)}]$ represents the elastic coefficients associated with the kth lamina. For a particular layer these coefficients depend on both the elastic properties of the material principal axes and the orientation of these axes with respect to the laminate axes. Once a reference surface for strains and curvatures is defined, then stress resultants and stress couples can be formulated with respect to this surface as

$$(N_x, N_y, N_{xy}) = \sum_{k=1}^{n} \int_{h_{k-1}}^{h_k} [\sigma_x^{(k)}, \sigma_y^{(k)}, \tau_{xy}^{(k)}]dz$$
(2.2.3.2)

$$(M_x, M_y, M_{xy}) = \sum_{k=1}^{n} \int_{h_{k-1}}^{h_k} [\sigma_x^{(k)}, \sigma_y^{(k)}, \tau_{xy}^{(k)}]zdz$$
(2.2.3.3)

Performing the above integration and summation,

$$\begin{bmatrix} N \\ M \end{bmatrix} = \begin{bmatrix} A & B \\ B & D \end{bmatrix}\begin{bmatrix} \varepsilon^O \\ \chi \end{bmatrix}$$
(2.2.3.4)

where

$$A_{ij} = \sum_{k=1}^{n} C_{ij}^{(k)} (h_k - h_{k-1})$$

$$B_{ij} = \frac{1}{2} \sum_{k=1}^{n} C_{ij}^{(k)} (h_k^2 - h_{k-1}^2) \qquad (2.2.3.5)$$

$$D_{ij} = \frac{1}{3} \sum_{k=1}^{n} C_{ij}^{(k)} (h_k^3 - h_{k-1}^3)$$

Equilibrium equations are the same as for the two-ply laminate given by equations (2.2.2.10), (2.2.2.11) and (2.2.2.12), and the compatibility equation (2.2.2.21). The governing differential equations of the laminate can be formulated either in terms of an Airy stress function $\phi(x,y)$ and the transverse deflection w, or in terms of the three displacements u^o, v^o and w. The system of two simultaneous fourth-order equations obtained in terms of $\phi(x,y)$ and $w(x,y)$ is identical to that of the two-ply laminate given in equations (2.2.2.22) and (2.2.2.23). The formulation in terms of the displacements is given by Whitney and Leissa [9], and Whitney [10]. The governing equations for cross-ply laminates are

$$L_1 u^o + L_2 v^o - L_4 w = 0$$

$$L_2 u^o + L_3 v^o - L_5 w = 0 \qquad (2.2.3.6)$$

$$- L_4 u^o - L_5 v^o + L_6 w = p$$

and the governing equations for angle-ply laminates are

$$L_1 u^O + L_2 v^O - L_1 w = 0$$

$$L_2 u^O + L_3 v^O - L_8 w = 0 \qquad\qquad (2.2.3.7)$$

$$- L_1 u^O - L_8 v^O + L_6 w = p$$

where L_i are operators given in [9,10]. It should be noted that these operators are different from those given in equations (2.2.2.22). P is the transverse load acting on the plate. These equations can be simplified significantly when the laminated plate is a symmetric one with respect to the middle plane, i.e., when the middle plane of the laminate is selected as the reference surface of the plate and the laminate is composed of pairs of laminas such that the two laminas of any particular pair are identical in thickness and orientation. Hence, under these conditions $B_{ij} = 0$, which implies no coupling between stretching and bending.

Pagano [12-14] has investigated the limitations of the classical plate theory (CPT) by comparing the solutions of several specific boundary value problems in this theory with the exact solutions (within the theory of linear elasticity); in particular, cylindrical bending of laminates and transverse deflection of rectangular bi-directional composites.

Pagano [12] formulated the cylindrical bending of a laminate composed of m orthotropic layers simply supported on the ends $x = 0$ and $x = \ell$, by assuming the plate to be in a state of plane strain. Since each layer is orthotropic, the strain-stress relations can be written as

$$\varepsilon_x = R_{11}\sigma_x + R_{13}\sigma_z, \quad \varepsilon_z = R_{13}\sigma_x + R_{33}\sigma_z$$

$$\gamma_{xz} = R_{55}\tau_{xz}$$

where R_{ij} are the reduced compliance coefficients for plane strain, defined in terms of S_{ij} the compliances with respect to the principal axes of the material. The equilibrium equations along with the strain-displacement relations are given as

$$\sigma_{x,x} + \tau_{xz,z} = 0, \quad \sigma_{z,z} + \tau_{xz,x} = 0$$

$$\varepsilon_x = u_{,x}, \quad \varepsilon_z = w_{,z}, \quad \gamma_{xz} = u_{,z} + w_{,x}$$

Note that all the stresses, strains and displacements are functions of x and z only. A solution of the following form is assumed:

$$\sigma_x^{(i)} = f_i''(z) \cdot \sin px$$

$$\sigma_z^{(i)} = -p^2 f_i(z) \cdot \sin px$$

$$\tau_{xz}^{(i)} = -p f_i'(z) \cdot \cos px$$

-21-

which satisfies the equations of equilibrium identically, and the eigenvalues $p = p(n)$ are determined from the boundary conditions. Substitution of these assumed solutions into the stress-strain and strain-displacements relations results in a fourth-order ordinary differential equation in the variable $f_i(z)$ for each layer which is solved exactly. In a subsequent work Pagano [13] solved the problem of bending for a simply supported rectangular laminate under transverse load. Each layer was assumed to be orthotropic. A solution to the governing equations of elasticity of the form

$$u(x,y,z) = U(z)\cos px.\sin qy$$

$$v(x,y,z) = V(z).\sin px.\cos qy$$

$$w(x,y,z) = W(z)\sin px.\sin py$$

and

$$(U,V,W) = (U^*,V^*,W^*).\exp(sz)$$

was assumed. The eigenvalues p and q as well as the constants U^*, V^*, and W^* were determined by substitution of the above assumed solution into the field equations and boundary conditions.

Comparison of the solutions obtained by Pagano [12,13] with that of the classical laminate plate theory solutions discussed previously [7-11] indicate clearly that the classical laminated plate theory (CPT) underestimates the

plate deflection and gives a very poor estimate for relatively
low values of S (span length/plate thickness), e.g., in the
case of cylindrical bending at S = 20, the error is approxi-
mately 20% and it grows significantly with lower values of S;
however, for large values of S the solution approaches asymp-
totically the CPT results. Another important point to note
is the validity of the Kirchhoff hypothesis, where the solu-
tion indicates that the assumption of linear displacement
within each layer may be reasonable; but, the deformed con-
figuration of the original normal plane cannot be described
by this hypothesis for low values of S. Meanwhile, it can be
seen that the deformed normal tends to straighten as the value
of S increases.

In summary, the above comparison clearly shows
the necessity of incorporating the influence of transverse
shear deformation.

Whitney [15] considered the bending of symmetric
angle-ply and cross-ply laminates where he included the trans-
verse shear deformation in the following way. Using the con-
ventional x,y,z coordinate system, the plate surfaces $z = \pm\frac{h}{2}$
are assumed to be free of shear tractions. Each layer is as-
sumed to be an orthotropic material. Neglecting the effect
of transverse normal stress σ_z on the gross response of the
laminate, the stress-strain relation for the kth layer can be
written as

$$
\begin{bmatrix} \sigma_x \\ \sigma_y \\ \tau_{yz} \\ \tau_{xz} \\ \tau_{xy} \end{bmatrix} = \begin{bmatrix} Q_{11} & Q_{12} & 0 & 0 & Q_{16} \\ Q_{12} & Q_{22} & 0 & 0 & Q_{26} \\ 0 & 0 & Q_{44} & Q_{45} & 0 \\ 0 & 0 & Q_{45} & Q_{55} & 0 \\ Q_{16} & Q_{26} & 0 & 0 & Q_{66} \end{bmatrix} \begin{bmatrix} \varepsilon_x \\ \varepsilon_y \\ \varepsilon_{yz} \\ \varepsilon_{xz} \\ \varepsilon_{xy} \end{bmatrix}
$$

where Q_{ij} is the reduced stiffness matrix. Furthermore, it is assumed that the transverse shear stresses of the kth layer have the following form:

$$
\sigma_{xz}^{(k)} = [Q_{55}^{(k)} f(z) + a_{55}^{(k)}] \phi_x(x,y)
$$

$$
+ [Q_{45}^{(k)} f(z) + a_{45}^{(k)}] \phi_y(x,y)
$$

$$
\sigma_{yz}^{(k)} = [Q_{45}^{(k)} f(z) + a_{45}^{(k)}] \phi_x(x,y)
$$

$$
+ [Q_{44}^{(k)} f(z) + a_{44}^{(k)}] \phi_y(x,y)
$$

In the above $a_{ij}^{(k)}$ are constants which can be determined from the condition of the continuity of shear tractions at the interface of adjacent layers.

Using the strain-displacement relations along with the stress-strain equations and the assumption that $w = w(x,y)$ yields

$$u^{(k)} = -zw_{,x} + [J(z) + g_1(z)^{(k)}]\phi_x + g_2(z)^{(k)}\phi_y$$

$$v^{(k)} = -zw_{,y} + g_3(z)^{(k)}\phi_x + [J(z) + g_4(z)^{(k)}]\phi_y$$

where

$$J(z) = \int f(z)dz$$

$$g_i(z)^{(k)} = \alpha_i z^{(k)} + d_i^{(k)}, \quad (i = 1,2,3,4)$$

and where the constants $d_i^{(k)}$ can be determined from the continuity condition of the displacements u and v at the interface of adjacent layers, noting that u = v = 0 at the midplane of the plate. These equations for $J(z)$ and $g_i(z)^{(k)}$ along with the strain-displacement (linear elasticity) relations and Hooke's law for the kth layer will yield three equations for the stress couples M_x, M_y, M_{xy} as functions of $w(x,y)$, $\phi_x(x,y)$ and $\phi_y(x,y)$ and their derivatives. Using these new equations along with the conventional equations of equilibrium given in equations (2.2.2.11) and (2.2.2.12) will result in three constitutive equations for w, ϕ_x and ϕ_y. These constitutive equations are rather formidable; however, for laminates in which $Q_{45}^{(k)} = a_{45}^{(k)} = 0$, they are considerably simplified [15]. This condition arises when the preferred directions of the layers coincide with the plate axes.

-25-

In order to assess this formulation, Whitney considered a simply supported rectangular laminated plate subjected to sinusoidal transverse loading. In order to obtain relevant numerical results, a knowledge of the nature of the function f(z) is necessary. From solutions provided in [12] and other references mentioned in [15], Whitney concluded that the choice of

$$f(z) = 1 - 4(\frac{z}{h})^2$$

was a judicious one for this class of boundary value problems. Bending curves given in [11] indicate that shear deformation increases the plate deflection; e.g., for a width to depth ratio of 20 this increase is about 15% for the plate with $E_{11}/E_{22} = 40$, while the laminate with $E_{11}/E_{22} = 3$ shows a much less pronounced effect, demonstrating the effect of anisotropy of each individual layer. It can be seen that despite the assumptions made on the functions τ_{xz}, τ_{yz} and f(z), this theory predicts rather accurately the gross response of laminated plates under transverse loads.

As is evident, bending theories of composite laminated plates have been investigated extensively. However, very little attention has been given to the extension and in particular the interlaminar shear problems. Puppo and Evensen [16] have proposed the following model for the study of interlaminar shear stresses in the laminate. It is assumed that

the laminate can be modeled as a set of anisotropic layers
separated by isotropic layers, where the isotropic layers
develop only shear stresses, acting as "adhesives" between
the anisotropic layers. It is also assumed that the state of
stress in each anisotropic layer is that of generalized plane
stress, and the in-plane stresses σ_x, σ_y, τ_{xy} and displace-
ments u, v are the averages of the actual values through the
thickness. For a model consisting of two layers, the equilib-
rium equations for the anisotropic layers are

$$\sigma_{x,x}^{(i)} + \tau_{xy,y}^{(i)} \mp \frac{\tau_{xz}^{*}}{h_i} = 0$$

$$\tau_{xy,x}^{(i)} + \sigma_{y,y}^{(i)} \mp \frac{\tau_{yz}^{*}}{h_i} = 0$$

where the superscript (i) indicates a particular layer, and
the positive and negative signs correspond to i=1 and i=2 re-
spectively. The interlaminar shear stresses τ_{xz}^{*} and τ_{yz}^{*} are
acting on the faces of the layers, but from the equilibrium
point of view it is assumed that they are acting on the middle
plane of each layer. This assumption is a valid one if the
laminate is symmetric or warping is prevented by external sup-
ports. The shear stresses in the isotropic layer are assumed
to be

$$\tau_{xz}^{*} = G\gamma_{xz} \simeq \frac{G}{h}(u_1 - u_2)$$

$$\tau_{yz}^{*} = G\gamma_{yz} \simeq \frac{G}{h}(v_1 - v_2)$$

-27-

where u, v are the displacement components, and G is the shear modulus of the isotropic layer, while the stress-strain relation for the anisotropic material is $\{\sigma\} = [Q_{ij}]\{\varepsilon\}$ where Q_{ij} is the reduced stiffness matrix. The solution is obtained when four functions u_1, v_1, u_2 and v_2 are found which satisfy the constitutive equations and the particular boundary conditions. For an infinite laminate under uniform unidirectional deformation, it is shown that the interlaminar shear stresses are zero. However, at the free edge of a finite width laminate, the interlaminar shear stress has a finite value. Results based on this theory indicate that the magnitude of the transverse shear τ_{xz}^* can be approximately 25% of the maximum axial stress σ_x, while in the classical laminate plate theory these shear stresses are ignored. Hence, it is evident that for a reasonable strength analysis the effect of the interlaminar shear stresses must be included.

Pipes and Pagano [17] considered the problem of a finite width symmetric angle-ply laminate under uniform axial strain, in order to study the character of the interlaminar shear stress. The stress-strain relations for each layer with respect to the plate axes are

$$
\begin{bmatrix} \sigma_x \\ \sigma_y \\ \sigma_z \\ \tau_{yz} \\ \tau_{xz} \\ \tau_{xy} \end{bmatrix}
=
\begin{bmatrix}
C_{11} & C_{12} & C_{13} & 0 & 0 & C_{16} \\
C_{12} & C_{22} & C_{23} & 0 & 0 & C_{26} \\
C_{13} & C_{23} & C_{33} & 0 & 0 & C_{36} \\
0 & 0 & 0 & C_{44} & C_{45} & 0 \\
0 & 0 & 0 & C_{45} & C_{55} & 0 \\
C_{16} & C_{26} & C_{36} & 0 & 0 & C_{66}
\end{bmatrix}
\begin{bmatrix} \varepsilon_x \\ \varepsilon_y \\ \varepsilon_z \\ \gamma_{yz} \\ \gamma_{xz} \\ \gamma_{xy} \end{bmatrix}
$$

and the strain-displacement relations are those of linear elasticity. The tractions are applied only on the ends of the laminate (x = constant) such that the stress components are independent of x. Hence the equilibrium equations are

$$
\tau_{xy,y} + \tau_{xz,z} = 0, \quad \sigma_{y,y} + \tau_{yz,z} = 0, \quad \tau_{yz,y} + \sigma_{z,z} = 0
$$

Integrating strain-displacement relations and enforcing the symmetry conditions of the displacements with respect to the xy and xz planes and the continuity conditions at the interfaces yields

$$
u = C_6 x + U(y,z), \quad v = V(y,z), \quad w = W(y,z)
$$

Since the strain ε_x is a constant, this type of displacement field is defined as "uniform axial extension" [17]. The constitutive equations of each layer are obtained by combining the stress-strain relations with the reduced equilibrium equations, the strain-displacement relations and the above displacement field. From the numerical results of a four layer,

-29-

$\pm 45°$ symmetric angle-ply laminate, it can be seen that the in-plane stresses converge to the values predicted by the classical plate theory away from the plate boundaries. However, the interlaminar shear stress τ_{xz} tends to approach infinity at the free edge, indicating the possibility of the presence of a singularity at the intersection of the interface and free-edge. Rybicki [18] has carried out a three-dimensional finite element analysis for the problem considered by Pipes and Pagano, i.e., a laminar plate subjected to uniform end displacements. Rybicki's results for the stress components are in close agreement with those of Pipes and Pagano except that Rybicki's interlaminar shearing stresses do not become singular at the plate edges. The fact that Rybicki did not obtain a singularity for the shearing stresses may be a consequence of his finite element model which does not permit such singularities. The question of whether these shearing stress components attain a large finite value or are actually singular at the plate edges is not satisfactorily resolved by either the Pipes and Pagano or the Rybicki calculation because of the inherent approximate nature of both of their numerical calculations.

In summary the classical laminate plate theory can be used effectively when predicting gross behavior of thin laminates; however, it fails to predict the interlaminar shear stresses and their effect on other laminate response. In order to predict the behavior of composite plates accurately, the

effect of transverse stresses must be included. The mathe-
matical models of Puppo and Evensen, and Pipes and Pagano
consider the effect of interlaminar shear for the special
case of symmetric laminates. These models can be used as a
guide in understanding the shear transfer behavior between
layers of a composite laminate, but they are inadequate to
investigate the failure by either delamination or fracture
within an individual layer. Other mathematical models are
needed to investigate these failure mechanisms in conjunction
with the free edge effects due to geometrical discontinuities.

2.2.4   STRESS ANALYSIS FOR LAMINATES CONTAINING FLAWS - A PROPOSED THEORY

The ultimate purpose of models and stress analy-
ses for composites is to enable strength analysis or the pre-
diction of load carrying capacity for the composite system.
The approach to be taken is clearly dependent on the mode of
failure anticipated. For laminates, failure is often asso-
ciated with crack growth and/or delamination. Thus a knowl-
edge of the local effects of flaws or cracks on the response
of laminates is needed to make accurate predictions of load
carrying capacity. The theories discussed above give a de-
scription of the stress field in laminar composites but do not
take into account the effects of material imperfections.

In the following section, an approximate, three-
dimensional model for laminates is developed and applied to
the problem of a through crack in a laminate.

SECTION III

AN APPROXIMATE THREE-DIMENSIONAL LAMINAR PLATE THEORY

Laminar composites have been developed whose strength to weight ratio is considerably higher than that of homogeneous materials. This had led to a considerable interest in the employment of composite plates for structural application. Consequently, a great deal of effort has been directed in both areas, analysis and experiments, to determine the behavior of such composite systems. In particular, it is clearly important to understand the failure mechanisms and develop criteria to predict failure conditions. The failure phenomena for composites is far more complicated than for the corresponding homogeneous structures because fiber-matrix debonding and interlaminar separation often are observed in conjunction with unstable crack growth. The present study attempts to (1) develop an approximate theory for laminar plates and (2) apply this theory to a laminate containing a through crack in order to predict the effect of such a flaw on the behavior of the composite system. The analysis is particularly directed toward developing a better understanding of the failure mechanisms, i.e., the interaction of cracks with delamination.

In the development of approximate theory for laminar plates, it must be, at the outset, realized that composite plates contain a truly three-dimensional distribution of stress even under two-dimensional loading conditions. The approach employed in this work is to extend the approximate

three-dimensional theories for homogeneous plates developed by Reissner [3] and Hartranft and Sih [1] to laminates. These theories are based on the variational principle of minimum complementary potential energy. An approximate form is assumed for the stress field and the complementary potential energy functional is minimized with respect to admissible variations of this field, i.e., those which satisfy (a) the equilibrium equations of three-dimensional elasticity and (b) the traction boundary conditions. The resulting solution is approximate in that the compatibility or displacement continuity conditions are only satisfied in an averaged sense. Thus some difficulties can arise in the application of such a theory to laminates because the interfacial conditions between layers requires continuity of displacements as well as tractions. The choices for the extension of the three-dimensional plate theories to laminar structures will be based, in part, on just this consideration.

The complementary potential energy principle for two (or more) isotropic material problems will be developed and the interfacial continuity conditions will be demonstrated. An approximate stress field will then be assumed and its consequences examined. This will lead to an approximate theory for laminar plates which will, in turn, be applied to the problem of a laminate containing a through crack subjected to an in-plane loading situation. It should be noted that the same approach is applicable to problems associated with bend-

ing of laminar plates. Only minor changes in the formulation are needed to consider plate bending.

The approximate theory to be presented here is capable of dealing with laminates developed from homogeneous, isotropic plies. On the other hand, more interest has been expressed in laminates which are manufactured from fiber reinforced layers, thereby exhibiting higher strength to weight ratios. Extensions of the present theory to laminates containing anisotropic plies, thus modeling the behavior of fibrous laminates, are now possible as a result of the knowledge gained from this idealized approach.

3.1 THE VARIATIONAL PRINCIPLE OF MINIMUM COMPLEMENTARY POTENTIAL ENERGY FOR COMPOSITES

The complementary potential energy principle is developed for two-material problems and the results are used to determine the corresponding variational principle for laminates.

Recall, the complementary potential energy (Φ) of an isotropic, homogeneous, body is defined as the strain energy of that body minus the work done on the portion of the body surface (S_u) over which displacements are specified, i.e.,

$$\Phi = \int_V \Psi dv - \int_{S_u} T_i \bar{u}_i ds \qquad (3.1.1)$$

where the strain energy density is

-34-

$$\Psi = \int_{o}^{\sigma_{ij}} \varepsilon_{ij} d\sigma_{ij}$$

Consider a body, made up of two materials, which is subjected to traction boundary conditions along its external surface, Figure 3.1.1. Traction boundary conditions are assumed over the entire external surface for convenience in writing so that the complementary potential energy reduces to the strain energy and the only interfacial surface (S_I) must be considered separately. Displacement boundary conditions can be handled in the standard manner and do not alter the significant points of the analysis to be discussed. The complementary potential energy of the body described is the sum of the strain energies of the portion made from material (1) plus that formed from material (2), i.e.,

$$\Phi = \int_{v(1)} \Psi_{(1)} dv + \int_{v(2)} \Psi_{(2)} dv \qquad (3.1.2)$$

This functional (Φ) is to be minimized with respect to the stress components subject to the constraints of

(1) equilibrium, $\sigma_{ij,j}^{(p)} = 0$, $p = 1,2$

(2) satisfaction of traction boundary conditions, $\sigma_{ij}^{(p)} n_j = T_i$ on $S_T^{(p)}$, $p = 1,2$, and

(3) continuity of tractions across S_I, $\sigma_{ij}^{(1)} n_j^{(1)} = -\sigma_{ij}^{(2)} n_j^{(2)}$

-35-

where $n_j^{(p)}$ are the components of the outward unit normal to the surface of the sub-region (p). Thus, on S_I,

$$n_j^{(2)} = - n_j^{(1)}$$

The minimization of a functional subject to a set of constraints can be accomplished with the use of Lagrange multipliers. For this case, the functional π is introduced as

$$\pi = \int_{v_1} \Psi_1 dv + \int_{v_2} \Psi_2 dv - \int_v \lambda_i^{(1)} \sigma_{ij,j}^{(1)} dv$$

$$- \int_{v_2} \lambda_i^{(2)} \sigma_{ij,j}^{(2)} dv - \int_{S_I} \beta_i (\sigma_{ij}^{(1)} n_j^{(1)}$$

$$+ \sigma_{ij}^{(2)} n_j^{(2)}) ds \qquad (3.1.3)$$

where $\lambda_i^{(1)}$, $\lambda_i^{(2)}$, and β_i (i = 1,3) are the Lagrange multipliers. The minimization of this functional π with respect to admissible variations of the stress components leads to the set of governing equations and material boundary conditions. This variational procedure will be carried out primarily to demonstrate that it leads to continuity conditions for the displacement components across the material interface S_I.

$$\delta\pi = \int_{V_1} \frac{\partial\Psi_1}{\partial\sigma_{ij}^{(1)}} \delta\sigma_{ij}^{(1)}dv + \int_{V_2} \frac{\partial\Psi_2}{\partial\sigma_{ij}^{(2)}} \delta\sigma_{ij}^{(2)}dv$$

$$- \int_{V_1} \lambda_i^{(1)}\delta(\sigma_{ij,j}^{(1)})dv - \int_{V_2} \lambda_i^{(2)}\delta(\sigma_{ij,j}^{(2)})dv$$

$$- \int_{S_I} \beta_i(n_j^{(1)}\delta\sigma_{ij}^{(1)} + n_j^{(2)}\delta\sigma_{ij}^{(2)})ds = 0 \qquad (3.1.4)$$

Application of the divergence theorem followed by collection of terms yields

$$\delta\pi = \int_{V_1} (\frac{\partial\Psi_1}{\partial\sigma_{ij}^{(1)}} + \lambda_{i,j}^{(1)})\delta\sigma_{ij}^{(1)}dv$$

$$+ \int_{V_2} (\frac{\partial\Psi_2}{\partial\sigma_{ij}^{(2)}} + \lambda_{i,j}^{(2)})\delta\sigma_{ij}^{(2)}dv$$

$$- \int_{S_I} [(\lambda_i^{(1)} + \beta_i)n_j^{(1)}\delta\sigma_{ij}^{(1)}$$

$$+ (\lambda_i^{(2)} + \beta_i)n_j^{(2)}\delta\sigma_{ij}^{(2)}]ds = 0 \qquad (3.1.5)$$

This result can be further simplified by recalling that on S_I
$n_j^{(1)}\sigma_{ij}^{(1)} + n_j^{(2)}\sigma_{ij}^{(2)} = 0$ which implies that

$$n_j^{(2)}\delta\sigma_{ij}^{(2)} = - n_j^{(1)}\delta\sigma_{ij}^{(1)}$$

Thus

$$\delta \pi = \int_{v_1} \left(\frac{\partial \Psi_1}{\partial \sigma_{ij}^{(1)}} + \lambda_{i,j}^{(1)} \right) \delta \sigma_{ij}^{(1)} dv$$

$$+ \int_{v_2} \left(\frac{\partial \Psi_2}{\partial \sigma_{ij}^{(2)}} + \lambda_{i,j}^{(2)} \right) \delta \sigma_{ij}^{(2)} dv$$

$$- \int_{S_I} \left(\lambda_i^{(1)} - \lambda_i^{(2)} \right) n_j^{(1)} \delta \sigma_{ij}^{(1)} ds = 0 \qquad (3.1.6)$$

In order that $\delta \pi = 0$ for all admissible $\delta \sigma_{ij}^{(1)}$ in v_1 and on S_I and all admissible $\delta \sigma_{ij}^{(2)}$ in v_2, it is necessary that

$$\frac{\partial \Psi_1}{\partial \sigma_{ij}^{(1)}} + \lambda_{i,j}^{(1)} = 0 \qquad \text{in } v_1$$

$$\frac{\partial \Psi_2}{\partial \sigma_{ij}^{(2)}} + \lambda_{i,j}^{(2)} = 0 \qquad \text{in } v_2 \qquad (3.1.7)$$

$$\left(\lambda_i^{(1)} - \lambda_i^{(2)} \right) = 0 \qquad \text{on } S_I$$

From equation (3.1.1) it is recognized that $\frac{\partial \Psi}{\partial \sigma_{ij}} = \varepsilon_{ij}$ and the first two sets of equations are the compatibility conditions in v_1 and v_2, respectively. They further imply that

$$\lambda_i^{(p)} = - u_i^{(p)}, \ p = 1,2, \ i = 1,2,3$$

Substitution of this result into the third set of equations (3.1.7) yields

$$u_i^{(1)} = u_i^{(2)} \text{ on } S_I$$

-38-

Thus, it has been demonstrated that the complementary strain energy for a nonhomogeneous body is the sum of the strain energies of the various constituents minus the work done over the portion of the external boundary over which displacements are prescribed. Minimization of the complementary potential energy with respect to admissible stress fields leads to the compatibility conditions within each material and continuity of displacements across material interfaces.

3.2 AN APPROXIMATE THREE-DIMENSIONAL THEORY FOR LAMINATES

The use of variational principles, e.g., the principle of minimum complementary potential energy, to develop approximate solutions is a standard technique. An approximate form is assumed for the variables, in this case the stress components, and it is substituted into the functional. Minimization of that functional with respect to admissible variations of the assumed functions (stress components) leads to the choice for those functions which best approximates the exact solution in an averaged sense.

The procedure to be employed for laminated plates is to assume that each of the stress components in each layer can be approximated as a product of a function of the out-of-plane variable z multiplied by a function of the in-plane variables x and y, i.e.,

$$\sigma_{ij}^{(p)} = f_{ij}^{(p)}(z)g_{ij}^{(p)}(x,y) \quad \text{no sum on } i,j,p \quad (3.2.1)$$

The purpose of this assumed form for the stress components is to reduce the governing equations from dependence on three independent variables to dependence on two variables for which many standard solution techniques exist. Substitution of the assumed form for the components into the equilibrium equations with the additional condition that the equations separate leads to the more specific assumption

$$\sigma_z^{(p)} = f_p(z)Z_z^{(p)}(x,y)$$

$$[\tau_{xz}^{(p)}, \tau_{yz}^{(p)}] = -f_p'(z)[Z_x^{(p)}(x,y), Z_y^{(p)}(x,y)]$$

$$\quad (3.2.2)$$

$$[\sigma_x^{(p)}, \sigma_y^{(p)}, \tau_{xy}^{(p)}] = f_p''(z)[S_x^{(p)}(x,y), S_y^{(p)}(x,y),$$

$$T_{xy}^{(p)}(x,y)]$$

The conditions of traction continuity across material interfaces are satisfied by taking

$$[Z_x^{(p)}, Z_y^{(p)}, Z_z^{(p)}] = [Z_x, Z_y, Z_z]$$

and

$$f_p(z) = f_{p+1}(z)$$

$$f_p'(z) = f_{p+1}'(z)$$

at the value of z corresponding to the interface between layers p and p+1.

It is perfectly reasonable to substitute this assumed form for the stress field into the complementary potential energy functional and minimize that functional with respect to $f^{(p)}(z)$, Z_z, Z_x, Z_y, $S_x^{(p)}$, $S_y^{(p)}$, and $T_{xy}^{(p)}$ subject to the conditions of equilibrium in order to develop an approximate solution for laminar composites. It is, however, advantageous to examine the resulting form of the strain components so as to choose the approximate solution which comes closest to satisfying the displacement continuity conditions across the material interfaces. For example, the strain component ε_x is given by

$$\varepsilon_x = \frac{1}{E}[\sigma_x - \nu(\sigma_y + \sigma_z)] = \frac{1}{E}[f''(z)(S_x - \nu S_y) - \nu f(z)Z_z]$$

In order for ε_x and thus u_x to be continuous it is necessary, though not sufficient, that $S_x^{(p)}$ and $S_y^{(p)}$ be the same for all layers. Examination of the shearing strain component γ_{xy} yields a similar condition for $T_{xy}^{(p)}$. Thus the assumed form for the stress field which will be adopted is:

$$\sigma_z^{(p)} = f_{(p)}(z)Z_z(x,y)$$

$$[\tau_{xz}^{(p)}, \tau_{yz}^{(p)}] = -f'_{(p)}(z)[Z_x(x,y), Z_y(x,y)] \qquad (3.2.3)$$

$$[\sigma_x^{(p)}, \sigma_y^{(p)}, \tau_{xy}^{(p)}] = f''_{(p)}(z)[S_x(x,y), S_y(x,y), T_{xy}(x,y)]$$

-41-

where $f_p(z)$ and $f_p'(z)$ must match their respective values for the adjacent layers. For notational purposes it is convenient to rewrite the assumed form for the stress components in an equivalent manner as:

$$\sigma_z^{(p)} = f(z)Z_z(x,y)$$

$$[\tau_{xz}^{(p)}, \tau_{yz}^{(p)}] = -f'(z)[Z_x(x,y), Z_y(x,y)]$$

$$[\sigma_x^{(p)}, \sigma_y^{(p)}, \tau_{xy}^{(p)}] = f''(z)[S_x(x,y), S_y(x,y), T_{xy}(x,y)]$$

where $f(z)$ must be continuous and have a continuous first derivative across the material interfaces.

Substitution of this assumed form for the stress components, equation (3.2.4), into the complementary potential energy functional and the equilibrium equations for a laminar plate with edge loading and traction-free surfaces ($f = f' = 0$ on surfaces) yields

$$\Phi = \sum_p \left[\frac{1}{2E_{(p)}} \int_{V_{(p)}} \{ f''^2 [S_x^2 + S_y^2 - 2\nu_{(p)}S_x S_y \right.$$

$$+ 2(1+\nu_{(p)})T_{xy}^2] + 2f'^2(1+\nu_{(p)})(Z_x^2 + Z_y^2)$$

$$- 2\nu_{(p)}ff''(Z_z)(S_x + S_y) + f^2 Z_z^2 \} dv$$

$$\left. - \int_{S_u^{(p)}} [f''(S_n \bar{U}_n^{(p)} + T_{ns}\bar{U}_s^{(p)}) - f'Z_n\bar{U}_z^{(p)}] ds \right. \quad (3.2.5)$$

and

$$Z_z = Z_{x,x} + Z_{y,y}$$

$$Z_x = S_{x,x} + T_{xy,y} \qquad (3.2.6)$$

$$Z_y = T_{xy,x} + S_{y,y}$$

where

$$S_n n_x - T_{ns} n_y = S_x n_x + T_{xy} n_y$$

$$S_n n_y + T_{ns} n_x = T_{xy} n_x + S_y n_y \qquad (3.2.7)$$

$$Z_n = Z_x n_x + Z_y n_y$$

and $\bar{U}_n^{(p)}$, $\bar{U}_s^{(p)}$, and $\bar{U}_z^{(p)}$ are the normal, tangential, and transverse components of the displacements prescribed on the edge $(S_n^{(p)})$ of layer p, respectively.

Lagrange multipliers (λ_i) are employed to insure satisfaction of the equilibrium equations, and the functional

$$\pi = \Phi - \iint [\lambda_1 (S_{x,x} + T_{xy,y} - Z_x)$$

$$+ \lambda_2 (T_{xy,y} + S_{y,y} - Z_y) + \lambda_3 (Z_{x,x} + Z_{y,y} - Z_y)]dxdy$$

$$(3.2.8)$$

is formed.

The variation of π with respect to S_x, S_y, T_{xy}, Z_x, Z_y, Z_z, and $f(z)$ with the continuity conditions enforced on $f(z)$ and $f'(z)$ is

$$\delta\pi = \sum_p \left[\frac{1}{2E_{(p)}} \int_{V_{(p)}} \{f''[2S_x\delta S_x + 2S_y\delta S_y - 2\nu_{(p)}(S_x\delta S_y \right.$$

$$+ S_y\delta S_x) + 4(1+\nu_{(p)})T_{xy}\delta T_{xy}] + 4f'^2(1+\nu_{(p)}) \times$$

$$\times (Z_x\delta Z_x + Z_y\delta Z_y) - 2\nu_{(p)}ff''[Z_z(\delta S_x + \delta S_y)$$

$$+ (S_x + S_y)\delta Z_z] + 2f^2 Z_z\delta Z_z\}dv - \int_{S_u^{(p)}} [f''(\delta S_n\bar{U}_n^{(p)}$$

$$+ \delta T_{ns}\bar{U}_s^{(p)} - f'\delta Z_n\bar{U}_z^{(p)}]ds]$$

$$- \iint [\lambda_1(\delta S_{x,x} + \delta T_{xy,y} - \delta Z_x)$$

$$+ \lambda_2(\delta T_{xy,x} + \delta S_{y,y} - \delta Z_y)$$

$$+ \lambda_3(\delta Z_{x,x} + \delta Z_{y,y} - \delta Z_z)]dxdy$$

$$+ \sum_p \left[\frac{1}{2E_{(p)}} \int_{V_{(p)}} \{2[S_x^2 + S_y^2 - 2\nu_{(p)}S_xS_y \right.$$

$$+ 2(1+\nu_{(p)})T_{xy}]f''\delta f'' + 4(1+\nu_{(p)})(Z_x^2 + Z_y^2)f'\delta f'$$

$$- 2\nu_{(p)}Z_z(S_x + S_y)(f\delta f'' + f''\delta f) + 2Z_z^2 f\delta f\}dv$$

-44-

$$- \int_{S_u^{(p)}} [(S_n \bar{U}_n^{(p)} + T_{ns} \bar{U}_s^{(p)}) \delta f'' - Z_n \bar{U}_z^{(p)} \delta f'] ds]$$

(3.2.9)

Note that $\delta \pi$ has been purposely separated into two parts. The first part contains only variations of the in-plane functions S_x, S_y, T_{xy}, Z_x, Z_y, and Z_z; while the second set of terms includes only variations of $f(z)$ and its derivatives. The integrals containing variations of the in-plane functions can be integrated through the thickness and those containing variations of $f(z)$ can be integrated in x and y. Thus $\delta \pi$ can be rewritten as:

$$\delta \pi = \int_A \{I_1 (S_x \delta S_x + S_y \delta S_y) + 2(I_1 - I_2) T_{xy} \delta T_{xy}$$

$$+ I_2 (S_x \delta S_y + S_y \delta S_x) + I_3 (Z_x \delta Z_x + Z_y \delta Z_y)$$

$$+ I_4 [Z_z (\delta S_x + \delta S_y) + (S_x + S_y) \delta Z_z] + I_5 Z_z \delta Z_z$$

$$- \lambda_1 (\delta S_{x,x} + \delta T_{xy,y} - \delta Z_x) - \lambda_2 (\delta T_{xy,x} + \delta S_{y,y} - \delta Z_y)$$

$$- \lambda_3 (\delta Z_{x,x} + \delta Z_{y,y} - \delta Z_z) \} dx dy$$

$$- \int_{C_u} (U_n \delta S_n + U_s \delta T_{ns} + U_z \delta Z_n) dC$$

$$+ \sum_p \int_{t_{p-1}}^{t_p} \{\alpha_1^{(p)} f''(z) \delta f''(z) + \alpha_2^{(p)} f'(z) \delta f'(z)$$

$$+ \alpha_3^{(p)} [f(z) \delta f''(z) + f''(z) \delta f(z)] + \alpha_4^{(p)} f(z) \delta f(z)$$

$$+ \beta_1^{(p)} \delta f''(z) + \beta_2^{(p)} \delta f'(z) \} dz$$

(3.2.10)

-45-

where

$$I_1 = \sum_p \frac{1}{E_{(p)}} \int_{t_{p-1}}^{t_p} f''^2(z) dz$$

$$I_2 = - \sum_p \frac{\nu_{(p)}}{E_{(p)}} \int_{t_{p-1}}^{t_p} f''^2(z) dz$$

$$I_3 = \sum_p \frac{2(1+\nu_{(p)})}{E_{(p)}} \int_{t_{p-1}}^{t_p} f'^2(z) dz$$

$$I_4 = - \sum_p \frac{\nu_{(p)}}{E_{(p)}} \int_{t_{p-1}}^{t_p} f(z) f''(z) dz$$

$$I_5 = \sum_p \frac{1}{E_{(p)}} \int_{t_{p-1}}^{t_p} f^2(z) dz$$

$$u_n = \sum_p \int_{t_{p-1}}^{t_p} \bar{U}_n^{(p)} f''(z) dz$$

$$u_s = \sum_p \int_{t_{p-1}}^{t_p} \bar{U}_s^{(p)} f''(z) dz$$

$$u_z = - \sum_p \int_{t_{p-1}}^{t_p} \bar{U}_z^{(p)} f'(z) dz$$

$$\alpha_1^{(p)} = \frac{1}{E_{(p)}} \iint_A [S_x^2 + S_y^2 - 2\nu_{(p)} S_x S_y + 2(1+\nu_{(p)}) T_{xy}^2] dx dy$$

$$\alpha_2^{(p)} = \frac{2(1+\nu_{(p)})}{E_{(p)}} \iint_A (Z_x^2 + Z_y^2) dx dy$$

$$\alpha_3^{(p)} = -\frac{\nu_{(p)}}{E_{(p)}} \iint_A Z_z (S_x + S_y) \, dxdy$$

$$\alpha_4^{(p)} = \frac{1}{E_{(p)}} \iint_A Z_z^2 \, dxdy$$

$$\beta_1^{(p)} = \int_{C_u} (S_n \bar{U}_n^{(p)} + T_{ns} \bar{U}_s^{(p)}) \, dC$$

$$\beta_2^{(p)} = -\int_{C_u} Z_n \bar{U}_z^{(p)} \, dC$$

The divergence theorem and the integration-by-parts technique are applied to the variational equation $\delta\pi = 0$ to obtain:

$$
\begin{aligned}
\delta\pi = \int_A \Big[& (I_1 S_x + I_2 S_y + I_4 Z_z + \lambda_{1,x}) \delta S_x \\
& + (I_1 S_y + I_2 S_x + I_4 Z_z + \lambda_{2,y}) \delta S_y \\
& + (2(I_1 - I_2) T_{xy} + \lambda_{1,y} + \lambda_{2,x}) \delta T_{xy} \\
& + (I_3 Z_x + \lambda_1 + \lambda_{3,x}) \delta Z_x \\
& + (I_3 Z_y + \lambda_2 + \lambda_{3,y}) \delta Z_y \\
& + (I_4 (S_x + S_y) + I_5 Z_z + \lambda_3) \delta Z_z \Big] \, dxdy
\end{aligned}
$$

$$- \int_{C_u} [(u_n + \lambda_n)\delta S_n + (u_s + \lambda_s)\delta T_{ns} + (u_z + \lambda_3)\delta Z_n]dc$$

$$+ \sum_p \int_{t_{p-1}}^{t_p} [\alpha_1^{(p)} f''''(z) + (2\alpha_3^{(p)} - \alpha_2^{(p)})f''(z) + \alpha_4^{(p)} f(z)$$

$$+ \beta_{1,zz}^{(p)} - \beta_{2,z}^{(p)}]\delta f(z)dz + \sum_p (\alpha_1^{(p)} f''(z) + \alpha_3^{(p)} f(z)$$

$$+ \beta_1^{(p)})\delta f'(z)\Big|_{t_{p-1}}^{t_p} + \sum_p (-\alpha_1^{(p)} f'''(z) + \alpha_2^{(p)} f'(z)$$

$$- \alpha_3^{(p)} f'(z) - \beta_{1,z}^{(p)} + \beta_2^{(p)})\delta f(z)\Big|_{t_{p-1}}^{t_p} \qquad (3.2.11)$$

where

$$\lambda_n = \lambda_1 n_1 + \lambda_2 n_2$$

$$\lambda_s = -\lambda_1 n_2 + \lambda_2 n_2$$

and (n_1, n_2) are the direction cosines of the normal to the plate edge.

The governing equations and boundary conditions are now apparent, i.e., the in-plane variables can be determined from

$$I_1 S_x + I_2 S_y + I_4 Z_z + \lambda_{1,x} = 0$$

$$I_1 S_y + I_2 S_x + I_4 Z_z + \lambda_{2,y} = 0$$

-48-

$$2(I_1 - I_2)T_{xy} + \lambda_{1,y} + \lambda_{2,x} = 0$$

$$I_3 Z_x + \lambda_1 + \lambda_{3,x} = 0$$

$$I_3 Z_y + \lambda_2 + \lambda_{3,y} = 0$$

$$I_4(S_x + S_y) + I_5 Z_z + \lambda_3 = 0$$

$$\text{(3.2.12)}$$

$$Z_z = Z_{x,x} + Z_{y,y}$$

$$Z_x = S_{x,x} + T_{xy,y}$$

$$Z_y = T_{xy,x} + S_{y,y}$$

with $\lambda_n = -u_n$, $\lambda_s = -u_s$, and $\lambda_3 = -u_z$ on the portion of the boundary over which displacements are prescribed. The boundary conditions associated with the in-plane variables S_x, S_y,... can be either of the traction type or averaged displacements. On the contour c along the plate edge, one can prescribe either

$$S_n = \bar{S}_n \quad \text{or} \quad \lambda_n = -\bar{u}_n$$

$$T_{ns} = \bar{T}_{ns} \quad \text{or} \quad \lambda_s = -\bar{u}_s$$

$$Z_n = \bar{Z}_n \quad \text{or} \quad \lambda_3 = -\bar{u}_z$$

The function $f(z)$ for the pth layer is governed by

$$\alpha_1^{(p)} f''''(z) + (2\alpha_3^{(p)} - \alpha_2^{(p)}) f''(z) + \alpha_4^{(p)} f(z)$$

$$= \beta_{2,z}^{(p)} - \beta_{1,zz}^{(p)} \qquad (3.2.13)$$

with the conditions that, $f(z)$, $f'(z)$, $(\alpha_1^{(p)} f''(z) + \alpha_3^{(p)} f$
$+ \beta_1^{(p)})$ and $[\alpha_1^{(p)} f'''(z) + (\alpha_3^{(p)} - \alpha_2^{(p)}) f'(z) + \beta_{1,z}^{(p)} - \beta_2^{(p)}]$
must be continuous across material interfaces. The traction-
free surface conditions are reflected by the requirement that
$f(z)$ and $f'(z)$ must be zero on the plate surfaces.

After some nontrivial manipulations the set of governing
differential equations can be separated into the form:

$$Z_x - a_6 \nabla^2 Z_x = \frac{\partial}{\partial x} (a_1 \nabla^2 \lambda_3 + a_2 \lambda_3)$$

$$Z_y - a_6 \nabla^2 Z_y = \frac{\partial}{\partial y} (a_1 \nabla^2 \lambda_3 + a_2 \lambda_3) \qquad (3.2.14)$$

$$a_3 \nabla^4 \lambda_3 + a_4 \nabla^2 \lambda_3 + a_5 \lambda_3 = 0$$

provided that

$$\frac{\partial Z_x}{\partial x} + \frac{\partial Z_y}{\partial y} = - a_7 \nabla^2 \lambda_3 - a_8 \lambda_3$$

$$a_1 = \frac{[\frac{I_4}{(I_1+I_2)} + \frac{I_2 I_3}{(I_1^2-I_2^2)} - \frac{I_3}{2(I_1-I_2)}] I_4}{[I_5(I_1+I_2)+I_3 I_4-2I_4^2]} + \frac{I_1}{(I_1^2-I_2^2)}$$

$$a_2 = \frac{[\frac{I_4}{(I_1+I_2)} + \frac{I_2 I_3}{(I_1^2-I_2^2)} - \frac{I_3}{2(I_1-I_3)}](I_1+I_2)}{[I_5(I_1+I_2)+I_3 I_4-2I_4^2]}$$

-50-

$$a_3 = I_4^2 - I_1 I_5$$

$$a_4 = -2I_4(I_1 - I_2) + I_1 I_3$$

$$a_5 = -(I_1^2 - I_2^2)$$

$$a_6 = \frac{I_3}{2(I_1 - I_2)}$$

$$a_7 = \frac{I_4}{[I_5(I_1 + I_2) + I_4(I_3 - 2I_4)]}$$

$$a_8 = \frac{(I_1 + I_2)}{[I_5(I_1 + I_2) + I_4(I_3 - 2I_4)]}$$

The other in-plane variables can be expressed in terms of λ_3, Z_x, and Z_y as

$$\lambda_1 = -I_3 Z_x - \frac{\partial}{\partial x}(\lambda_3)$$

$$\lambda_2 = -I_3 Z_y - \frac{\partial}{\partial y}(\lambda_3)$$

$$T_{xy} = \frac{1}{(I_1 - I_2)} \frac{\partial^2 \lambda_3}{\partial x \partial y} + \frac{I_3}{2(I_1 - I_2)} \left(\frac{\partial Z_x}{\partial y} + \frac{\partial Z_y}{\partial x}\right)$$

$$S_x = \frac{1}{(I_1^2 - I_2^2)} \left\{ I_1 \frac{\partial^2 \lambda_3}{\partial x^2} - I_2 \frac{\partial^2 \lambda_3}{\partial y^2} + [I_1 I_3 - I_4(I_1 - I_2)] \frac{\partial Z_x}{\partial x} \right.$$
$$\left. - [I_2 I_3 + I_4(I_1 - I_2)] \frac{\partial Z_y}{\partial y} \right\}$$

$$S_y = \frac{1}{(I_1^2 - I_2^2)} \left\{ I_1 \frac{\partial^2 \lambda_3}{\partial y^2} - I_2 \frac{\partial^2 \lambda_3}{\partial x^2} + [I_1 I_3 - I_4(I_1 - I_2)] \frac{\partial Z_y}{\partial y} \right.$$
$$\left. - [I_2 I_3 + I_4(I_1 - I_2)] \frac{\partial Z_x}{\partial x} \right\} \qquad (3.2.15)$$

3.3 APPLICATION OF THE APPROXIMATE THEORY TO A LAMINAR PLATE CONTAINING A THROUGH CRACK

For this analysis, the crack length is taken as small in comparison with the in-plane dimensions of the plate. The stress field in the vicinity of the crack is thus independent of local boundary effects and the plate can be modeled as infinite in the two, in-plane directions. This assumption simplifies the analysis significantly while maintaining the essential characteristics of the crack laminar plate problem.

In particular, the problem of a laminar plate (symmetric about its mid-plane) containing a crack in a uniaxial far-field, stress state will be considered (Figure 3.3.1). The crack is directed normal to the loading direction, thus modeling the most damaging type of flaw. This problem can be expressed as the superposition of two auxiliary problems. The first auxiliary problem is that of an uncracked plate subjected to the same loading conditions as the actual cracked plate. For the second auxiliary problem, the cracked plate configuration is considered with no boundary loads. Instead, the crack faces are loaded with tractions of equal magnitude but opposite sense to those found at the crack location in the first problem. Thus the superposition of the two problems yields the cracked plate with traction free crack faces and remote loading as originally described.

The first of the auxiliary problems, an uncracked plate in a far, uniform stress field, has nonsingular stress compo-

nents and as such does not contribute to the crack-tip singularity. Therefore, the stress field in the vicinity of the crack tips for the case of crack face loading is identical to that for the remote loading situation of the actual cracked plate. It is mathematically advantageous to consider the crack face loading problem because it leads to stress fields which die-out far from the crack and can thus be treated by transform techniques.

The problem of a composite plate, made up of isotropic layers distributed symmetrically about its mid-plane, containing a through crack will be analyzed for the case of symmetric crack face loading. The loading is required to be symmetric about the plate mid-plane as well as the x = 0 line to eliminate any bending effects. The crack is directed along the x-axis, Figure (3.3.1). In general, the loading on the crack face will include normal pressure and transverse shearing tractions. The symmetry conditions require that these shearing tractions be zero on the intersection of the mid-plane of the plate with the crack faces. They also have to die-out at the top and bottom plate surfaces. Thus, except in the case of very thick plates their effect will be small in comparison with the pressure loading and the crack face shearing tractions will be omitted from this analysis.

Consider the region x,y,z > 0. The boundary and symmetric conditions from three-dimensional elasticity are:

on y = 0

$$\tau_{xy} = \tau_{yz} = 0$$

$$\sigma_y = p(x,z), \quad 0 \leq x \leq a$$ (3.3.1)

$$u_y = 0 \quad , \quad x > a$$

on x = 0

$$\tau_{xy} = \tau_{xz} = 0$$

$$u_x = 0$$

and on z = 0

$$\tau_{xz} = \tau_{yz} = 0$$

$$u_z = 0$$

The equivalent boundary conditions for the approximate theory
are:

on y = 0

$$T_{xy} = Z_y = 0$$

$$S_y = P(x), \quad 0 \leq x \leq a$$ (3.3.2)

$$\lambda_2 = 0 \quad , \quad x > a$$

on x = 0

$$T_{xy} = Z_x = 0$$

$$\lambda_1 = 0$$

and $f(z)$ is required to be symmetric in z to model the sym-
metry conditions on the $z = 0$ plane. Further $f(z)$ and $f'(z)$
are zero on the plate surface $z = \pm h/2$.

The governing equations (3.2.14) are to be solved subject
to the boundary conditions (3.3.2). Further, the functions
S_x, S_y, T_{xy}, Z_x, Z_y, and Z_z must die-out at large distances
from the crack.

3.3.1 SOLUTION PROCEDURE FOR THE IN-PLANE VARIATIONS OF THE STRESS FIELD

As indicated earlier, the solution procedure will
be based on applying the Fourier transform to the x variable
to determine the nine in-plane variables S_x, S_y,... It is
convenient to recognize the symmetry properties of these vari-
ables in advance, thus reducing the Fourier transform to sine
and cosine transforms for the odd and even functions, respec-
tively. It is observed that the functions S_x, S_y, Z_y, Z_z,
λ_2, and λ_3 are even in x while T_{xy}, Z_x, and λ_1 are odd in x.
Therefore define

$$S_x^c(s,y) = \int_0^\infty S_x(x,y)\cos(sx)dx, \text{ etc.}$$

and

$$T_{xy}^s(s,y) = \int_0^\infty T_{xy}(x,y)\sin(sx)dx, \text{ etc.}$$

Application of Fourier sine and cosine transforms
to the governing set of equations (3.2.4) leads to the follow-

ing set of equations:

$$a_3 \frac{d^4\lambda_3^c}{dy^4} + (a_4 - 2a_3 s^2) \frac{d^2\lambda_3^c}{dy^2} + (a_3 s^4 - a_4 s^2 + a_5)\lambda_3^c = 0$$

$$\frac{d^2 Z_x^s}{dy^2} - (s^2 + \frac{1}{a_6})Z_x^s = s[\frac{a_1}{a_6} \frac{d^2\lambda_3^c}{dy^2} + (\frac{a_2}{a_6} - \frac{a_1}{a_6} s^2)\lambda_3^c]$$

$$\frac{d^2 Z_y^c}{dy^2} - (s^2 + \frac{1}{a_6})Z_y^c = - \frac{a_1}{a_6} \frac{d^3\lambda_3^c}{dy^3} - (\frac{a_2}{a_6} - \frac{a_1}{a_6} s^2) \frac{d\lambda_3^c}{dy}$$

$$(3.3.1.1)$$

provided that

$$s Z_x^s + \frac{dZ_y^c}{dy} = - a_7 \frac{d^2\lambda_3^c}{dy^2} + (a_7 s^2 - a_8)\lambda_3^c$$

The general solution to equations (3.3.3.1) which satisfies the asymptotic conditions at infinity can be written in the form

$$\lambda_3^c(s,y) = 2Re[A_1(s)e^{-ry}]$$

$$Z_x^s(s,y) = \frac{q}{s} B(s)e^{-qy} + Re[P_1(s)e^{-ry}] \qquad (3.3.1.2)$$

$$Z_y^c(s,y) = B(s)e^{-qy} + Re[P_2(s)e^{-ry}]$$

where

$$r = \pm [s^2 - \frac{a_4}{2a_3} \pm i \sqrt{\frac{a_5}{a_3} - (\frac{a_4}{2a_3})^2}]^{1/2}$$

-56-

$$q = \sqrt{s^2 + \frac{1}{a_6}}$$

and

$$P_1(s) = -2s \frac{[a_2 - a_1(s^2 - r^2)]}{[1 + a_6(s^2 - r^2)]} A_1(s)$$

$$P_2(s) = -2r \frac{[a_2 - a_1(s^2 - r^2)]}{[1 + a_6(s^2 - r^2)]} A_1(s)$$

The additional transformed functions of the in-plane variables can be expressed in terms of λ_3^c, Z_x^s, and Z_y^c through equations (3.2.15). In particular, the functions T_{xy}^s, S_y^c, and λ_2^c are obtained to study the boundary conditions:

$$T_{xy}^s(s,y) = \frac{1}{(I_1 - I_2)} \left[-s \frac{d\lambda_3^c}{dy} + \frac{I_3}{2} \left(\frac{d}{dy} Z_x^s - s Z_y^c \right) \right]$$

$$S_y^c(s,y) = \frac{1}{(I_1^2 - I_2^2)} \left\{ I_1 \frac{d^2 \lambda_3^c}{dy^2} + s^2 I_2 \lambda_3^c \right.$$

$$+ [I_1 I_3 - I_4(I_1 - I_2)] \frac{dZ_y^c}{dy} \qquad (3.3.1.3)$$

$$\left. - [I_2 I_3 + I_4(I_1 - I_2)] s Z_x^s \right\}$$

$$\lambda_2^c(s,y) = -I_3 Z_y^c - \frac{d\lambda_3^c}{dy}$$

The general solution is now substituted into the boundary conditions (transformed appropriately). The condition $Z_y^c(s,o) = 0$ yields

$$B(s) = \text{Re} \left\{ 2r \left[\frac{a_2 - a_1(s^2 - r^2)}{1 + a_6(s^2 - r^2)} \right] A_1(s) \right\} \qquad (3.3.1.4)$$

-57-

while the condition $T^S_{xy}(s,o) = 0$ relates the real and imaginary parts of $A_1(s)$ as

$$Re\{2[1 + \frac{I_3}{2}(1 - \frac{q^2}{s^2})(\frac{a_2-a_1(s^2-r^2)}{1+a_6(s^2-r^2)})]rA_1(s)\} = 0$$

It is convenient to express this result symbolically as $Im[A_1(s)] = \beta_1(s)Re[A_1(s)]$ where

$$\beta_1(s) = -\{r_R[s^2 - \frac{I_3}{2a_6}(\frac{(a_2-k_1a_1)(1+a_6k_1)-a_1a_6k_3^2}{(1+a_6k_1)^2+(a_6k_3)^2})$$

$$+ r_i\frac{I_3}{2a_6}k_3[\frac{a_1+a_2a_6}{(1+a_6k_1)^2+(a_6k_3)^2}]\} \div$$

$$\div \{r_R\frac{I_3}{2a_6}k_3[\frac{a_1+a_2a_6}{(1+a_6k_1)^2+(a_6k_3)^2}]$$

$$- r_i[s^2 - \frac{I_3}{2a_6}(\frac{(a_2-k_1a_1)(1+a_6k_1)-a_1a_6k_3^2}{(1+a_6k_1)^2+(a_6k_3)^2})]\}$$

$$(3.3.1.5)$$

and

$$k_1 = \frac{a_4}{2a_3}$$

$$- ik_3 = \sqrt{\overline{(\frac{a_4}{2a_3})^2 - \frac{a_5}{a_3}}}$$

The set of mixed boundary conditions

$$S_y(x,o) = - p(x), \quad x<a$$

$$\lambda_2(x,o) = 0 \qquad , \quad x\geq a$$

remain to be satisfied. These conditions can be expressed in terms of the transformed functions as

$$\frac{2}{\pi} \int_0^\infty S_y^c(s,o)\cos(sx)ds = -p(x), \quad x<a$$

(3.3.1.6)

$$\frac{2}{\pi} \int_0^\infty \lambda_2^c(s,o)\cos(sx)ds = 0, \quad x\geq a$$

The functions $S_y^c(s,o)$ and $\lambda_2^c(s,o)$ can be expressed in terms of the one unknown function $\text{Re}[A_1(s)]$ as

$$\lambda_2^c(s,o) = f_1(s)\text{Re}[A_1(s)]$$

(3.3.1.7)

$$S_y^c(s,o) = f_2(s)\text{Re}[A_1(s)]$$

where

$$f_1(s) = \text{Re}[r(1 + i\beta)]$$

$$f_2(s) = \frac{2}{(I_1^2-I_2^2)}\text{Re}\{(1+i\beta)[I_1 r^2 + I_2 s^2 + (-qr(I_1+I_2)I_3$$

$$+ (r^2 I_1 + s^2 I_2)I_3 + (s^2-r^2)(I_1-I_2)I_4] \times$$

$$\times [\frac{a_2-a_1(s^2-r^2)}{1+a_6(s^2-r^2)}]\}$$

(3.3.1.8)

Thus the mixed boundary conditions can be expressed in the form of a set of dual integral equations as

-59-

$$\int_0^\infty g(s)R(s)\cos(sx)ds = -\frac{\pi}{2}p(x), \quad x<a$$

$$(3.3.1.9)$$

$$\int_0^\infty R(s)\cos(sx)ds = 0, \quad x \geq a$$

where

$$R(s) = f_1(s)Re[A_1(s)]$$

and

$$g(s) = \frac{f_2(s)}{f_1(s)}$$

This set of dual integral equations can be reduced to a single integral equation by the introduction of an auxiliary function, w(x), defined as

$$w(x) = \begin{cases} \frac{2}{\pi} \int_0^\infty R(s)\cos(sx)ds, & x<a \\ \\ 0 & , \quad x \geq a \end{cases}$$

$$(3.3.1.10)$$

Then $R(s) = \int_0^\infty w(x)\cos(sx)dx$ and the set of equations is satisfied for all functions w(x) which satisfy

$$\int_0^\infty \{g(s) \int_0^a w(x)\cos(sx)dx\}\cos(sx)ds = -\frac{\pi}{2}p(x) \quad (3.3.1.11)$$

This equation (3.3.1.11) contains the crack tip singularity and corresponding care must be taken in the solu-

tion procedure. Exact three-dimensional solutions for symmetric crack problems [19], indicate that on all interior points in the immediate vicinity of the leading crack edge the local stress and displacement fields must be of the form:

$$\sigma_x = \frac{k_1(z)}{\sqrt{2\rho}} \left[\cos\left(\frac{\theta}{2}\right) + \frac{1}{2}\sin(\theta)\sin\left(\frac{3}{2}\theta\right)\right]$$

$$\sigma_y = \frac{k_1(z)}{\sqrt{2\rho}} \left[\cos\left(\frac{\theta}{2}\right) - \frac{1}{2}\sin(\theta)\sin\left(\frac{3}{2}\theta\right)\right]$$

$$\sigma_z = \nu(\sigma_x + \sigma_y) \tag{3.3.1.12}$$

$$\tau_{xy} = \frac{k}{\sqrt{2\rho}} \left[\frac{1}{2}\sin(\theta)\cos\left(\frac{3}{2}\theta\right)\right]$$

$$\tau_{xz}, \tau_{yz} = 0(1) \text{ as } \rho \to 0$$

where (ρ, θ) are local polar coordinates in the plane normal to the crack edge, Figure (3.3.1).

The auxiliary function $w(x)$ corresponds to $\lambda_2(x,o)$ and, as such, is expected to be locally proportional to the square root of the distance from the crack tip. This information is used to introduce a second auxiliary function, $\psi(t)$, in an attempt to remove the inherent singularity from equation (3.3.1.11). Define $\psi(t)$ by the integral equation

$$w(x) = \int_x^a \frac{\psi(t)t}{\sqrt{t^2 - x^2}} \, dt, \quad x < a \tag{3.3.1.13}$$

Substitution into equation (3.3.1.11) yields, after some simplifications,

$$\int_0^a t\psi(t) \left[\int_0^\infty \frac{g(s)}{s} J_0(st)\sin(sx)ds\right]dt = - \int_0^x p(x)dx, \quad x<a$$

(3.3.1.14)

where J_0 is the zero order Bessel function of the first kind. If the expectations mentioned above are correct, equation (3.3.1.14) will be a nonsingular integral equation for $\psi(t)$ which is amenable to numerical solution procedures[*]. The function $g(s)$ can be written in the form

$$\frac{g(s)}{s} = C + g*(s)$$

(3.3.1.15)

and C is given in the Appendix where $g*(s) = O(s^{-2})$ as $s\to\infty$. Substitution into equation (3.3.1.14) and use of the known solution to Abel's equation leads to the Fredholm integral equation (see reference [20] for details)

$$C\sqrt{t}\psi(t) + \int_0^a \sqrt{\eta}\psi(\eta) \sqrt{t\eta} \int_0^\infty sg*(s)J_0(s\eta)J_0(st)dsd\eta$$

$$= - \frac{2}{\pi} \sqrt{t} \frac{p(x)}{\sqrt{t^2-x^2}} dx$$

(3.3.1.16)

---

[*] A posteriori checks of the numerical results do indeed indicate that $\psi(t)$ is a well behaved function.

-62-

This equation can be reduced to standard form by the following nondimensionalizations

$$\eta = a\xi, \quad t = a\tau, \quad x = a\beta, \quad s = \frac{\theta}{a}$$

and

$$\Phi(\tau) = \sqrt{\tau}\psi(a\tau)$$

Then equation (3.3.1.16) can be written as

$$C\Phi(\tau) + \int_0^1 \Phi(\xi)K(\xi,\tau)d\xi$$

$$= -\frac{2}{\pi}\sqrt{\tau}\int_0^\tau \frac{p(x)}{\sqrt{\tau^2-\beta^2}}d\beta \qquad (3.3.1.17)$$

where

$$K(\xi,\tau) = \sqrt{\xi\tau}\int_0^\infty \theta g^*\left(\frac{\theta}{a}\right)J_0(\theta\xi)J_0(\theta\tau)d\theta$$

The accuracy of the numerical solution procedure to be employed is improved by separating $g^*(s)$ as

$$g^*(s) = \frac{H}{s^2+N^2} + h(s) \qquad (3.3.1.18)$$

where $h(s) = O(s^{-6})$ as $s \to \infty$. The constants H and N^2 are given in the Appendix. The kernel $K(\xi,\tau)$ can be rewritten as

$$K(\xi,\tau) = \sqrt{\xi\tau} \; \{a^2 H I_0(\xi aN) K_0(\tau aN)$$

$$+ \int_0^\infty \theta h(\frac{\theta}{a}) J_0(\theta\xi) J_0(\theta\tau) d\theta\}, \quad 0<\xi\leq\tau$$

where I_0 and K_0 are the zero-order modified Bessel functions of the first and second kind, respectively.

The case of crack face loading which does not vary with x is considered, i.e., $p(x) = p$. The kernel is now evaluated numerically and the integral equation is approximated by a set of algebraic equations via Simpson's rule. Numerical solutions for $\Phi(\tau)$ are thereby obtained.

The original unknown function, R(s), is obtained by substitution into equations (3.3.1.13) and (3.3.1.10). Carrying out the indicated integrations, R(s) can be written as

$$R(s) = \frac{\pi}{2} \frac{a}{s} p\{\Psi(1) J_1(as)$$

$$- \int_0^1 \frac{d}{d\xi} [\frac{\Psi(\xi)}{\sqrt{\xi}}] J_1(as\xi)\xi d\xi\} \qquad (3.3.1.19)$$

The unknown transformed functions S_x^c, S_y^c, etc., can be determined directly from R(s) by back substitution.

It is expected that damage resulting from either crack propagation or interfacial delamination will originate in the most highly stressed region, the vicinity of the crack

tip. Thus our main objective is to obtain the best approximate solution for the near tip crack field. Referring to equation (3.3.1.19) it can be shown that the singularity at the crack tip is associated with $\Phi(1)$ and that integral expression in this equation has no contribution to it. Because an asymptotic description of the crack tip field is sought, the integral expression in equation (3.3.1.19) is dropped and the functions S_x^c, S_y^c, etc., are expressed in terms of the simplified equation for $R(s)$. These transformed functions are inverted asymptotically for large s. Adopting polar coordinates r, r_1, r_2, and θ, θ_1, θ_2 as shown in Figure (3.3.1), it is found that

$$S_x(x,y)^* = -\frac{a}{\sqrt{r_1 r_2}}\, P\Psi(1)C\{\frac{ay}{r_1 r_2}\, \sin[\tfrac{3}{2}(\theta_1+\theta_2)]$$

$$-\frac{r_o}{a}\, \cos[\theta_o - \tfrac{1}{2}(\theta_1+\theta_2)]\} + O(1)$$

$$S_y(x,y) = +\frac{a}{\sqrt{r_1 r_2}}\, P\Psi(1)C\{\frac{ay}{r_1 r_2}\, \sin[\tfrac{3}{2}(\theta_1+\theta_2)]$$

$$+\frac{r_o}{a}\, \cos[\theta_o - \tfrac{1}{2}(\theta_1+\theta_2)]\} + O(1)$$

$$T_{xy}(x,y) = -\frac{a}{\sqrt{r_1 r_2}}\, P\Psi(1)C\{\frac{ay}{r_1 r_2}\, \cos[\tfrac{3}{2}(\theta_1+\theta_2)]\} + O(1)$$

---

* e_1, b_1, b_2, C, m_2 are given in the Appendix A.

$$Z_z(x,y) = -\frac{a}{\sqrt{r_1 r_2}} P\Psi(1) \left[\frac{e_1(k_1 b_2 + k_3 b_1)}{m_2}\right] \times$$

$$\times \left\{\frac{r_o}{a} \cos\left[\theta_o - \frac{1}{2}(\theta_1 + \theta_2)\right]\right\} + O(1)$$

$$Z_x(x,y) = aP\Psi(1) \frac{1}{m_2} \left\{\left[\frac{e_1}{2}(b_1 k_3 + b_2 k_1 - \frac{b_2}{a_6})\right] \times\right.$$

$$\times \int_0^\infty \frac{1}{s} J_1(as)\sin(sx)e^{-sy}ds$$

$$\left. + \frac{e_1}{2}(b_1 k_3 + b_2 k_1 + \frac{b_2}{a_6}) \int_0^\infty y J_1(as)\sin(sx)e^{-sy}ds\right\}$$

$$Z_y(x,y) = aP\Psi(1) \frac{e_1}{2m_2} (b_1 k_3 + b_2 k_1 + \frac{b_2}{a_6}) \times$$

$$\times \int_0^\infty y J_1(as)\cos(sx)e^{-sy}ds \qquad (3.3.1.20)$$

Note that $Z_x(x,y)$ and $Z_y(x,y)$ are nonsingular. Further, approaching the crack tip (a,o), i.e., taking the limit $r \to a$, $\theta \to 0$, $r_2 \to 2a$, $\theta_2 \to 0$, the near tip fields can be written as

$$\sigma_x = \frac{K\sigma_p(z)\sqrt{a}}{\sqrt{2r_1}} \left[\cos(\frac{\theta_1}{2}) - \frac{1}{2}\sin(\theta_1)\sin(\frac{3\theta_1}{2})\right] + O(1)$$

$$\sigma_y = \frac{K\sigma_p(z)\sqrt{a}}{\sqrt{2r_1}} \left[\cos(\frac{\theta_1}{2}) + \frac{1}{2}\sin(\theta_1)\sin(\frac{3\theta_1}{2})\right] + O(1)$$

$$\tau_{xy} = \frac{K\sigma_p(z)\sqrt{a}}{\sqrt{2r_1}} \left[\frac{1}{2}\sin(\theta_1)\cos(\frac{3\theta_1}{2})\right] + O(1)$$

$$\sigma_z = \frac{K\sigma_T(z)\sqrt{a}}{\sqrt{2r_1}} \left[\cos(\frac{\theta_1}{2})\right] + O(1)$$

$$\tau_{xz} = \tau_{yz} = 0(1) \tag{3.3.1.21}$$

where

$$K = a\Psi(1)e_1C$$

$$\sigma_p(z) = Pf''(z)$$

and

$$\sigma_T(z) = P(b_1k_3+b_2k_1)\frac{1}{C}f(z)$$

Note that the stress field in the vicinity of the crack tip, as given above, contains the usual square root singularity in the plane normal to the crack front. The dependence of the stress components on the in-plane variable (r_1,θ_1) obtained here is in complete agreement with the exact three-dimensional solution for a crack in an elastic medium [19]. Note, the results of this approximate solution indicate that the transverse shearing stress components do not exhibit an in-plane singularity, a possibility considered by other authors [17]. The dependence of the near tip stress field on the through-the-thickness coordinate, z, will be discussed in the following section.

3.3.2 THROUGH-THE-THICKNESS VARIATION OF THE NEAR-TIP STRESS FIELD

Two possible approaches may be proposed for the determination of $f_i(z)$. The variational principle, Section 3.2, yields equations and matching conditions for the functions $f_i(z)$ which govern the stress distribution in the thickness direction of the ith layer. Functions obtained from these equations give the "best" choice for $f_i(z)$ consistent with the initial approximations, i.e., the function of z which on the average over the entire plate is closest to describing the true stress field. The possibility of using this approach was considered but an alternative direction was chosen instead. Exact asymptotic analysis [19] described earlier indicates that at all interior points near the leading edge of the crack, the plate is in a state of plane strain, i.e.,

$$\sigma_z = \nu(\sigma_x + \sigma_y) \qquad (3.3.2.1)$$

Within each layer, the plane strain condition can be employed to obtain $f_i(z)$ in the vicinity of the crack tip. Supposition of the requirement that the approximate solution should satisfy equation (3.3.2.1) leads to the following differential equations for $f_i(z)$:

$$f_i''(z) + p_i^2 f_i(z) = 0 \qquad (3.3.2.2)$$

where p_i^2 is equal to the asymptotic value of the function

$- Z_z/\nu_i(S_x + S_y)$ at the crack tip, i.e.,

$$p_i^2 = \frac{1}{\nu_i} \left[\frac{e_1}{2m_6} (b_1 k_3 + b_2 k_1) \right]$$

It can be shown in general that the solutions to equation (3.3.2.2) do not possess sufficient free parameters to satisfy both of the free surface conditions ($f = f' = 0$).

Hartranft and Sih [1] have used the condition in equation (3.3.2.1) to derive the z-distribution of the stresses through a single layer plate with a crack. Their results in terms of the function $f(z)$ is Acos(pz); where p is the free parameter in the theory and A is arbitrary. Such an approximate analytical solution, however, cannot be expected to hold throughout the thickness of the plate. This is mainly because experimental observation has shown that there exists a layer of material near the plate surface which behaves very differently from that in the bulk. Specifically, the fracture testing of through cracks in finite thickness plates has evidenced two surface layers of the material commonly referred to as the "shear lips" that undergo a considerable amount of plastic deformation. However, the interior portion of the fractured plate remains essentially brittle. This is analogous to the flow of fluids in a pipe where the viscous action dominates in a layer of fluid close to the pipe wall while the flow characteristics in the bulk can be adequately described by using the potential flow theory.

In order to impose a limitation on the analytical result in [1], Hartranft and Sih introduced two narrow slices of finite thickness (boundary layers[*]) $\varepsilon h/2$ close to the plate surface, where the variation ε was chosen as $\varepsilon = 1/(2+8h/a)$. The same approach will be carried out here for laminated plates. The non-dimensional boundary layer of thickness ε (to be chosen later) is introduced in the outer most layers of the composite plate. In this thin strip the function $f(z)$ is chosen such that it satisfies the traction-free condition on the exterior surface and equilibrium in the interior region. The three layer symmetric composite, Figure (3.3.1), is chosen as the simplest nontrivial example. The numeral 1 is used to refer to the interior layer while the outside layers are denoted by 2. The solutions to equation (3.3.2.2) which satisfy continuity of f_1 and f_1' across the material interfaces are:

$$f_1(z) = A\cos(p_1 z), \quad 0 \leq z \leq h_1$$

$$f_2(z) = A\{\cos(p_1 h_1)\cos[p_2(z-h_1)] \quad\quad (3.3.2.3)$$

$$- \frac{p_1}{p_2} \sin(p_1 h_1)\sin[p_2(z-h_1)]\}, \quad h_1 \leq z \leq h_1 + h_2$$

where

---

[*] There exists a small but finite distance to the boundary within which the resolution of experimental measurements and accuracy of any numerical solution breaks down.

$$p_1^2 = \frac{1}{\nu_1} \left[\frac{e_1}{2m_6} (b_1 k_3 + b_2 k_1) \right]$$

(3.3.2.4)

$$p_2^2 = \frac{\nu_1}{\nu_2} p_1^2$$

See Appendix A for b_1, b_2, e_1, m_6, k_1 and k_3.

The functions $f_i(z)$ given by equation (3.3.2.3) which satisfy the plane strain conditions are not general enough to allow imposition of the free surface conditions at $z = h_1 + h_2$. It is reasonable to introduce a boundary layer adjacent to the free surface within which an arbitrary function $f_2(z)$ is constructed such that the traction-free conditions $f_2(h_1+h_2) = f_2'(h_1+h_2) = 0$ are satisfied along with the requirements that $f_2(z)$ and its first and second derivatives must be continuous at $z = h_1 + h_2(1-\varepsilon)$. This arbitrary function can be represented by the following fourth order polynomial

$$f_2(z) = \alpha_1(z-h_1-h_2)^4 + \alpha_2(z-h_1-h_2)^3 + \alpha_3(z-h_1-h_2)^2$$

$$+ \alpha_4(z-h_1-h_2) + \alpha_5,$$ (3.3.2.5)

$$h_1 + h_2(1-\varepsilon) \le z \le h_1+h_2$$

The five coefficients (α_i, $i = 1,2,..,5$) are determined from the conditions mentioned before.

At this point the functions $f_i(z)$ ($i = 1,2$) can be expressed solely in terms of the parameter p_1, which de-

pends on the behavior of the functions S_x, S_y, and $Z_y(x,y)$. The dependency of $f_i(z)$ on p_1 is found by using an iterative procedure, which consists of selecting an initial value of p_1 that specifies a given set of the coefficients of asymptotic behavior of S_x, S_y and $Z_z(x,y)$. This leads to a new value of p_1 obtained from equation (3.3.2.1) and the procedure is repeated until it converges to any one of a set of discrete values for p_1 which satisfy equation (3.3.2.2). This iterative procedure should be modified such that the solution for p_1 converges to that value which best approximates the actual load applied on the crack surface.

The crack tip stress field as given by equations (3.3.1.21) is now completely determined and there remains simply the numerical calculation of the stress intensity factor, $k_1(z)$ which can be expressed in the form

$$k_1(z) = K\sigma_p(z)\sqrt{a}$$

The newly defined function

$$\sigma_p(z) = Pf_i''(z), \quad (i = 1,2)$$

represents the equivalent load distribution on the crack faces which is compatible with the variational theory. To recapitulate, the in-plane stress components are proportional to $f_i''(z)$, and the transverse normal stress σ_z is equal to

-72-

$\nu_i(\sigma_x+\sigma_y)$ except in the boundary layer, while the transverse shear stresses τ_{xz} and τ_{yz} are non-singular. Thus, the singular stress field in the vicinity of the crack tip can be characterized by the non-dimensional stress intensity parameter K and the eigenvalues p_1 and p_2 which govern the functions $f_i(z)$.

It should be pointed out that the behavior of the laminate may be qualitatively different in the vicinity of the material interfaces than that within each layer. Such an effect may have significant influence on the load transfer from one layer to the next. This line of reasoning suggests the possibility of introducing additional boundary layers or transition regions at the material interfaces. However, the introduction of such boundary layers is not required by this formulation, because the functions $f_i(z)$ given in equation (3.3.2.3) do satisfy the traction continuity conditions at the interfaces.

In order to carry out the numerical analysis it is necessary to assume a value for ε, the non-dimensional boundary layer thickness. For laminates the boundary layer thickness will in general depend on the elastic constants E_1/E_2, ν_1, ν_2 and geometric parameters h_2/h_1 and $(h_1+h_2)/a$, but sufficient data for modeling the functional dependence is not yet available. Hence as a first attempt in modeling laminates the present formulation includes boundary layers at the exterior surfaces but no interfacial transition layers. This

non-dimensional boundary layer thickness was assumed to be of the form

$$\varepsilon = \frac{1}{2+16(\frac{h_1+h_2}{a})} \left(\frac{h_2}{h_1}\right) \qquad (3.3.2.6)$$

The consequence of this choice will be discussed in the following section.

3.3.3 NUMERICAL RESULTS AND DISCUSSION

Numerical results are obtained for the dependence of the crack-tip stress field on the geometric and material parameters (h_2/h_1, h_1/a, E_1/E_2, ν_1 and ν_2) of the layered plate containing a through crack for two formulations. The first does not and the second include the boundary layers discussed in Section 3.3.2. The amplitude of the singular stress field, equation (3.3.1.21), is presented in the non-dimensional form

$$K = k_1(z)/(\sigma_p(z)\sqrt{a})$$

where $\sigma_p(z) = Pf_1''(z)$ is the crack face load distribution. The results for K as a function of the composite plate parameters are presented graphically.

Results for the formulation without any boundary layers are presented first in Figures 3.3.3.1 - 3.3.3.4. In this case no attempt has been made to satisfy the boundary

conditions on the plate surfaces $z = \pm(h_1 + h_2)$. As a consequence, the parameter p_1 which governs the z dependence of the stress field given by equation (3.3.2.3) can be chosen arbitrarily. Note, however, that for $p_1(h_1 + h_2)$ greater than $\pi/2$, the crack face load distribution changes from compression to tension at $z = \frac{\pi}{2p_1}$ for $\nu_1 = \nu_2$ and no longer adequately models the physical problem under consideration. For this reason, the results are confined to the range $0 < p_1 < \pi/2$.

Referring to Figures 3.3.3.1 - 3.3.3.4, and defining the symbol $P_1 = p_1 h_1$, note that the stress intensification parameter K is strongly influenced by the value of p_1 chosen, i.e., as p_1 is decreased, K increases for finite h_1/a. In the limit h_1/a becomes large, K approaches unity for all values of p_1. The reason for the p_1 dependence is clear when one recalls the z dependence of the near tip field, equation (3.3.2.3). As p_1 decreases the rate of change of this field with respect to z is correspondingly decreased. In fact, as p_1 approaches zero, the crack tip stress field becomes independent of z and reduces to the two-dimensional plane strain solution for which K equals 1.0.

The dependence of K on the relative layer thickness h_2/h_1 is also seen in these graphs. As h_2/h_1 increases, the stress intensification parameter, K, correspondingly increases for finite h_1/a approaching 1.0 for large h_2/h_1. This result is directly associated with the increase in plate

thickness and the approach of the plane strain condition at large h_2/h_1. The dependence of K on h_2/h_1 is more pronounced at low values of p_1.

Figures 3.3.3.1 - 3.3.3.4 show that the dependence of K on the relative layer stiffness E_1/E_2 is rather weak. Results for the formulation which includes boundary layers and satisfies the mathematical boundary conditions are to be presented next. They exhibit a stronger K dependence on E_1/E_2.

Boundary layers at the free surfaces are included in the refined formulation in order to (a) satisfy the mathematical boundary conditions and (b) model the physically observed surface phenomena referred to as the shear lips zone as discussed in Section 3.3.2. In this formulation the parameter p_1 is no longer arbitrary. Numerical results for $\nu_1 = \nu_2$ (for which $p_2 = p_1$) suggest that $p_1(h_1+h_2)$ is almost constant and approximately equal to $\pi/2$. Deviations are attributed to the specific form of the boundary layer solution. Thus, except near the free surfaces

$$f(z) \approx \cos(\frac{\pi}{2} \frac{z}{h_1+h_2})$$

This implies that near the crack tip the normal stress components σ_x, σ_y, and σ_z attain a maximum at the center plane of the composite plate and approach zero near the top and bottom surfaces of the plate.

-76-

Numerical results are obtained for the dependence of the stress intensification factor K on the geometric and material properties of the laminate associated with the refined formulation which includes boundary layers. Results are presented graphically in the form of plots for K as a function of h_1/a at various values of E_1/E_2, h_2/h_1 with $\nu_1 = \nu_2 = .3$ in Figures 3.3.3.5 - 3.3.3.14.

Attention is directed to the influence of the relative stiffness of the inside layer to the outer layers (E_1/E_2) on the amplitude of the stress field in the vicinity of the crack tip. Figures 3.3.3.5 - 3.3.3.9 indicate that K decreases as E_1/E_2 increases if the other parameters are held constant. As E_1/E_2 increases the load is carried increasingly by the middle layer. In the limit as E_2 goes to zero, the actual plate half thickness is reduced from h_1+h_2 to h_1 and the stress intensity factor is expected to decrease accordingly[*]. The influence of h_2/h_1 on this effect can be seen by comparing Figures 3.3.3.5 - 3.3.3.9. As h_2/h_1 increases, the effect of changes of E_1/E_2 on K becomes less pronounced. To understand these interactions, recall that at finite E_1/E_2

---

[*] In the present model, it is not possible to account completely for this effect. The load distribution permitted in this formulation for finite but small E_2 is qualitatively different than that for $E_2 = 0$, i.e., for E_2 finite, $p_1 \approx \frac{\pi}{2} (\frac{1}{h_1+h_2})$ while at $E_2 = 0$, $p_1 \approx \frac{\pi}{2} \frac{1}{h_1}$.

increasing h_2/h_1 causes the outer layers to carry a larger portion of the applied load and for very large h_2/h_1 the laminate behavior should be almost independent of the material properties of the inside layer.

Figures 3.3.3.10 - 3.3.3.13 explicitly demonstrate the influence of the parameter h_2/h_1 on K. If h_1/a is held constant increasing h_2/h_1 increases the total plate thickness and K is observed to increase accordingly.

Figure 3.3.3.14 is a plot of K against h_1/a for the special condition in which the total plate thickness to crack length is held constant ($\frac{h_1+h_2}{a} = 3.0$). Note that for finite h_2/h_1, K decreases as E_1/E_2 increases. In this case, load is transferred to the middle layer and the "apparent" plate thickness is decreased. Calculations were also carried out for the special case $E_1/E_2 = 1.0$. For $E_1/E_2 = 1.0$, the stress intensification parameter K is not expected to vary with h_1/h_2 as long as the total plate thickness to crack length ratio is held constant. The slight variation observed is associated with the boundary layer thickness dependence on h_1/h_2 (equation (3.3.2.6)) which is inappropriate for this special case.

In summary, the approximate three-dimensional stress analysis presented here for a laminate containing a through crack indicates that the amplitude of the near tip stress field tends to increase with plate thickness. The

stress intensification parameter K was found to decrease as the relative stiffness of interior layer to outer layers (E_1/E_2) is increased. Poisson's ratio influences are to be studied in subsequent work.

3.3.4 LIMITATIONS OF PRESENT THEORY AND FUTURE WORK

The present formulation includes boundary layers at the top and bottom surfaces of the composite plate; however, it does not allow for a transition layer at the material interfaces. Such an interfacial boundary layer is not required by this variational formulation as all equilibrium and traction conditions can be satisfied without the introduction of interfacial layers. However, the effect of not including these transition layers in this approximate formulation is that the crack face load distribution is fixed in the z direction independent of the material properties of the layers. The physics of the problem suggests that the major portion of the load per unit thickness should be transmitted in the stiffer layers. Interfacial transition layers are needed in the approximate theory to take into account this type of load distribution - layer property interaction. Extensions of the present model to include these layers are currently under study. A stronger dependence of the stress distribution in the laminate on the material properties of the constituents is expected in the improved model.

Further theoretical and experimental work is also needed to employ the approximate stress analyses as presented

here for the prediction of laminate strength. The possibility

of defining equivalent fracture toughness as a failure crite-

rion for composite plates is being considered. Some related

work for finite thickness homogeneous plates containing

through cracks is discussed in Section IV of this report.

SECTION IV

EXPERIMENTAL MEASUREMENT OF THE EFFECT OF PLATE
THICKNESS ON THE STRAIN ENERGY RELEASE RATE

The results of an experimental program to determine the effects of plate thickness on the failure of homogeneous plates containing through cracks subjected to tensile loading are presented here. This work is a prerequisite to experimental determination of strength for laminated plates containing flaws where a large number of material and geometric parameters will have to be considered.

In this study, compliance measurements and critical load tests were performed for a set of specimens covering a range of plate thicknesses as well as crack lengths. The results of these tests enable an indirect calculation for the average through-the-thickness of the energy release rate; i.e., the rate at which the strain energy of the plate is decreased as the crack extends.

The energy release rate (or the stress intensity factor which is directly related to it) is the basic parameter used for failure prediction in two-dimensional elastic fracture mechanics[*]. However, for finite thickness specimens, the averaged energy release rate is expected to depend on the

_____

[*]Reference is made to the plane stress and plane strain formulations of two-dimensional elasticity.

ratio of the plate thickness to the crack length. An approximate stress analysis which takes this thickness effect into account has been carried out by Hartranft and Sih [1,28], (Figure 4.1) and is extended to laminates in Section III of this report. The experimental results obtained here will be compared to the predictions of that approximate, three-dimensional model. An analogous theory has been developed [28] and a corresponding program carried out [29] for the bending of finite thickness plates with through cracks.

4.1 CALCULATION OF ENERGY RELEASE RATE FROM EXPERIMENTAL RESULTS

Let U be the strain energy of the cracked plate. If the crack extends under constant displacement conditions so that no external work is done to the plate, then the energy release rate per unit of new crack surface area A created is defined as

$$G = -\frac{\partial U}{\partial A} \qquad (4.1.1)$$

For the present experimental investigation, the test specimen is loaded in tension by concentrated loads P as shown in Figure 4.2. The points of application of the loads are displaced a distance $\delta = \delta(P)$ during loading. Thus the strain energy stored in the specimen as a result of the loads P is

$$U = \frac{1}{2} P\delta \qquad (4.1.2)$$

provided the plate response is completely elastic. If the crack in the loaded plate then extends under fixed grip conditions, i.e., if δ is held constant during crack growth, then

$$G = -\frac{\partial U}{\partial A} = -\frac{1}{2} \delta \left.\frac{\partial P}{\partial A}\right|_{\delta \text{ constant}} \tag{4.1.3}$$

At this point, it is convenient to define an apparent plate stiffness $k = P/\delta$. Then

$$\frac{\partial \delta}{\partial A} = P \frac{\partial(1/k)}{\partial A} + \frac{1}{k}\frac{\partial P}{\partial A} = 0$$

Thus

$$\left.\frac{\partial P}{\partial A}\right|_{\delta \text{ constant}} = -kP \frac{\partial(1/k)}{\partial A}$$

Substitution of this result into equation (4.1.3) gives

$$G = \frac{1}{2} P^2 \frac{\partial(\delta/P)}{\partial A} \tag{4.1.4}$$

Thus, the critical energy release rate (the value at fracture initiation) can be determined from experimental results for the load P_c at fracture and the specimen compliance δ/P as a function of crack surface area.

4.2 THE EXPERIMENTAL PROGRAM

Plexiglas was chosen as the material for the test speci-
mens. It possesses the following desirable characteristics:

a. Plexiglas exhibits comparatively little plasticity
   up to failure.

b. A cost material, plexiglas is very nearly isotropic.

c. Since plexiglas is transparent, the detection of
   crack extension in it is relatively easy.

The specimens were 16 inches long and 3 inches wide.
Their thickness varied from 1/16 to 3/4 inch. After the
specimens were cut from a sheet of cast material, two holes
were drilled in order to mount them on the loading pins.
Another small hole of approximately 1/8 inch in diameter was
drilled in the center of the specimen so that a jeweler's saw
could be used to cut the crack. Twelve specimens for each
thickness were prepared, (see Figure 4.3).

4.3 TESTING PROCEDURE

An Instron universal testing machine with 10,000 lb
capacity was used to apply the tensile load between the grips.
A specimen was tested with the small hole of 1/8 inch radius
without a crack to determine the load-displacement relation-
ship for zero crack length. The displacements in each test
were measured between the points of load application and also

-84-

for an 8 inch gage length, 4 inches from each side of the crack. Those two different methods of measuring the displacement were used in order to study the importance of the displacement gage length. Each specimen was accurately centered before loading. The load was applied in small increments. At each increment the relative displacement between the two points in consideration (points of load application or 8 inch gage length) was measured with 2 dial indicators read to an accuracy of ±0.001 inches. During the load application, the displacement had a constant rate of 0.02 inches per minute. For each specimen, the loading was applied five or more times until a repeatable load-displacement curve was obtained. After determining the load-displacement curve for the specimen with the small hole, a small crack of 1/4 inch length was cut with a jeweler's saw. The specimen was then mounted on the machine and subjected to tension, applying the load in small increments and measuring the displacements for each load increment.

Following this testing procedure in which the load-displacement curve was determined, the crack was lengthened by an increment of 1/4 inch and tested again. The procedure was continued until the crack length of 1 1/2 inches was reached. This is the maximum crack length advisable for avoiding effect of finite width [30]. Details of the test apparatus are shown in Figures 4.4 and 4.5. The same procedure was performed for each different thickness. Figure 4.6 shows typical load-displacement curves. A second series of tests were car-

ried out to determine the critical loads for each plate thickness and crack length. In Figure 4.7, the critical load is plotted against crack length for the case of 3/8 inch thick specimens.

4.4 EXPERIMENTALLY DETERMINED ENERGY RELEASE RATES

Table 4.1 contains a listing of the experimentally determined compliances (δ/P) and fracture loads (P_{cr}) for the specimens tested. For each thickness considered, compliance was plotted against crack length and corresponding crack surface area to determine the quantity

$$\frac{\partial(\delta/P)}{\partial A}$$

needed in equation (4.1.4) for calculation of the energy release rate. A sample graph for compliance against crack surface area corresponding to a specimen of thickness 3/8 inch is shown in Figure 4.7. Energy release rates were then calculated using equation (4.1.4) and are included in Table 4.1.

4.5 COMPARISON OF EXPERIMENTALLY DETERMINED ENERGY RELEASE RATES WITH THE HARTRANFT-SIH MODEL

Hartranft and Sih [1] carried out an approximate three-dimensional analysis for a finite thickness plate containing a through crack under tensile loading, Figure 4.1. In this refined theory, the rate at which energy is released with crack extension is found to vary through the plate thickness.

An average, over the plate thickness, of the energy release rate per unit of new crack lnegth created is given in the form

$$\bar{G} = f(h/2a, \nu, p, \varepsilon) \frac{\pi \sigma^2 a(1-\nu^2)}{E} \qquad (4.5.1)$$

where σ is the applied stress, 2a is the crack length, h is the plate thickness, ν is Poisson's ratio, and E is Young's modulus. The parameter ε is a measure of the boundary layer-thickness at the plate surfaces where observed behavior is qualitatively from that of the specimen interior. These surface layers were introduced to account for phenomena such as shear lip formation. In the specimen interior the variation of the near tip stress field with the thickness coordinate z is given by the multiplicative functional coefficient

$$f(z) = \cos pz$$

The value of p is to be chosen from experimental observations.

It should be noted that if the crack extends without change in shape of its leading edge, the average energy release rate per unit increase of crack length and the energy release rate per unit of new crack surface created are identical. With this assumption, the energy release rate $\bar{G}$ (equation (4.5.1)) and the experimentally determined energy release rate at fracture are both plotted against the non-

dimensional thickness parameter h/2a in Figure 4.9. A least squares procedure has been used to fit the experimental curve through the data. The asymptotic value of the Hartranft-Sih equation for $\bar{G}$ at large $\frac{h}{2a}$ where the specimen is in a state of plane strain and $\bar{G} \rightarrow \frac{\pi\sigma^2 a(1-\nu^2)}{E}$ has been chosen to agree with the experimental results.

In two-dimensional elasticity, the energy release rate G is used as a failure criterion for thick specimens where plane strain conditions are assumed to hold. A critical value of the energy release rate G_{1c} known as the fracture toughness is obtained experimentally for a given material. Failure of a structural component of the same material containing a flaw is predicted at the level of loading such that

$$G(\text{load, geometry}) \rightarrow G_{1c}$$

Here, an attempt is made to extend the fracture toughness concept beyond the plane strain range. A thickness dependent energy release rate at fracture has been determined experimentally for plexiglas, Figure 4.9, and an approximate formula, equation (4.5.1), can be used to determine the dependence of the energy release rate on specimen loading and geometry. The $\bar{G}$ obtained in equation (4.5.1) can be equated to the G_{exp} for given h/a to determine the failure load, i.e.,

$$P_{cr} = [\frac{G_{exp}9h^2E}{af\pi(1-\nu^2)}]^{1/2} \qquad (4.5.2)$$

where f is given in equation (4.5.1). These calculations

have been carried out for each of the specimens tested and a comparison of P_{cr}(exp) with P_{cr} (predicted) is given in Table 4.2.

A graphical comparison of experimental and predicted values for P_{cr} is shown in Figure 4.10. The quantity $P_{cr}\sqrt{a}/h$ is plotted against the thickness parameter h/2a. This parameter ($P_{cr}\sqrt{a}/h$) is seen to be relatively insensitive to h/2a for h/2a > .35 and in that range experimental and predicted values are in good agreement. The experimental results for the range h/2a < .35 are observed to depend strongly on the actual plate thickness h and continuation of the curve through these points would be deceiving.

In considering the results presented in Table 4.2 and Figure 4.10, note that for each plate thickness tested (with the exception of h = 0.5") the G_{exp} is found to increase with h/2a until a maximum value, then decrease slightly and level out. These results are typical of those obtained many experimental programs in fracture mechanics. The level portion of the curve for large h/2a is known as the plane strain region. The peak is associated with plane stress and the left-most portion where G_{exp} increases with h/2a is thought to be the consequence of a nonlinear necking phenomenon. Tests corresponding to this range where plasticity is considered to be important and the Hartranft-Sih elastic model is not expected to be accurate are marked with superscript (*).

With the exception of the results for 0.5" thickness
specimens which are suspect, the experimental values and the
predictions for critical load are in reasonable agreement
over the range where the nonlinear effects are thought to
be negligible. These results are based on a rather arbitrary
choice for the parameters p and ε contained in equation
(4.5.1). Further theoretical and experimental work is being
carried out presently to develop a rational procedure for
choosing these or other related parameters. Similar sequences
of tests are needed for other materials to substantiate the
present results. Even with these limitations, the initial
results obtained here are very encouraging in that they sug-
gest a possible procedure for overcoming the testing restric-
tions on specimen thickness based on two-dimensional plane
strain analyses, and for using fracture mechanics to predict
failure of three-dimensional structural components. This
kind of information is necessary before reasonable strength
analyses can be carried out for laminated plates containing
flaws where the stress fields near the flaws are expected to
be three-dimensional in character.

TABLE 4.1 - EXPERIMENTALLY DETERMINED ENERGY RELEASE RATES FOR FINITE THICKNESS PLATES

Thickness h	Crack Length 2a	$\frac{1}{2} P_{cr}^2$	$\frac{\partial(\frac{\Delta}{P})}{\partial(2a)}$	$G_{exp} = \frac{1}{2} P_{cr}^2 \cdot \frac{1}{h} \cdot \frac{\partial(\frac{\Delta}{P})}{\partial(2a)}$ $\frac{lb-in}{in^2}$
1/16"	1/2	12.50×10^4	0.028×10^{-4}	5.75
1/16"	3/4	10.10×10^4	0.045×10^{-4}	7.10
1/16"	1	5.80×10^4	0.076×10^{-4}	7.05
1/16"	1 1/4	3.80×10^4	0.102×10^{-4}	6.20
1/16"	1 1/2	3.20×10^4	0.114×10^{-4}	5.80
1/8 "	1/2	28.90×10^4	0.029×10^{-4}	6.72
1/8 "	3/4	16.50×10^4	0.050×10^{-4}	6.65
1/8 "	1	12.50×10^4	0.064×10^{-4}	6.40
1/8 "	1 1/4	9.50×10^4	0.096×10^{-4}	7.25
1/8 "	1 1/2	6.50×10^4	0.134×10^{-4}	6.97
1/4 "	1/2	95.0×10^4	0.017×10^{-4}	6.45
1/4 "	1	57.5×10^4	0.036×10^{-4}	8.25
1/4 "	1 1/2	10.3×10^4	0.170×10^{-4}	7.05
3/8 "	1/2	173.0×10^4	0.016×10^{-4}	7.35
3/8 "	3/4	105.0×10^4	0.025×10^{-4}	7.00
3/8 "	1	63.0×10^4	0.045×10^{-4}	7.55
3/8 "	1 1/4	41.1×10^4	0.085×10^{-4}	9.25
3/8 "	1 1/2	25.8×10^4	0.125×10^{-4}	8.60

TABLE 4.1 - (Continued)

Thickness h	Crack Length 2a	$\frac{1}{2} P^2_{cr}$	$\frac{\partial(\frac{\Delta}{P})}{\partial(2a)}$	$G_{exp} = \frac{1}{2} P^2_{cr} \frac{1}{h} \frac{\partial(\frac{\Delta}{P})}{\partial(2a)}$ $\frac{lb\text{-}in}{in^2}$
1/2 "	3/4	300.0×10^4	0.012×10^{-4}	7.20
1/2 "	1	242.0×10^4	0.016×10^{-4}	7.75
1/2 "	1 1/4	92.5×10^4	0.040×10^{-4}	7.40
1/2 "	1 1/2	60.5×10^4	0.065×10^{-4}	7.80
1/2 "	1/2	450.0×10^4	0.007×10^{-4}	6.30
5/8 "	1	283×10^4	0.015×10^{-4}	7.03
5/8 "	1 1/4	162.0×10^4	0.028×10^{-4}	7.25
5/8 "	1 1/2	91.0×10^4	0.046×10^{-4}	6.50
5/8 "	1/2	510.0×10^4	0.0085×10^{-4}	6.80
3/4 "	1/2	585.0×10^4	0.0080×10^{-4}	6.30
3/4 "	1	386.0×10^4	0.0125×10^{-4}	6.45
3/4 "	1 1/4	250.0×10^4	0.0210×10^{-4}	7.00
3/4 "	1 1/2	200.0×10^4	0.0280×10^{-4}	7.45

TABLE 4.2 – COMPARISON OF PREDICTED AND EXPERIMENTAL VALUES
FOR FAILURE LOAD

h	a	G_{exp} lb-in/in^2	P_{cr} exp.	pred.	h/2a
3/4 "	3/4"	7.45	20 $(10)^2$lbs	21.5$(10)^2$lbs	1/2
3/4 "	5/8"	7.0	22.5 $(10)^2$lbs	22.5$(10)^2$lbs	3/5
3/4 "	1/2"	6.45	28 $(10)^2$lbs	25 $(10)^2$lbs	3/4
3/4 "	1/4"	6.30	34 $(10)^2$lbs	35 $(10)^2$lbs	3/2
*5/8 "	3/4"	6.50	13.5 $(10)^2$lbs	16.4$(10)^2$lbs	5/12
5/8 "	5/8"	7.25	18 $(10)^2$lbs	19.6$(10)^2$lbs	1/2
5/8 "	1/2"	7.03	24 $(10)^2$lbs	21.5$(10)^2$lbs	5/8
5/8 "	1/4"	6.80	32 $(10)^2$lbs	29.2$(10)^2$lbs	5/4
1/2 "	3/4"	7.80	11 $(10)^2$lbs	15.0$(10)^2$lbs	1/3
1/2 "	5/8"	7.40	13.7 $(10)^2$lbs	16.0$(10)^2$lbs	2/5
1/2 "	1/2"	7.75	22 $(10)^2$lbs	17.8$(10)^2$lbs	1/2
1/2 "	1/4"	6.30	30 $(10)^2$lbs	23.0$(10)^2$lbs	1
*3/8 "	3/4"	8.60	7.2 $(10)^2$lbs	11.5$(10)^2$lbs	1/4
3/8 "	5/8"	9.25	9.5 $(10)^2$lbs	12.0$(10)^2$lbs	3/10
3/8 "	1/2"	7.55	11.25$(10)^2$lbs	13.7$(10)^2$lbs	3/8
3/8 "	3/8"	7.0	14.5 $(10)^2$lbs	15.0$(10)^2$lbs	1/2
3/8 "	1/4"	7.35	18.7 $(10)^2$lbs	18.5$(10)^2$lbs	3/4
*1/4 "	3/4	7.05	4.55$(10)^2$lbs	8.2$(10)^2$lbs	1/6
1/4 "	1/2	8.25	10.8 $(10)^2$lbs	9.6$(10)^2$lbs	1/4
1/4 "	1/4"	6.45	13.8 $(10)^2$lbs	13.2$(10)^2$lbs	1/2
*1/8 "	3/4"	6.97	3.6 $(10)^2$lbs	4.0$(10)^2$lbs	1/12
1/8 "	5/8"	7.25	4.4 $(10)^2$lbs	4.5$(10)^2$lbs	1/10
1/8 "	1/2"	6.40	5.0 $(10)^2$lbs	5.0$(10)^2$lbs	1/8
1/8 "	3/8"	6.65	5.8 $(10)^2$lbs	5.6$(10)^2$lbs	1/6
1/8 "	1/4"	6.72	7.6 $(10)^2$lbs	7.0$(10)^2$lbs	1/4
*1/16"	3/4"	5.80	2.5 $(10)^2$lbs	2.4$(10)^2$lbs	1/24
*1/16"	5/8"	6.20	2.8 $(10)^2$lbs	2.6$(10)^2$lbs	1/20
*1/16"	1/2"	7.02	3.4 $(10)^2$lbs	2.9$(10)^2$lbs	1/16
1/16"	3/8"	7.10	4.5 $(10)^2$lbs	3.1$(10)^2$lbs	1/12
1/16"	1/4"	5.75	5.0 $(10)^2$lbs	3.6$(10)^2$lbs	1/8

SECTION V

A PENNY-SHAPED CRACK IN AN ISOTROPIC LAYER SANDWICHED
BETWEEN TWO ORTHOTROPIC HALF-SPACES

There is considerable interest in the possible struc-
tural applications of fiber-reinforced laminar composites.
These composites are produced by adhering sheets of fiber
reinforced material to create a laminar structure. Separa-
tion of the individual layers through debonding, a process
known as delamination, is perhaps the most often observed
mode of failure for this type of composite system. The aim
of this study is to determine the influence of the geometric
and material properties of the composite on the loading con-
ditions under which delamination will occur. A flaw is pos-
tulated to exist within an adhesive layer in the form of a
penny-shaped crack parallel to the plane of the layers. The
shape chosen for the flaw clearly simplifies the mathematical
analysis, yet it also models the physical situation realisti-
cally. Kassir and Sih [32] have demonstrated that cracks of
arbitrary shape subjected to stress fields, which are approx-
imately uniform relative to the scale of the flaw, will tend
to grow into the shape of a circular disk of discontinuity.
A stress analysis, for a model of fiber-reinforced composite,
will be described which yields a measure of the stress inten-
sification along the edge of the flaw as a function of the
thickness of the bond and the elastic properties of both the
adhesive and the fiber-reinforced layers. The rate at which
energy could be made available for the creation of new sur-

-94-

face associated with enlargement of the flaw is determined thereby enabling prediction of the conditions under which delamination will occur for a given adhesive.

5.1 MODEL FOR FIBER REINFORCED LAMINATE

Consider the composite made up of a number of fiber-reinforced layers bonded together by relatively thin layers of adhesive materials. One of the adhesive layers contains a penny-shaped crack which is parallel to the bonding surfaces, Figure (5.1). The stated purpose of the analysis is to describe accurately the solution in the vicinity of the flaw and the influence of the geometric and material properties of the composite system on that solution. With this in mind, the details of the composite structure are ignored everywhere except in the neighborhood of the crack. The sequences of reinforced and adhesive layers above and below the layer which contains the flaw are idealized as two identical, transversely isotropic half-spaces with preferred directions normal to the layers, Figure (5.2). The elastic properties of these half-spaces are chosen to model the averaged effects of the outer layers on the solution in the vicinity of the flaw. The parameters in this model which can be varied to represent the influences of the composite structure on the local behavior about the crack are: the ratio of adhesive layer thickness to crack radius, the Young's modulus and Poisson's ratio for the adhesive, and the five material properties of the transversely isotropic half-spaces. For example, the relative

-95-

stiffness of the half-spaces parallel to the bond plane as compared to their stiffness normal to that plane is taken to be a measure of the stiffness and quantity of the fiber reinforcements.

Solutions will be presented for the problem of pressure loading on the surfaces of the penny-shaped crack. The superposition principle for linear elasticity can be used to demonstrate that the sum of these solutions plus the corresponding ones for the remote tensile loading of the same body without the crack gives the solutions for remote tensile loading normal to the bond line of the composite containing the flaw. The solution for the remote loaded composite which does not contain a crack is nonsingular and thus will not effect the total solution in the immediate vicinity of the crack edge. Therefore, as far as the near-tip solution is concerned, formulation of the problem for either pressure loading on the crack faces or remote tensile loading lead to identical results. The former is amenable to solution by transform procedures [33] and will be considered.

5.2 FORMULATION OF GOVERNING EQUATIONS

For convenience, the superscript (1) will be used to refer to the isotropic layer containing the crack, while symbols with a superscript (2) will be associated with the half-spaces. The governing equations for the layer and half-spaces can be expressed in terms of Airy stress functions as

$$\left(\frac{\partial^2}{\partial r^2} + \frac{1}{r}\frac{\partial}{\partial r} + \frac{\partial^2}{\partial z^2}\right)^2 \phi^{(1)} = 0$$

and [34]   (5.2.1)

$$\left(\frac{\partial^2}{\partial r^2} + \frac{1}{r}\frac{\partial}{\partial r} + \frac{1}{S_1^2}\frac{\partial^2}{\partial z^2}\right)\left(\frac{\partial^2}{\partial r^2} + \frac{1}{r}\frac{\partial}{\partial r} + \frac{1}{S_2^2}\frac{\partial^2}{\partial z^2}\right)\phi^{(2)} = 0$$

where

$$S_1 = \alpha + \beta, \quad S_2 = \alpha - \beta$$

$$\alpha = \sqrt{\frac{F+H}{2}}, \quad \beta = \sqrt{\frac{F-H}{2}}$$

$$F = \frac{1}{2}\left[\frac{\tilde{E}^{(2)}/\tilde{G}^{(2)} - 2\tilde{\nu}^{(2)}(1+\nu^{(2)})}{\tilde{E}^{(2)}(1-\nu^{2(2)}/E^{(2)})}\right]$$

$$H = \left[\frac{1-\tilde{\nu}^{(2)}E^{(2)}/\tilde{E}^{(2)}}{\tilde{E}^{(2)}(1-\nu^{2(2)})/E^{(2)}}\right]^{1/2}$$

Here, $E^{(2)}$ and $\nu^{(2)}$ are the Young's modulus and the Poisson's ratio, respectively, in planes parallel to the interface, while, $\tilde{E}^{(2)}$, $\tilde{\nu}^{(2)}$, and $\tilde{G}^{(2)}$ are the Young's modulus, Poisson's ratio, and shear modulus in the transverse direction for material (2). Solutions will be presented for choices of material properties such that β is real.

The continuity conditions across the material interface are

$$\sigma_z^{(1)}(h,r) = \sigma_z^{(2)}(h,r)$$

$$\tau_{rz}^{(1)}(h,r) = \tau_{rz}^{(2)}(h,r)$$

$$\hspace{10cm} (5.2.2)$$

$$u_r^{(1)}(h,r) = u_r^{(2)}(h,r)$$

$$u_z^{(1)}(h,r) = u_z^{(2)}(h,r)$$

The mixed boundary conditions on the z = 0 plane are

$$\sigma_z^{(1)}(o,r) = -p, \quad r<a$$

$$u_z^{(1)}(o,r) = 0, \quad r \geq a \hspace{3cm} (5.2.3)$$

$$\tau_{rz}^{(1)}(o,r) = 0$$

Let $G^{(i)}(z,\xi)$, i = 1,2, be the Hankel transforms of the Airy stress functions $\phi^{(i)}(z,r)$ given by

$$G^{(i)}(z,\xi) = \int_{0}^{\infty} r\phi^{(i)}(z,r)J_0(\xi,r)dr$$

Application of the Hankel transform to the governing differential equations (5.2.1) results in the following equations for the transforms of the Airy stress functions:

$$\left(\frac{d}{dz^2} - \xi^2\right)^2 G^{(1)}(z,\xi) = 0 \hspace{3cm} (5.2.4)$$

$$\left(\frac{1}{s_1^2}\frac{d^2}{dz^2} - \xi^2\right)\left(\frac{1}{s_2^2}\frac{d}{dz^2} - \xi^2\right)G^{(2)}(z,\xi) = 0 \qquad (5.2.5)$$

The well-known solutions to these equations are:

$$G^{(1)}(z,\xi) = (A^{(1)}(\xi) + B^{(1)}(\xi)\xi z)\cosh\xi z$$

$$+ (C^{(1)}(\xi) + D^{(1)}(\xi)\xi z)\sinh\xi z \qquad (5.2.6)$$

$$G^{(2)}(z,\xi) = A^{(2)}(\xi)e^{-\xi(\alpha+\beta)z} + B^{(2)}(\xi)e^{-\xi(\alpha-\beta)z}$$

$$+ C^{(2)}(\xi)e^{\xi(\alpha+\beta)z} + D^{(2)}(\xi)e^{\xi(\alpha-\beta)z} \qquad (5.2.7)$$

Here, the function $C^{(2)}(\xi)$ and $D^{(2)}(\xi)$ are required to be identically zero so that the solution will remain bounded for large z.

The stress components and the displacements for the layer and the half-space can be expressed in terms of the transformed stress functions $G^{(1)}(z,\xi)$ and $G^{(2)}(\xi,z)$, respectively as

$$\sigma_r^{(1)}(z,r) = \int_0^\infty \left\{\left[\frac{\nu^{(1)}}{1+\nu^{(1)}}G_{,zzz}^{(1)} - \xi^2 G_{,z}^{(1)}\right] \times\right.$$

$$\left. \times J_0(\xi,r) - \frac{1}{r}\frac{(1+2\nu^{(1)})}{(1+\nu^{(1)})}\xi^2 G_{,z}^{(1)}J_1(\xi,r)\right\}d\xi$$

$$\sigma_z^{(1)}(z,r) = \int_0^\infty \xi[G_{,zzz}^{(1)} - \frac{2-\nu^{(1)}}{1-\nu^{(1)}} \xi^2 G_{,z}^{(1)}]J_0(\xi,r)d\xi$$

$$\tau_{rz}^{(1)}(z,r) = \int_0^\infty \xi^2[\frac{\nu^{(1)}}{(1-\nu^{(1)})} G_{,zz}^{(1)} + \xi^2 G^{(1)}]J_1(\xi,r)d\xi$$

$$U_r^{(1)}(z,r) = \frac{(1+\nu^{(1)})}{E^{(1)}(1-\nu^{(1)})} \int_0^\infty \xi^2 G_{,z}^{(1)}J_1(\xi,r)d\xi$$

$$U_z^{(1)}(z,r) = \frac{(1+\nu^{(1)})}{E^{(1)}(1-\nu^{(1)})} \int_0^\infty \xi[(1-2\nu^{(1)})G_{,zz}^{(1)}$$

$$- 2(1-\nu^{(1)})\xi^2 G^{(1)}]J_0(\xi,r)d\xi$$

$$\sigma_r^{(2)}(z,r) = - \int_0^\infty \xi[aG_{,zzz}^{(2)} - \xi^2 G_{,z}^{(2)}]J_0(\xi,r) \qquad (5.2.8)$$

$$+ \frac{1}{r} (b-1)\xi^2 G_{,z}^{(2)}J_1(\xi,r)d\xi$$

$$\sigma_z^{(2)}(z,r) = \int_0^\infty \xi[dG_{,zzz}^{(2)} - C\xi^2 G_{,z}^{(2)}]J_0(\xi,r)d\xi$$

$$\tau_{rz}^{(2)}(z,r) = - \int_0^\infty \xi^2[aG_{,zz}^{(2)} - \xi^2 G^{(2)}]J_1(\xi,r)d\xi$$

$$U_r^{(2)}(z,r) = \frac{(1-b)(1+\nu^{(2)})}{E^{(2)}} \int_0^\infty \xi^2 G_{,z}^{(2)}J_1(\xi,r)d\xi$$

$$U_z^{(2)}(z,r) = \int_0^\infty \xi\{\frac{(2\tilde{\nu}^{(2)}a+d)}{\tilde{E}^{(2)}} G_{,zz}^{(2)} - [\frac{(1+b)\tilde{\nu}^{(2)}+C}{\tilde{E}^{(2)}}] \times$$

$$\times \xi^2 G^{(2)}\}J_0(\xi,r)d\xi$$

-100-

where

$$a = -\frac{\tilde{\nu}^{(2)}(1+\nu^{(2)})}{1-\tilde{\nu}^{(2)}E^{(2)}/\tilde{E}^{(2)}}$$

$$b = [\tilde{\nu}^{(2)} - \tilde{\nu}^{(2)}(E^{(2)}/\tilde{G}^{(2)} - \tilde{\nu}^{(2)}E^{(2)}/\tilde{E}^{(2)})]/ \times$$

$$\times [1 - \tilde{\nu}^{2(2)}E^{(2)}/\tilde{E}^{(2)}]$$

$$c = [\tilde{E}^{(2)}/\tilde{G}^{(2)} - \tilde{\nu}^{(2)}(1+\nu^{(2)})]/[1 - \tilde{\nu}^{2(2)}E^{(2)}/\tilde{E}^{(2)}]$$

$$d = [\tilde{E}^{(2)}(1 - \nu^{2(2)})/E^{(2)}]/[1 - \tilde{\nu}^{2(2)}E^{(2)}/\tilde{E}^{(2)}]$$

The general solutions for $G^{(i)}(z,\xi)$, equation (5.2.6), and equation (5.2.7) are substituted into the above expressions for the stress and displacement components and the boundary conditions, equations (5.2.2) and (5.2.3) are applied. Five of the unknown functions of ξ can be expressed in terms of the sixth, reducing the problem to the set of dual integral equations with the mixed boundary conditions on the $z = 0$ plane.

$$\int_0^\infty \xi^3 A^{(1)}(\xi)J_0(\xi,r)d\xi = 0, \ r \geq a$$

$$\int_0^\infty \xi^4 f(\xi)A^{(1)}(\xi)J_0(\xi,r)d\xi = -p, \ r < a$$

(5.2.9)

where $f(\xi)$, a complicated function of the geometric and material parameters of the composite, is given in the Appendix

-101-

B.   The other unknown functions $B^{(1)}(\xi)$, $C^{(1)}(\xi)$, $D^{(1)}(\xi)$, $A^{(2)}(\xi)$, $B^{(2)}(\xi)$ can be expressed in terms of $A^{(1)}(\xi)$, see the Appendix B.

Solution procedures have been developed for this set of dual integral equations [28] and the method of solution will be briefly outlined here for completeness.   The first of equations (5.2.9) is satisfied by introducing the function

$$W(r) = \int_0^\infty \xi^3 A^{(1)}(\xi) J_0(\xi,r) d\xi \qquad (5.2.10)$$

with the condition $W(r) = 0$ for $r > a$.   The Hankel transform is applied to equation (5.2.10) to obtain

$$\xi^2 A^{(1)}(\xi) = \int_0^a rW(r) J_0(\xi,r) dr$$

The second equation (5.2.9) may thus be written as

$$\int_0^\infty \xi^2 f(\xi)\{\eta W(\eta) J_0(\xi\eta) d\eta\} J_0(\xi,r) d\xi = p(r), \quad r < a \qquad (5.2.11)$$

Since $W(x)$ is associated with the displacement field it must be bounded at $x \pm a$ and of order $(x \pm a)^{1/2}$ [28] as $|x| \to a$, i.e.,

$$W(x) = \phi(a)(a^2 - x^2)^{1/2} + \ldots$$

For this reason, $W(r)$ is expressed in the form

$$W(r) = \begin{cases} \displaystyle\int_r^a \frac{\tau(\phi)}{\sqrt{\tau^2 - r^2}}\,d\tau, & 0 \le r \le a \\[4mm] 0, & r > a \end{cases}$$

where $\phi(\tau)$ is continuous on the interval $[0,a]$.

The expression for $W(r)$ is substituted into equation (5.2.11). The resulting equation is multiplied by r and then integrated in r from $r = 0$ to $r = R$. After a formal change in order of integration and application of the identity

$$\int_0^\tau \frac{\xi\eta J_0(\xi,\eta)d\eta}{\sqrt{\tau^2\,\eta^2}}\,d\eta = \sin(\xi\tau)$$

the following equation is obtained

$$R \int_0^a \tau\phi(\tau) \int_0^\infty f(\xi)\sin(\xi\tau)J_1(\xi R)d\xi d\tau = \int_0^R p(r)rdr$$

where $J(\xi R)$ is the first order Bessel function of the first kind.

For the special case of constant pressure the above equation is reduced to:

$$\int_0^a \tau\phi(\tau) \int_0^\infty f(\xi)\sin(\xi\tau)J_1(\xi R)d\xi d\tau = \frac{pR}{2} \qquad (5.2.12)$$

By making the substitution

$$f^*(\xi) = -f(\xi)2\nu^{(1)}(1-\nu^{(1)}) - 1.0$$

-103-

and applying the identity

$$\int_0^\infty \sin(\xi\tau)J_1(\xi R)d\xi = \begin{cases} 0 & , \ 0<R<\tau \\ \dfrac{\tau}{R\sqrt{R^2-\tau^2}}, & 0\le\tau\le R \end{cases} \quad (5.2.13)$$

equation (5.2.12) can be expressed in the form of an Abel equation as

$$\int_0^R \frac{\tau^2\phi(\tau)d\tau}{\sqrt{R^2-\tau^2}} = -\ 2\nu^{(1)}(1-\nu^{(1)})R\ \frac{pR}{2}$$

$$-\ R\int_0^a \tau\phi(\tau)\int_0^\infty f^*(\xi)\sin(\xi\tau)J_1(\xi R)d\xi d\tau$$

The solution of the Abel equation yields a Fredholm integral equation of the second kind for $\phi(\tau)$

$$\tau\phi(\tau) = \frac{2}{\pi}\ \{\int_0^\tau \frac{p'RdR}{\sqrt{\tau^2-R^2}}$$

$$-\int_0^a \eta\phi(\eta)\int_0^\infty f^*(\xi)\sin(\xi\eta)\sin(\xi\tau)d\xi d\eta\}0<\tau<a$$

where

$$p' = -\ 2\nu^{(1)}(1-\nu_1^{(1)})p$$

This equation can be rewritten in a convenient nondimensional form, i.e., the substitutions

$$\tau = at, \quad \eta = as, \quad \tau\phi(\tau) = \frac{2}{\pi} p'a\Phi(\tau)$$

lead to

$$\Phi(t) + \int_0^1 \Phi(s)k(s,t)ds = t \qquad\qquad (5.2.14)$$

with the symmetric kernel

$$k(s,t) = \frac{2}{\pi} \int_0^\infty f^*(\frac{\xi}{a})\sin(\xi s)\sin(\xi t)d\xi, \quad 0<t<1; \quad 0<s<1$$

The equation (5.2.14) is solved numerically for $\Phi(t)$.

The function $\Phi(t)$ can be determined exactly for the case of a limitingly thin adhesive layer. Note that the function $f(\xi)$ reduces to a constant, say f_0, for $h = 0$. Refer back to equation (5.2.12), divide by f_0 and use the identity, equation (5.2.13), to reduce equation (5.2.12) to the Abel integral equation

$$\int_0^R \frac{\tau^2\phi(\tau)}{\sqrt{R^2-\tau^2}}d\tau = \frac{pR^2}{2f_0}, \quad R\leq a$$

Solution of this equation and application of the normalization described above gives

$$\Phi(t) = -\frac{t}{2\nu^{(1)}(1-\nu^{(1)})f_0}, \quad \text{for } h = 0$$

-105-

Returning to the solution of the original set of dual integral equations, $A^{(1)}(\xi)$ takes the form

$$A^{(1)}(\xi) = - \frac{2p'a}{\pi\xi^4} \Phi(1)\cos(\xi a)$$

$$+ \int_0^1 \frac{1}{\xi^4} \cos(\xi at)\frac{d}{dt} [\Phi(t)]dt \qquad (5.2.15)$$

where $\Phi(1)$ is to be interpreted as the limit of $\Phi(t)$ as t approaches 1.0 from below. Once the function $\Phi(t)$ is evaluated from the Fredholm integral equation, equation (5.2.15) may be substituted into equations (5.2.6) and (5.2.7) to obtain $G^{(1)}$ and $G^{(2)}$, from which the displacements and stresses at every point may be calculated.

5.3 LOCAL STRESS FIELD

It is not difficult to show that the integral expression in equation (5.2.15) remains bounded at the crack edge r = a and that the contribution to the singular behavior of the stresses is fully described by the leading term in equation (5.2.15). The desired explicit representation of the portion of the solution that becomes unbounded at the penny-shaped crack border may be obtained by recourse to Laurent series expansions and the use of elementary Bessel-integral identities. Adopting polar coordinates ρ and θ, as shown in Figure (5.3), it is found that

$$\sigma_r = k_1(2\rho)^{-1/2} \cos \frac{\theta}{2} [1 - \sin \frac{\theta}{2} \sin \frac{3}{2}\theta]$$

$$\sigma_z = k_1(2\rho)^{-1/2} \cos \frac{\theta}{2} [1 + \sin \frac{\theta}{2} \sin \frac{3}{2}\theta]$$

$$\tau_{rz} = k_1(2\rho)^{-1/2} \cos \frac{\theta}{2} [\sin \frac{\theta}{2} \cos \frac{3\theta}{2}]$$

where k_1 is the stress intensity factor defined as

$$k_1 = \frac{2}{\pi} \Phi(1)p\sqrt{a}$$

5.4 NUMERICAL RESULTS

Numerical solutions for the stress intensity factor were obtained for the special case $\nu^{(1)} = \nu^{(2)} = \tilde{\nu}^{(2)} = 3$, $\tilde{G}^{(2)} = \tilde{E}^{(2)}/2(1+\tilde{\nu}^{(2)})$. For this choice of $\tilde{G}^{(2)}$, β, equation (5.2.1) is real for $1 < \frac{E^{(2)}}{\tilde{E}^{(2)}} < [1/\tilde{\nu}^{(2)}]^2$ and the general solution to equation (5.2.5) for the transformed Airy stress function, equation (5.2.7) is correct. Alternate expressions for $\tilde{G}^{(2)}$ are possible which results in real values for β over other ranges of $E^{(2)}/\tilde{E}^{(2)}$.

Numerical results for the variation of stress intensity factor over the range of material's properties discussed above are exhibited in Figures (5.4) to (5.6). In these plots, the stress intensity factor has been normalized by its value for a penny-shaped crack of the same radius and subjected to the same pressure loading but contained in an in-

finite isotropic body ($k_1 = \frac{2}{\pi} p\sqrt{a}$) [24]. Thus values of the normalized stress intensity factor which are less than 1.0 indicate that less load is transferred to the crack tip by the laminar composite than would be transferred in an equivalent homogeneous, isotropic body. The dependence of the stress intensity factor on the degree of anisotropy of the center layers $E_2/\tilde{E}_2$ is illustrated in Figures (5.4) and (5.5) for various values of the relative stiffness of the cracked layer to that of the half spaces (in the direction normal to the crack face), $E_1/\tilde{E}_2$ at a number of distinct ratios of layer thickness to crack diameter. Increasing the relative stiffness of the half spaces parallel to the crack face reduces the load transfer to the crack tip. Further, any deviation of the stress intensity factor from the one-material result ($k_1 = \frac{2}{\pi} p\sqrt{a}$) is amplified as the layer thickness to crack diameter ratio h/a is decreased. This effect is demonstrated in Figure (5.6). It should be noted that the slope of the stress intensity factor layer thickness curves is infinite at h/a = 0. This mathematical result has been demonstrated earlier in connection with a different physical problem [28].

5.5 DISCUSSION

The primary purpose of these calculations is associated with the use of this boundary value problem as a model to study the effect of the geometric and material properties of the fiber reinforced, laminar composite system on a flaw in

an adhesive bond. With this interpretation in mind, the predictions are that load transfer to the flaw is decreased as the relative stiffness of the layer material to that of the adhesive is increased and, in particular, as the volume percentage or stiffness of the reinforcing fiber is increased, producing a higher apparent stiffness for the layers parallel to the interfaces. The effects are more pronounced when the adhesive layers are thin or the flaw is large.

These estimates of load transfer can be related to the prediction of conditions for delamination via a knowledge of the energy necessary to create new surface for the bonding material. The rate at which energy would be made available for the creation of new surface if the crack expanded uniformly is readily attainable from the numerical results presented above via the energy release rate equation for cracks in an isotropic material [24]:

$$G = \frac{4(1-\nu^{2(1)})}{E^{(1)}} \, k_1^2$$

Thus crack extension is predicted when G is greater than the corresponding material property $G_c = 2\pi a^2 \gamma$ of the adhesive. This analysis thus provides a quantitative criterion for choice of bonding material in terms of its stiffness and energy required to create new surface.

APPENDIX A – PARAMETERS ARISING IN SOLUTION FOR IN-PLANE STRESS VARIATIONS

$$k_1 = \frac{a_4}{2a_3}$$

$$- ik_3 = \sqrt{\left(\frac{a_4}{2a_3}\right)^2 - \frac{a_5}{a_3}}$$

$$b_1 = -2 \frac{a_1}{a_6} \frac{\left[\left(k_1 + \frac{1}{a_6}\right)\left(\frac{a_2}{a_1} - k_1\right) - k_3^2\right]}{\left[\left(k_1 + \frac{1}{a_6}\right)^2 + k_3^2\right]}$$

$$b_2 = 2 \frac{a_1}{a_6} \frac{k_3\left(\frac{1}{a_6} + \frac{a_2}{a_1}\right)}{\left[\left(k_1 + \frac{1}{a_6}\right)^2 + k_3^2\right]}$$

$$c_1 = 4a_6$$

$$c_2 = I_3 b_1 - 2k_1 a_6$$

$$c_3 = \frac{I_3}{2}(k_3 b_2 - k_1 b_1) - \frac{1}{2}(k_1^2 - k_3^2)a_6$$

$$d_1 = 2k_3 a_6 - I_3 b_2$$

$$d_2 = k_1 k_3 a_6 + \frac{I_3}{2}(k_3 b_1 + k_1 b_2)$$

$$d_3 = I_3\left[\frac{1}{4} k_1 k_3 b_1 + \frac{1}{8}(k_1^2 + k_3^2)b_2\right] - \frac{1}{4} k_3(k_3^2 - 3k_1^2)a_6$$

$$e_1 = \frac{c_1}{d_1}$$

$$e_2 = \frac{1}{d_1} (c_2 - c_1 \frac{d_2}{d_1})$$

$$e_3 = \frac{1}{d_1} [c_3 - c_2 \frac{d_2}{d_1} - c_1(\frac{d_3}{d_1} - (\frac{d_2}{d_1})^2)]$$

$$m_2 = 2(1 - \frac{k_3}{2} e_1)$$

$$m_3 = - (k_1 + k_3 e_2 + \frac{k_1 k_3}{2} e_1)$$

$$m_4 = - [\frac{(k_1^2 - k_3^2)}{4} + k_3 e_3 + \frac{k_1 k_3}{2} e_2 - \frac{k_3}{8} (k_3^2 - 3k_1^2)e_1]$$

$$m_6 = \frac{2}{(I_1^2 - I_2^2)} [(I_1 + I_2) - e_1\{I_1 k_3 + \frac{b_1 k_3}{2} [\frac{(I_1 + I_2)I_3}{2}$$

$$+ I_4(I_1 - I_2) - I_1 I_3] - \frac{b_2}{2} [\frac{(I_1 + I_2)I_3}{2} (\frac{1}{a_6} k_1)$$

$$- (I_4(I_1 - I_2) - I_1 I_3)k_1]\}]$$

$$m_7 = \frac{2}{(I_1^2 - I_2^2)} [-I_1(k_1 + k_3 e_2) + \frac{b_1}{2} \{-(I_1 + I_2)I_3 [\frac{1}{4a_6} k_3 e_1$$

$$+ (\frac{k_1}{2} + \frac{k_3}{2} e_2 + \frac{k_1 k_3}{4} e_1)] - [I_4(I_1 - I_2) - I_1 I_3](k_1 + k_3 e_2)\}$$

$$+ \frac{b_2}{2} \{-(I_1 + I_2)I_3 [\frac{e_1}{8a_6^2} + \frac{1}{2a_6} (\frac{k_1}{2} e_1 - e_2) + \frac{(k_1^2 - k_3^2)}{8} e_1$$

$$+ \frac{k_1}{2} e_2 - \frac{k_3}{2}] - [I_4(I_1 - I_2) - I_1 I_3](k_1 e_2 - k_3)\}]$$

$$m_8 = \frac{2}{(I_1^2 - I_2^2)} \left[-I_1 k_3 e_3 + \frac{b_1}{2} \left\{ -\frac{(I_1 + I_2) I_3}{2} \left[(e_3 - \frac{1}{8a_6^2} e_1) k_3 \right. \right. \right.$$

$$\left. + \frac{1}{2a_6} (k_1 + k_3 e_2 + \frac{k_1 k_3}{2} e_1) + \frac{(k_1^2 - k_3^2)}{4} + \frac{k_1 k_3}{2} e_2 \right.$$

$$\left. - \frac{1}{8} (k_3^3 - 3k_1^2 k_3) e_1 \right] - [I_4(I_1 - I_2) - I_1 I_3](k_3 e_3) \Big\}$$

$$+ \frac{b_2}{2} \left\{ \frac{(I_1 + I_2) I_3}{2} \left[\frac{1}{8a_6^3} e_1 + \frac{1}{4a_6^2} (\frac{k_1 e_1}{2} - e_2) \right. \right.$$

$$\left. - \frac{2}{a_6} (\frac{(k_1^2 - k_3^2)}{4} e_1 + k_1 e_2 - k_3 - 2e_3) - \frac{1}{8} (k_1^2 - 3k_3^2) k_1 e_1 \right.$$

$$\left. - \frac{(k_1^2 - k_3^2)}{4} e_2 - k_1 e_3 + \frac{k_1 k_3}{2} \right]$$

$$\left. \left. - [I_4(I_1 - I_2) - I_1 I_3](k_1 e_3) \right\} \right]$$

$$C = \frac{m_6}{m_2}$$

$$H = \frac{m_7}{m_2} - \frac{m_6}{m_2} \frac{m_3}{m_2}$$

$$N^2 = -\frac{\left[m_8 - \frac{(m_6 m_4 + m_7 m_3)}{m_2} + m_6 (\frac{m_3}{m_2})^2 \right]}{\left[m_7 - m_6 \frac{m_3}{m_2} \right]}$$

APPENDIX B - FUNCTION f(ξ) RELATED TO THE SECOND EQUATION
(5.2.9)

$$f(\xi) = \frac{1}{1-\nu^{(1)}} \frac{H(\xi)}{G(\xi)}$$

where:

$$H(\xi) = \frac{1}{g_4(\xi)} = \{\{(\frac{1+\nu^{(1)}}{E^{(1)}})(1 - \frac{1}{2\nu^{(1)}})$$

$$+ \frac{(1-b)(1+\nu^{(2)})(s_1-s_2)}{2E_2 s\nu^{(1)}}$$

$$- [1 + as_1s_2 - ds_1s_2(s_1+s_2)\xi h]\}\sinh\xi h$$

$$+ \{- \frac{(1+\nu^{(1)})\xi h}{2E_1\nu^{(1)}} + \frac{(1-b)(1+\nu^{(2)})(s_1-s_2)}{2E_2 s\nu^{(1)}} \times$$

$$\times [- (1 + as_1s_2)\xi h]\}\cosh\xi h\}$$

$$- \frac{1}{g_3(\xi)} \{\{- \frac{(1-\nu^{(1)^2})}{E_1\nu^{(1)}} - (\frac{s_1-s_2}{2\tilde{E}^{(2)}s\nu^{(1)}}) \times$$

$$\times [(2\tilde{\nu}^{(2)}a+d)(s_1+s_2)(-\xi h) + [(1+b)\tilde{\nu}^{(2)} + c] \times$$

$$\times a(s_1+s_2)(\xi h)]\}\cosh\xi h + \frac{(1+\nu^{(1)})\xi h}{2E^{(1)}_\nu{}^{(1)}}$$

$$- (\frac{s_1-s_2}{2\tilde{E}^{(2)}s\nu^{(1)}})[(2\tilde{\nu}^{(2)}a+d)[(s_1+s_2)$$

$$+ s_1s_2(c+ds_1s_2)(-\xi h)] - [(1+b)\tilde{\nu}^{(2)} + c] \times$$

-113-

$$\times \; [a(s_1+s_2) + [d(s_1^2+s_1s_2+s_2^2) - c](-\xi h)]]\}\sinh\xi h\}$$

$$G(\xi) = -\frac{1}{g_4(\xi)}\left\{\left\{\frac{(1+\nu^{(1)})(-\xi h)}{E^{(1)}(1-2\nu^{(1)})} + \frac{(1-b)(1+\nu^{(2)})(s_1-s_2)}{E^{(2)}s(1-2\nu^{(1)})}\times\right.\right.$$

$$\times\; [(1 + as_1s_2(-\xi h) - 2\nu^{(1)}ds_1s_2(s_1+s_2)]\}\sinh\xi h$$

$$+\; -\frac{(1+\nu^{(1)})}{E^{(1)}(1-2\nu^{(1)})} + \frac{(1-b)(1+\nu^{(2)})(s_1-s_2)}{E^{(2)}s}\times$$

$$\times\; [(1 + as_1s_2) - \frac{ds_1s_2(s_1+s_2)\xi h}{1-2\nu^{(1)}}]\}\cosh\xi h\}$$

$$+\; \frac{1}{g_3(\xi)}\left\{\left\{\frac{(1+\nu^{(1)})\xi h}{E^{(1)}(1-2\nu^{(1)})} - \frac{s_1-s_2}{\tilde{E}^{(2)}s}\times\right.\right.$$

$$\times\; [(2\tilde{\nu}^{(2)}a+d)[(s_1+s_2) + \frac{s_1s_2(c+ds_1s_2)(-\xi h)}{1-2\nu^{(1)}}$$

$$-\; [(1+b)\tilde{\nu}^{(2)} + c][a(s_1+s_2) + (d[s_1^2+s_1s_2+s_2^2] - c)\times$$

$$\times\; (-\frac{\xi h}{1-2\nu^{(1)}})]]\}\cosh\xi h + \{-\frac{2(1+\nu^{(1)})}{E^{(1)}}$$

$$-\; (\frac{s_1+s_2}{\tilde{E}_2s})[\frac{(2\tilde{\nu}^{(2)}a+d)}{1+2\nu^{(1)}}\;[(-\xi h)(s_1+s_2)$$

$$+\; s_1s_2(c+ds_1s_2)(-2\nu^{(2)}] - [\frac{(1+b)\tilde{\nu}^{(2)}+c}{1-2\nu^{(1)}}]\times$$

$$\times\; [a(s_1+s_2)(-\xi h) + (d[s_1^2+s_1s_2+s_2^2] - c)\times$$

$$\times\; (-2\nu^{(1)})]]\}\sinh\xi h\}$$

with:

$$s = [d(s_1^3 - s_2^3) + (c + cas_1s_2 + ads_1^2s_2^2)(s_1 - s_2)]$$

$$g_3(\xi) = \frac{1+\nu^{(1)}}{E^{(1)}} \left[\left(\frac{\xi h}{1-2\nu^{(1)}} \right) \cosh\xi h - \sinh\xi h \right]$$

$$+ \frac{s_1-s_2}{\tilde{E}^{(2)}s(1-2\nu^{(1)})} \{ (2\tilde{\nu}^{(2)}a+d) \{ [(\xi h)(s_1+s_2)$$

$$+ s_1s_2(c+ds_1s_2)]\sinh\xi h$$

$$+ [s_1s_2(c+ds_1s_2)(\xi h)]\cosh\xi h \}$$

$$- [(1+b)\tilde{\nu}^{(2)} + c]\{ [a(s_1+s_2)(\xi h)$$

$$+ (d[s_1^2+s_1s_2+s_2^2] - c]\sinh\xi h$$

$$+ [d(s_1^2+s_1s_2+s_2^2) - c][\xi h]\cosh\xi h \}\}$$

and

$$g_4(\xi) = - \{ \frac{(1+\nu_1)}{E^{(1)}(1-2\nu^{(1)})} [\xi h\sinh\xi h + 2(1-\nu^{(1)})\cosh\xi h]$$

$$+ \frac{(1-b)(1+\nu^{(2)})(s_1-s_2)}{E^{(2)}s(1-2\nu^{(1)})} \{ [(1 + as_1s_2)\xi h$$

$$+ ds_1s_2(s_1+s_2)]\sinh\xi h + [ds_1s_2(s_1+s_2)\xi h]\cosh\xi h \}\}$$

Coefficients of equations (5.2.6) and (5.2.7)

$$C^{(1)}(\xi) = \frac{L(\xi)}{g_4(\xi)} A^{(1)}(\xi)$$

$$B^{(1)}(\xi) = [\frac{C^{(1)}(\xi)-(1-2\nu^{(1)})f(\xi)}{(1-2\nu^{(1)})}]A^{(1)}(\xi)$$

$$D^{(1)}(\xi) = - \frac{A^{(1)}(\xi)}{2\nu^{(1)}}$$

$$A^{(2)}(\xi) = \frac{M(\xi)}{s(1-\nu^{(1)})} e^{\xi s_1 h} A^{(1)}(\xi)$$

$$B^{(2)}(\xi) = - \frac{N(\xi)}{s(1-\nu^{(1)})} e^{\xi s_2 h} A^{(1)}(\xi)$$

where:

$$L(\xi) = \{\{\frac{1+\nu^{(1)}}{E^{(1)}} [(1 - \frac{1}{2\nu^{(1)}}) - \frac{(1-\nu^{(1)})f(\xi)\xi h}{1-2\nu^{(1)}}]$$

$$+ \frac{(1-b)(1+\nu^{(2)})(s_1-s_2)}{E^{(2)}s} [(1 + as_1s_2) [\frac{1}{2\nu^{(1)}}$$

$$- \frac{(1+\nu^{(1)})f(\xi)\xi h}{1-2\nu^{(1)}}] - ds_1s_2(s_1+s_2)(\frac{\xi h}{2\nu^{(1)}}$$

$$+ \frac{2\nu^{(1)}(1-\nu^{(1)})f(\xi)}{1-2\nu^{(1)}})]\}\sinh\xi h + \{\frac{1+\nu^{(1)}}{E^{(1)}} [- \frac{\xi h}{2\nu^{(1)}}$$

$$- \frac{(1-\nu^{(1)})f(\xi)}{1-2\nu^{(1)}}] + \frac{(1-b)(1+\nu^{(2)})(s_1+s_2)}{E^{(2)}s} \times$$

$$\times [(1 + as_1s_2)[(1+\nu^{(1)})f(\xi) - \frac{\xi h}{2\nu^{(1)}}]$$

-116-

$$- \frac{ds_1 s_2 (s_1 + s_2)(1 - \nu^{(1)})f(\xi)\xi h}{1 - 2\nu^{(1)}}]\}\cosh\xi h\}$$

$$M(\xi) = \{(1 - as_2^2)[\frac{1}{2\nu^{(1)}} + [\frac{C^{(1)}(\xi) - (1 - \nu^{(1)})f(\xi)}{1 - 2\nu^{(1)}}](\xi h)]$$

$$- (ds_2^3 - s_2 c)[\frac{L(\xi)}{g_4(\xi)} - \frac{\xi h}{2\nu^{(1)}}$$

$$+ 2\nu^{(1)}[\frac{C^{(1)}(\xi) - (1 - \nu^{(1)})f(\xi)}{1 - 2\nu^{(1)}}]]\}\sinh\xi h$$

$$+ \{(1 + as_2^2)[\frac{L(\xi)}{g_4(\xi)} - \frac{\xi h}{2\nu^{(1)}} - (1 - 2\nu^{(1)}) \times$$

$$\times [\frac{C^{(1)}(\xi) - (1 - \nu^{(1)})f(\xi)}{1 - 2\nu^{(1)}}]] - (ds_1^3 - cs_2) \times$$

$$\times [\frac{C^{(1)}(\xi) - (1 - \nu^{(1)})f(\xi)}{1 - 2\nu^{(1)}}]\xi h\}\cosh\xi h$$

$$N(\xi) = \{(1 - as_1^2)[\frac{1}{2\nu^{(1)}} + [\frac{C^{(1)}(\xi) - (1 - \nu^{(1)})f(\xi)}{1 - 2\nu^{(1)}}]\xi h]$$

$$- (ds_1^3 - s_1 c)[\frac{L(\xi)}{g_4(\xi)} - \frac{\xi h}{2\nu^{(1)}}$$

$$- 2\nu^{(1)}[\frac{C^{(1)}(\xi) - (1 - \nu^{(1)})f(\xi)}{1 - 2\nu^{(1)}}]]\}\sinh\xi h$$

$$+ \{(1 - as_1^2)[\frac{L(\xi)}{g_4(\xi)} - \frac{\xi h}{2\nu^{(1)}} - (1 - 2\nu^{(1)}) \times$$

$$\times [\frac{C^{(1)}(\xi) - (1 - \nu^{(1)})f(\xi)}{1 - 2\nu^{(1)}}]] - (ds_1^3 - cs_1) \times$$

$$\times [\frac{C^{(1)}(\xi) - (1 - \nu^{(1)})f(\xi)}{1 - 2\nu^{(1)}}]\xi h\}\cosh\xi h$$

REFERENCES

1. Hartranft, R. J. and Sih, G. C., "An Approximate Three-Dimensional Theory of Plate with Application to Crack Problems", Int. J. Engng. Sci., Vol. 8, 1970, pp. 711-729.

2. Chamis, C. C. and Sendeckyj, G. P., "Critique on Theories Predicting Thermoelastic Properties of Fibrous Composites", J. Composite Materials, Vol. 2, No. 3, July 1968, pp. 332-358.

3. Reissner, E., "On Bending of Elastic Plates", Quarterly of Applied Mathematics, Vol. 5, 1947, pp. 55-68.

4. Calcote, L. R., "The Analysis of Laminated Composite Structure", Van Nostrand Reinhold Company.

5. Timoshenko, S. P. and Woinowsky-Krieger, "Theory of Plates and Shell", McGraw-Hill Book Company.

6. Smith, C. B., "Some New Types of Orthotropic Plates Laminated of Orthotropic Material", J. of Applied Mechanics, Vol. 20, TRANS. ASME, Vol. 75, 1953, pp. 286-288.

7. Reissner, E. and Stavsky, Yl, "Bending and Stretching of Certain Types of Heterogeneous Aeolotropic Elastic Plates", J. of Applied Mechanics, Vol. 28, No. 3, TRANS. ASME, Vol. 83, 1961, pp. 402-408.

8. Dong, S. B., Pister, K. S. and Taylor, R. L., "On the Theory of Laminated Anisotropic Shells and Plates", J. of the Aerospace Sciences, Vol. 29, 1962, pp. 969-975.

9. Whitney, J. M. and Leissa, A. W., "Analysis of Heterogeneous Anisotropic Plates", J. of Applied Mechanics, Vol. 36, June 1969, pp. 261-266.

10. Whitney, J. M., "The Effect of Boundary Conditions on the Response of Laminated Composites", J. Composite Materials, Vol. 4, April 1970, pp. 192-203.

11. Whitney, J. M., "Bending-Extensional Coupling in Laminated Plates Under Transverse Loading", J. Composite Materials, Vol. 3, January 1969, pp. 20-28.

12. Pagano, N. J., "Exact Solutions for Composite Laminates in Cylindrical Bending", J. Composite Materials, Vol. 3, July 1969, pp. 398-411.

13. Pagano, N. J., "Exact Solutions for Rectangular Bi-Directional Composites and Sandwich Plates", J. Composite Materials, Vol. 4, January 1970, pp. 20-35.

14. Pagano, N. J., "Influence of Shear Coupling in Cylindrical Bending of Anisotropic Laminates", J. Composite Materials, Vol. 4, July 1970, pp. 330-343.

15. Whitney, J. M., "The Effect of Transverse Shear Deformation on the Bending of Laminated Plates", J. Composite Materials, Vol. 3, July 1969, pp. 534-547.

16. Puppo, A. H. and Evensen, H. A., "Interlaminar Shear in Laminated Composites Under Generalized Plane Stress", J. Composite Materials, Vol. 4, April 1970, pp. 204-220.

17. Pipes, R. B. and Pagano, N. J., "Interlaminar Stresses in Composite Laminates Under Uniform Axial Extension", J. Composite Materials, Vol. 4, October 1970, pp. 538-548.

18. Rybicki, E. F., "Approximate Three-Dimensional Solutions for Symmetric Laminates Under In-Plane Loading", J. Composite Materials, Vol. 5, July 1971, pp. 354-360.

19. Hartranft, R. J. and Sih, G. C., "The Use of Eigenfunction Expansions in the General Solution of Three-Dimensional Crack Problems", J. of Mathematics and Mechanics, Vol. 19, 1969, pp. 123-138.

20. Sih, G. C., Hilton, P. D. and Wei, R. P., "Exploratory Development of Fracture Mechanics of Composite Systems", Air Force Report AFML-TR-70-112, 1970.

21. Sih, G. C. and Hartranft, R. J., "Variation of Strain Energy Release Rate with Plate Thickness", International Journal of Fracture Mechanics, in press.

22. Erdogan, F., Tuncel, O. and Paris, P. C., "An Experimental Investigation of the Crack Tip Stress-Intensity Factors in Plates Under Cylindrical Bending", Journal of Basic Engineering, TRANS. ASME, Series D, Vol. 84, 1962, pp. 542-546.

23. Wynn, R. H. and Smith, C. W., "An Experimental Investigation of Fracture Criteria for Combined Extension and Bending", J. Basic Engineering, TRANS. ASME, December 1969.

24. Sih, G. C. and Liebowitz, H., "Mathematical Theories of Brittle Fracture", Mathematical Fundamentals of Fracture, H. Liebowitz, editor, Academic Press, New York, 1968, pp. 67-190.

25. Irwin, G. R. and Kies, J. A., "Critical Energy Rate Analysis of Fracture Strength", Welding Research Supplement, April 1954, pp. 193-198.

26. Irwin, G. R., Kies, J. A. and Smith, H. L., "Fracture Strength Relative to Onset and Arrest of Crack Propagation", Proc. ASTM, 58, 1958, pp. 640-657.

27. Muskhelishvili, N. I., Some Basic Problems of the Mathematical Theory of Elasticity, Noordhoff, Groningen, 1954.

28. Hartranft, R. J. and Sih, G. C., "Effect of Plate Thickness on the Bending Stress Distribution Around Through Cracks", J. of Mathematics and Physics, Vol. 47, No. 3, September 1968, pp. 276-291.

29. Smith, D. G. and Smith, C. W., "Influence of Precatastrophic Extension and Other Effects on Local Stresses in Cracked Plates Under Bending Fields", Experimental Mechanics, 1971, pp. 394-401.

30. Dixon, J. R., "Stress Distribution Around a Central Crack in a Plate Loaded in Tension; Effect of Finite Width of Plate", J. of the Royal Aeronautical Society, Vol. 64, March 1960.

31. Srawley, J. E. and Brown, W. F., "Testing Methods, Fracture Toughness Testing and its Applications", ASTM STP No. 381.

32. Kassir, M. K. and Sih, G. C., "Three-Dimensional Stress Distribution around an Elliptical Crack Under Arbitrary Loadings", J. of Applied Mechanics, 33, 1966, pp. 601-611.

33. Sneddon, I. N., Fourier Transforms, McGraw-Hill, 1951.

34. Lekhnitskii, S. G., Theory of Elasticity of an Anisotropic Elastic Body, Holden-Day, 1963.
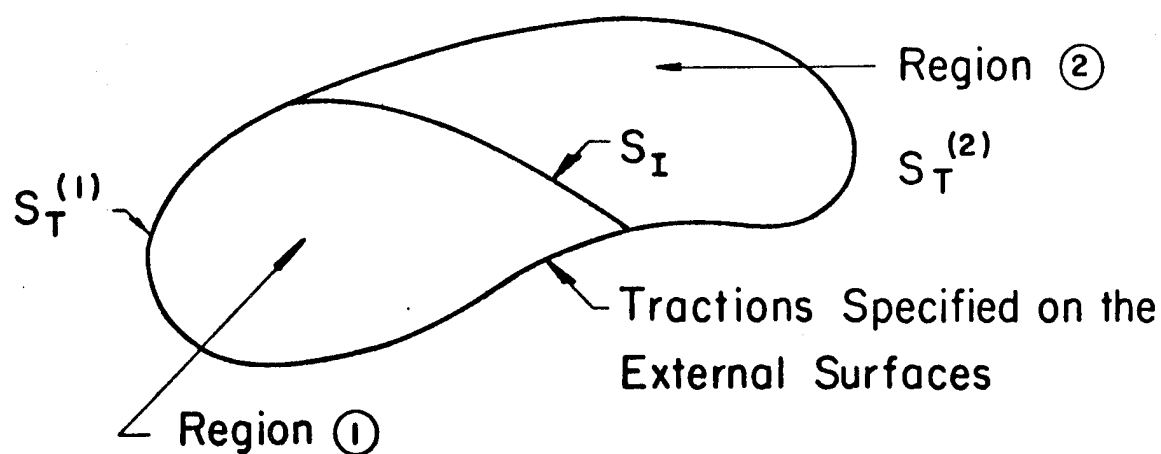
Figure 3.1.1 - A General Two-Phase Composite
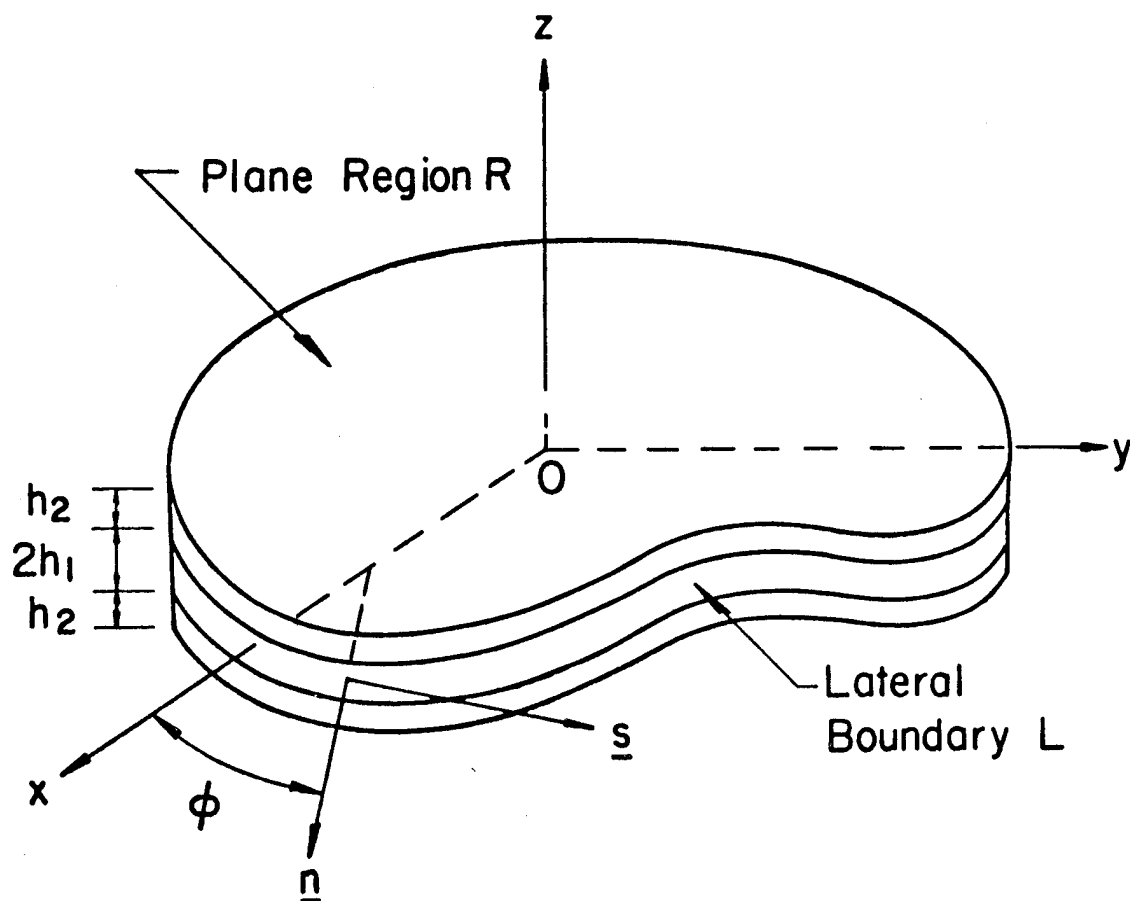
Figure 3.2.1 - Laminated Plate
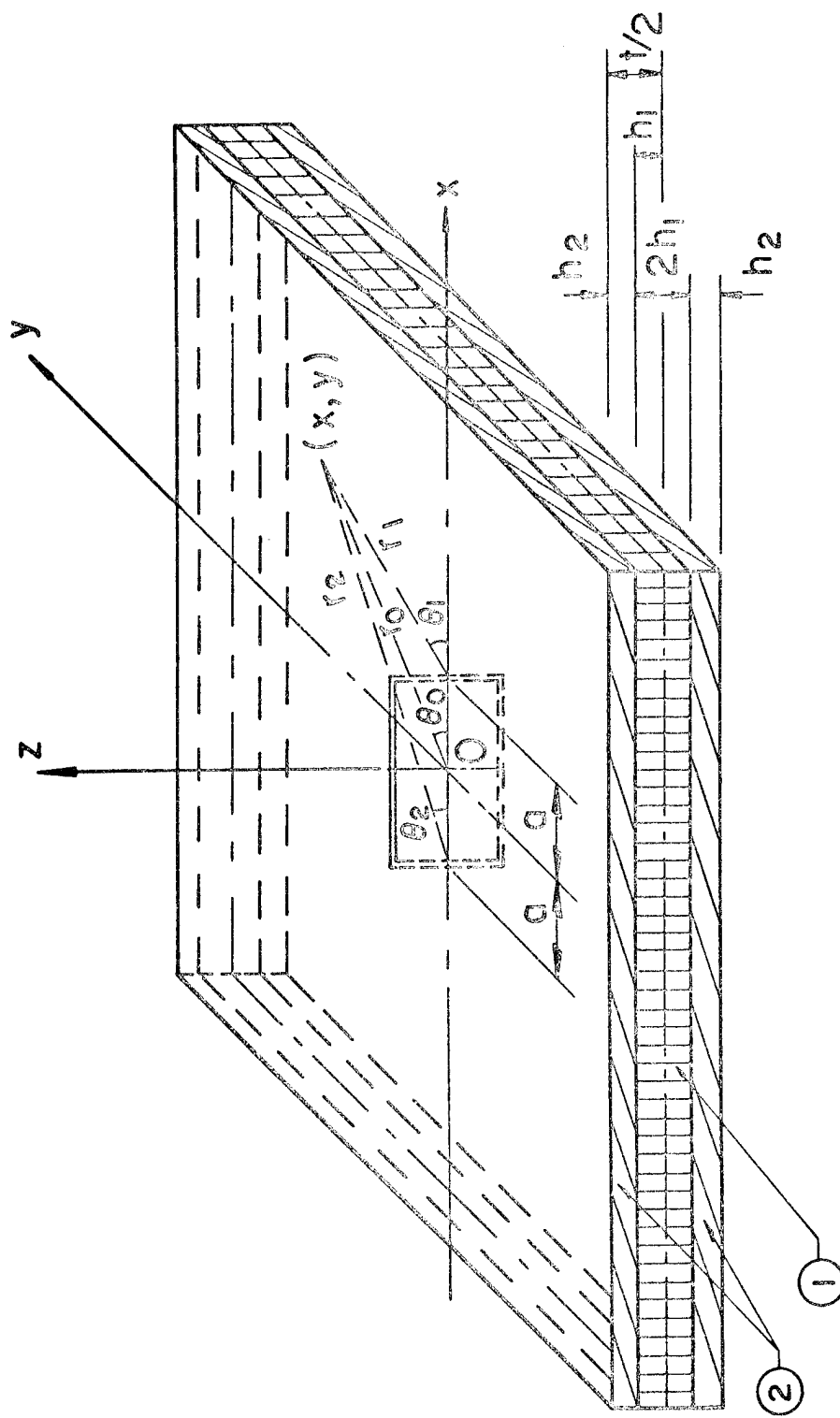
Figure 3.3.1 — Three Layer Composite Plate Containing a Through Crack
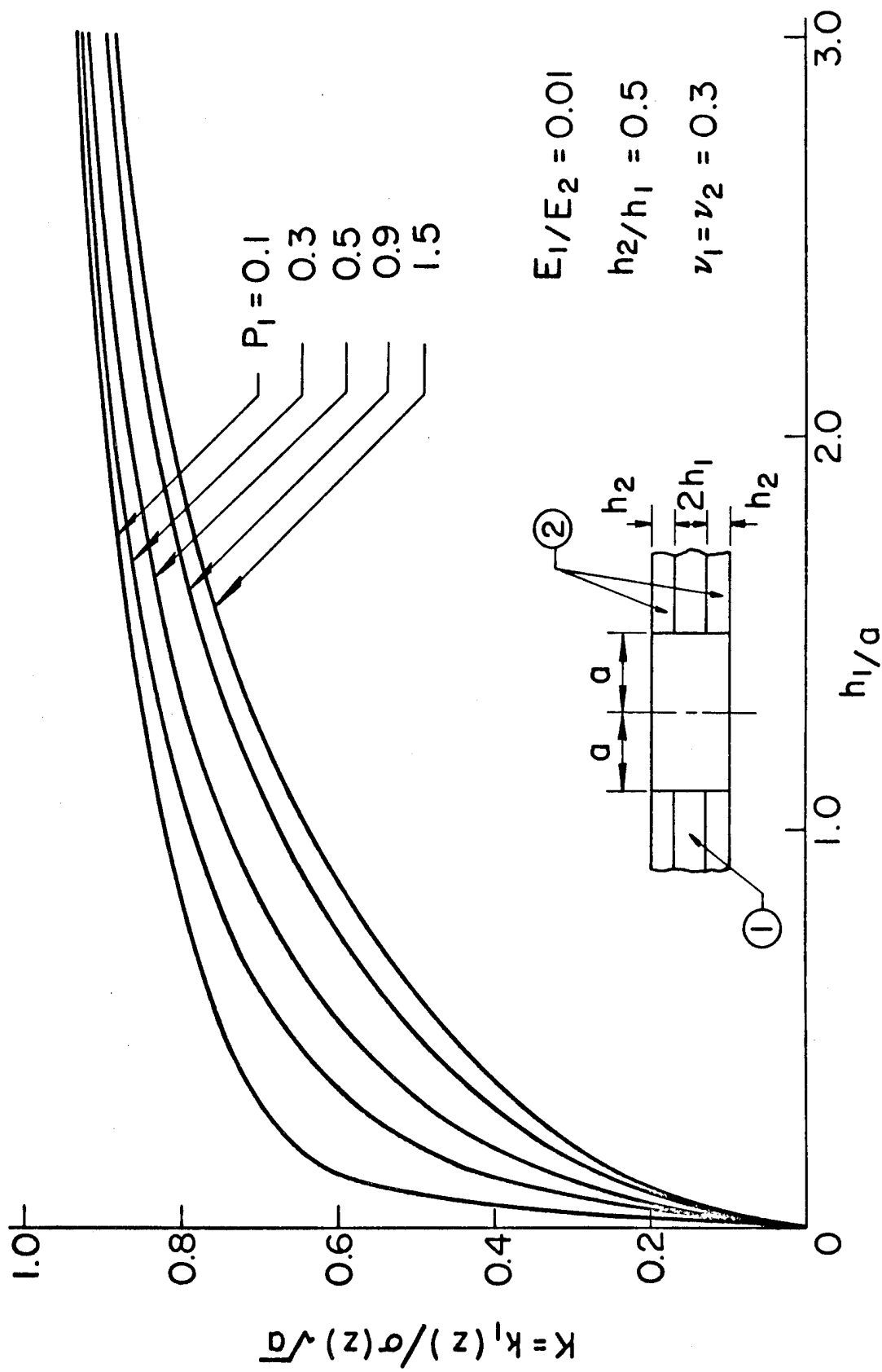
Figure 3.3.3.1 – Dimensionless Stress Intensity Factor as a Function of Normalized Layer Thickness for Formulation without Boundary Layer
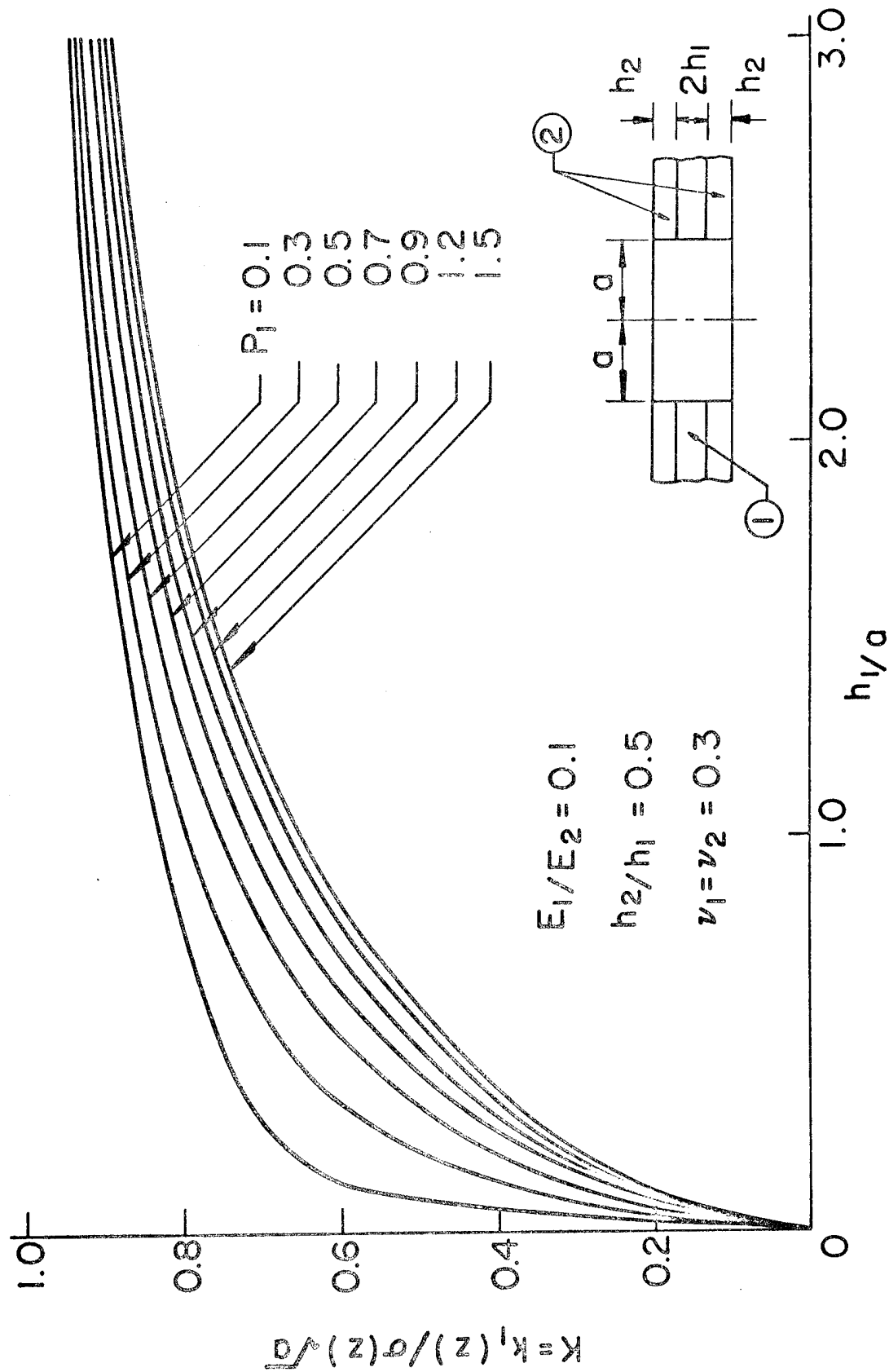
Figure 3.3.3.2 – Dimensionless Stress Intensity Factor as a Function of Normalized Layer Thickness for Formulation without Boundary Layer
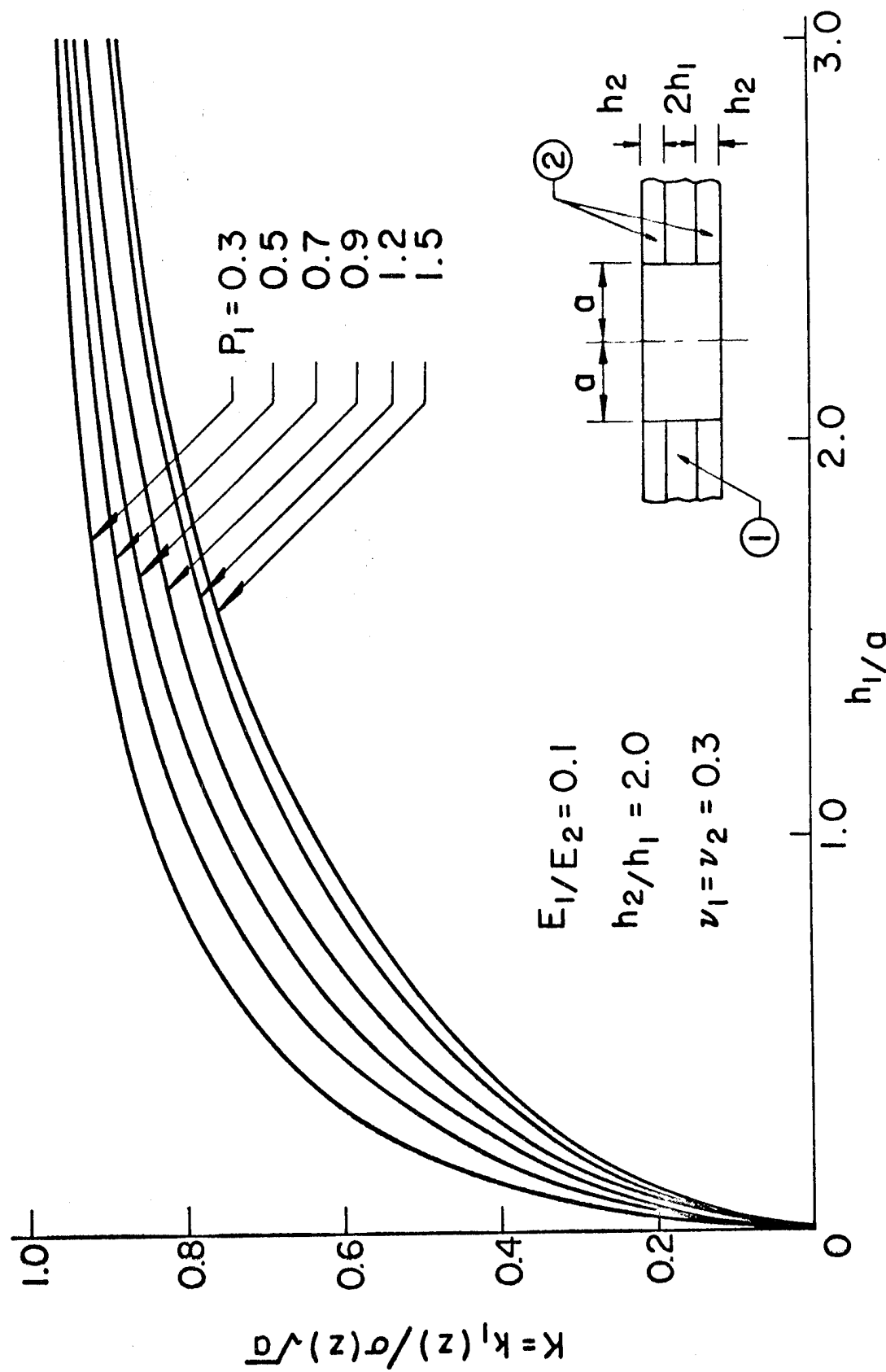
Figure 3.3.3.3 – Dimensionless Stress Intensity Factor as a Function of Normalized Layer Thickness for Formulation without Boundary Layer
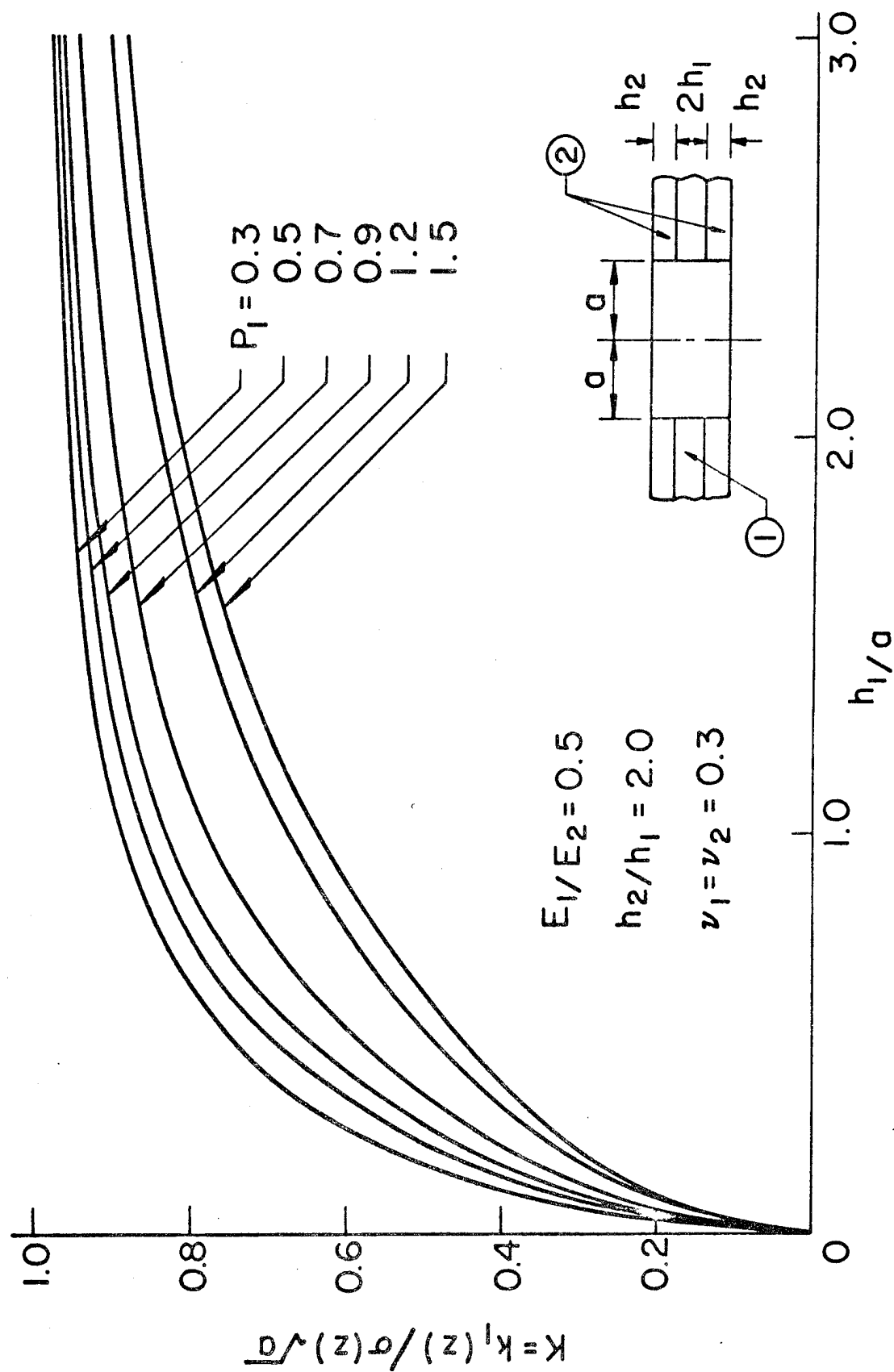
Figure 3.3.3.4 - Dimensionless Stress Intensity Factor as a Function of Normalized Layer Thickness for Formulation without Boundary Layer
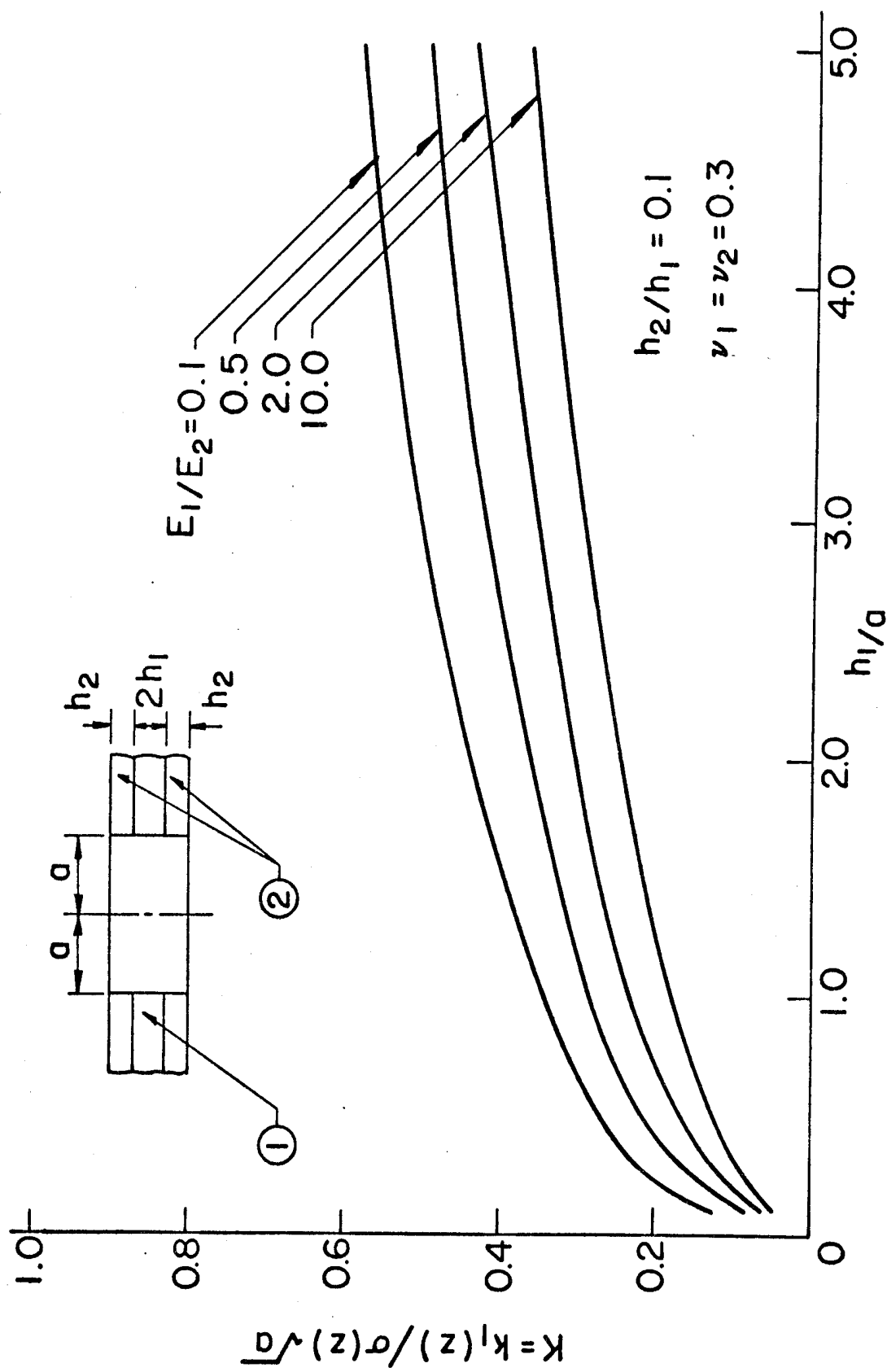
Figure 3.3.3.5 — Dimensionless Stress Intensity Factor at Various Ratios of Material Stiffness for Formulation including Boundary Layers
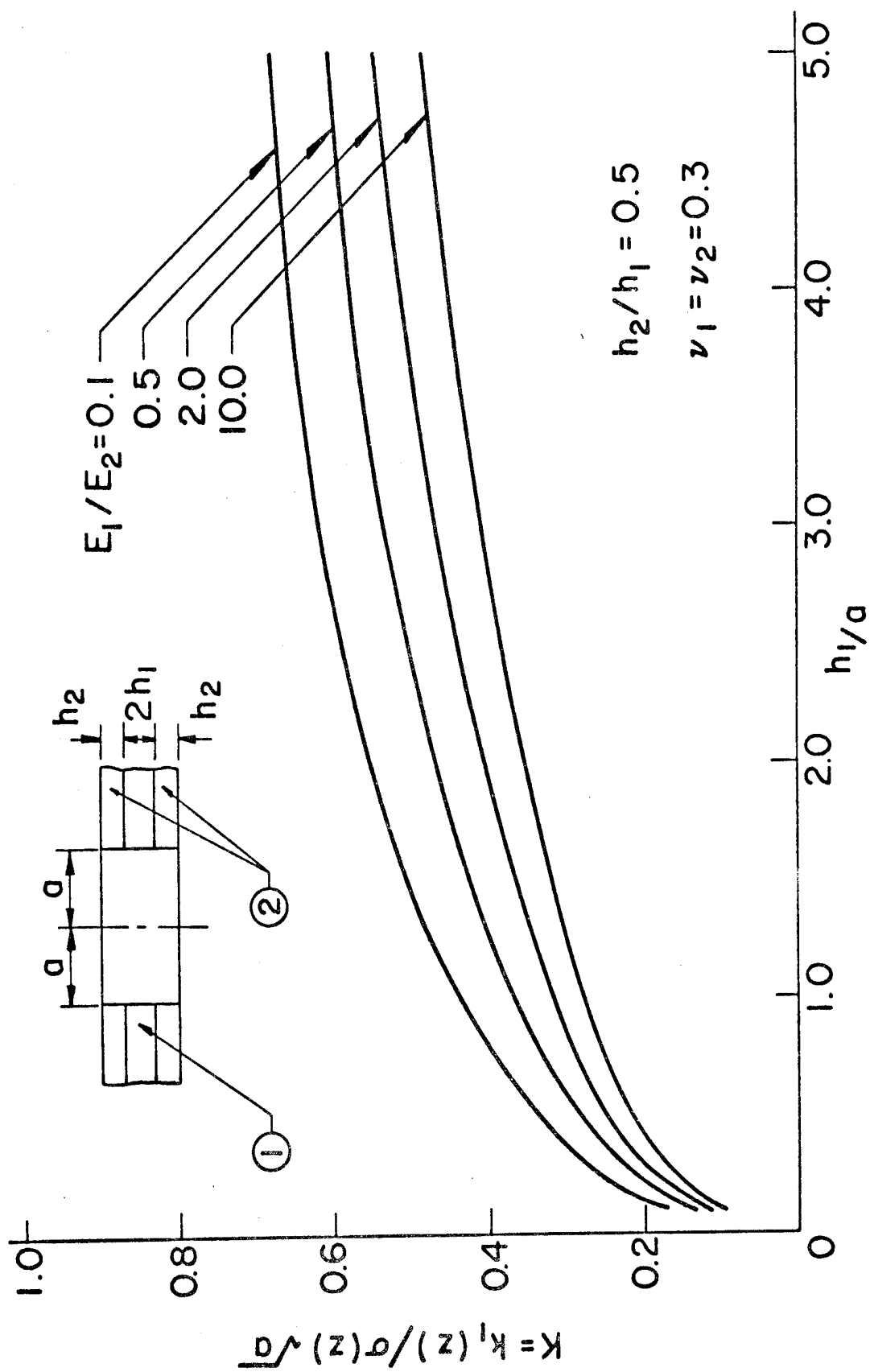
Figure 3.3.3.6 - Dimensionless Stress Intensity Factor at Various Ratios of Material Stiffness for Formulation including Boundary Layers
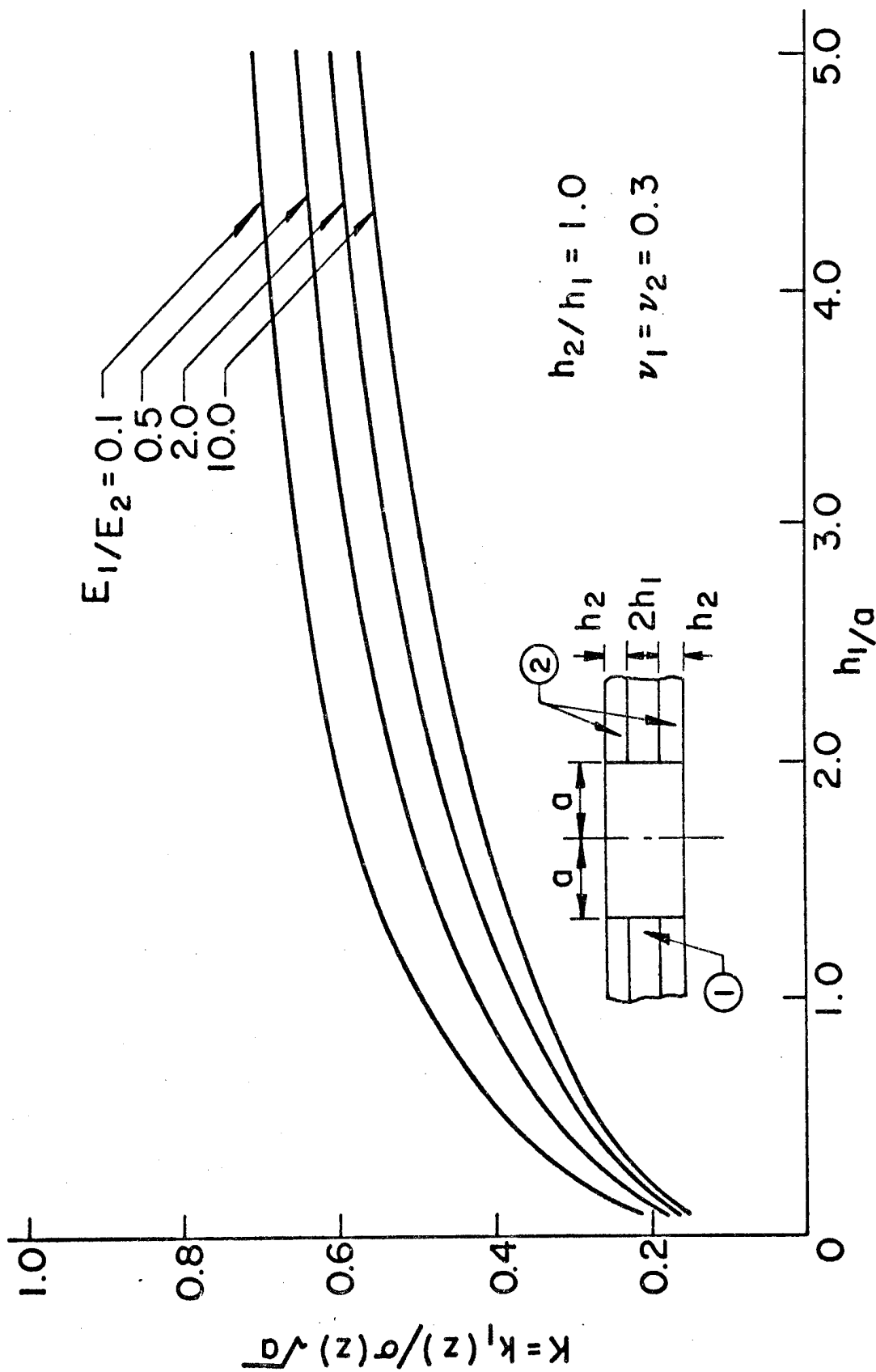
Figure 3.3.3.7 - Dimensionless Stress Intensity Factor at Various Ratios of Material Stiffness for Formulation including Boundary Layers
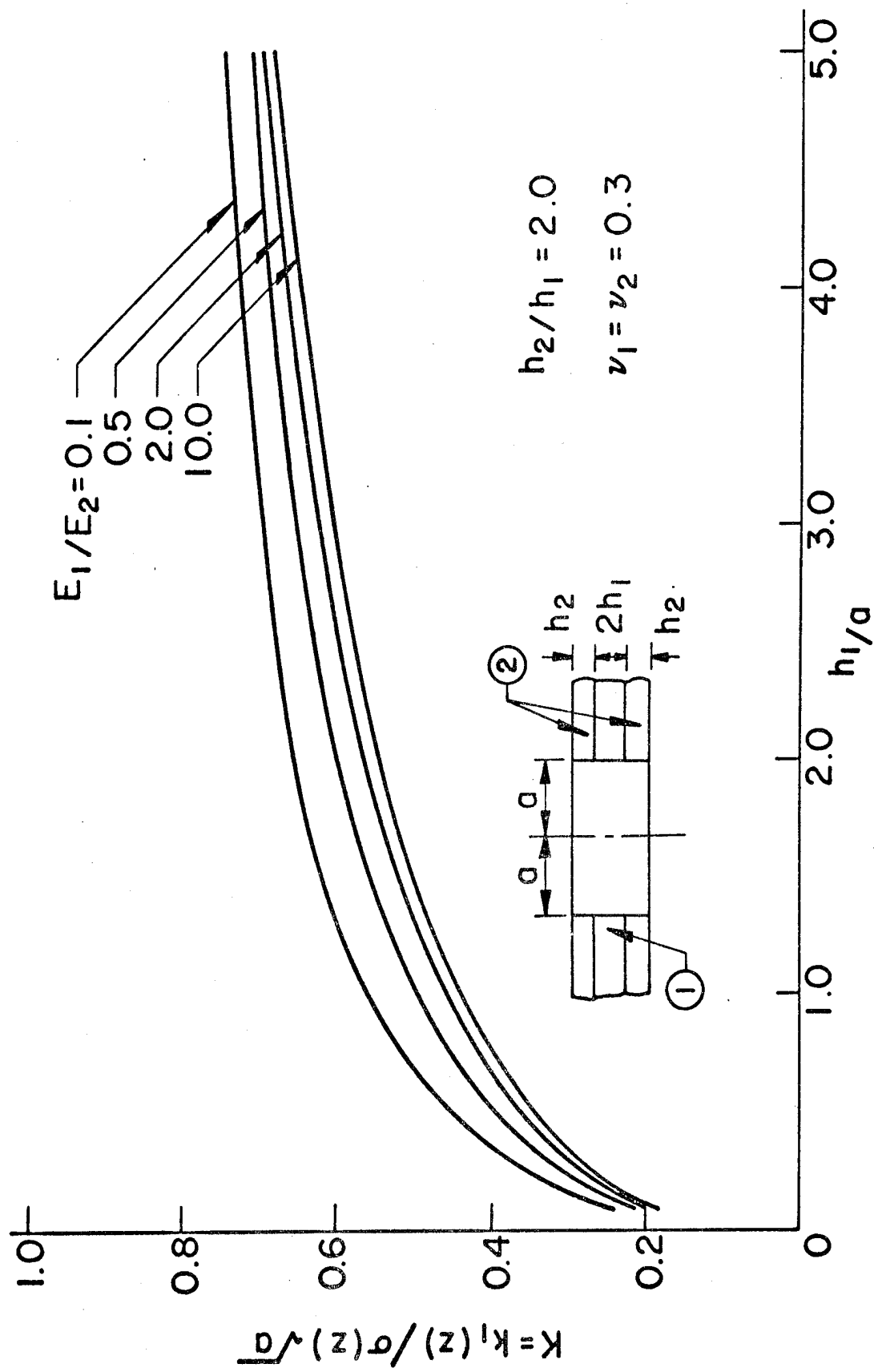
Figure 3.3.3.8 – Dimensionless Stress Intensity Factor at Various Ratios of Material Stiffness for Formulation including Boundary Layers

$E_1/E_2 = 0.1$

10.0

$h_2/h_1 = 10.0$

$\nu_1 = \nu_2 = 0.3$

h_2
$2h_1$
h_2

②

a

a

①

h_1/a

$K = k_1(z)/\sigma(z)\sqrt{a}$

1.0

0.8

0.6

0.4

0.2

0

1.0   2.0   3.0   4.0   5.0
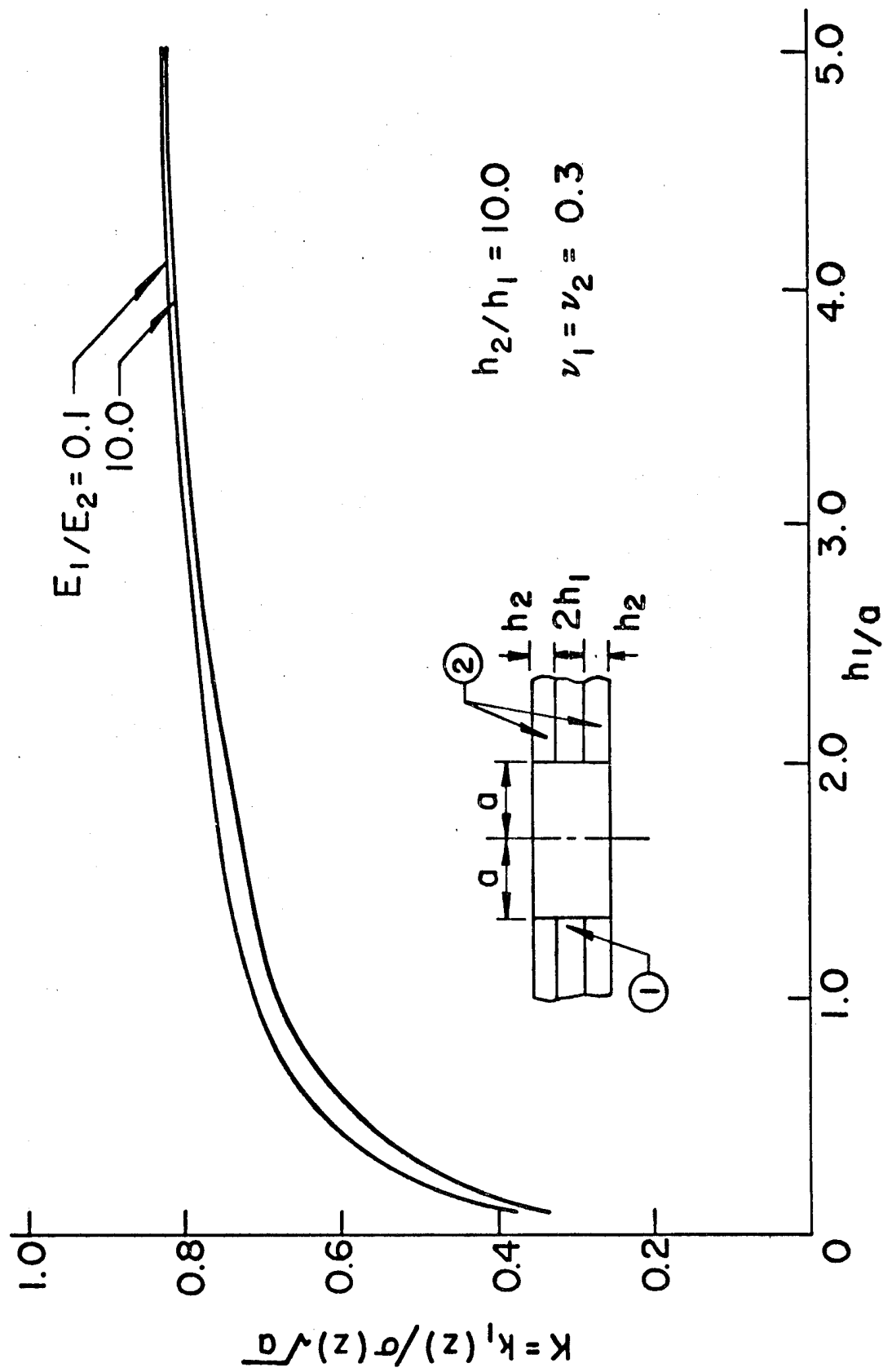
Figure 3.3.3.9 – Dimensionless Stress Intensity Factor at Various Ratios of Material Stiffness for Formulation including Boundary Layers
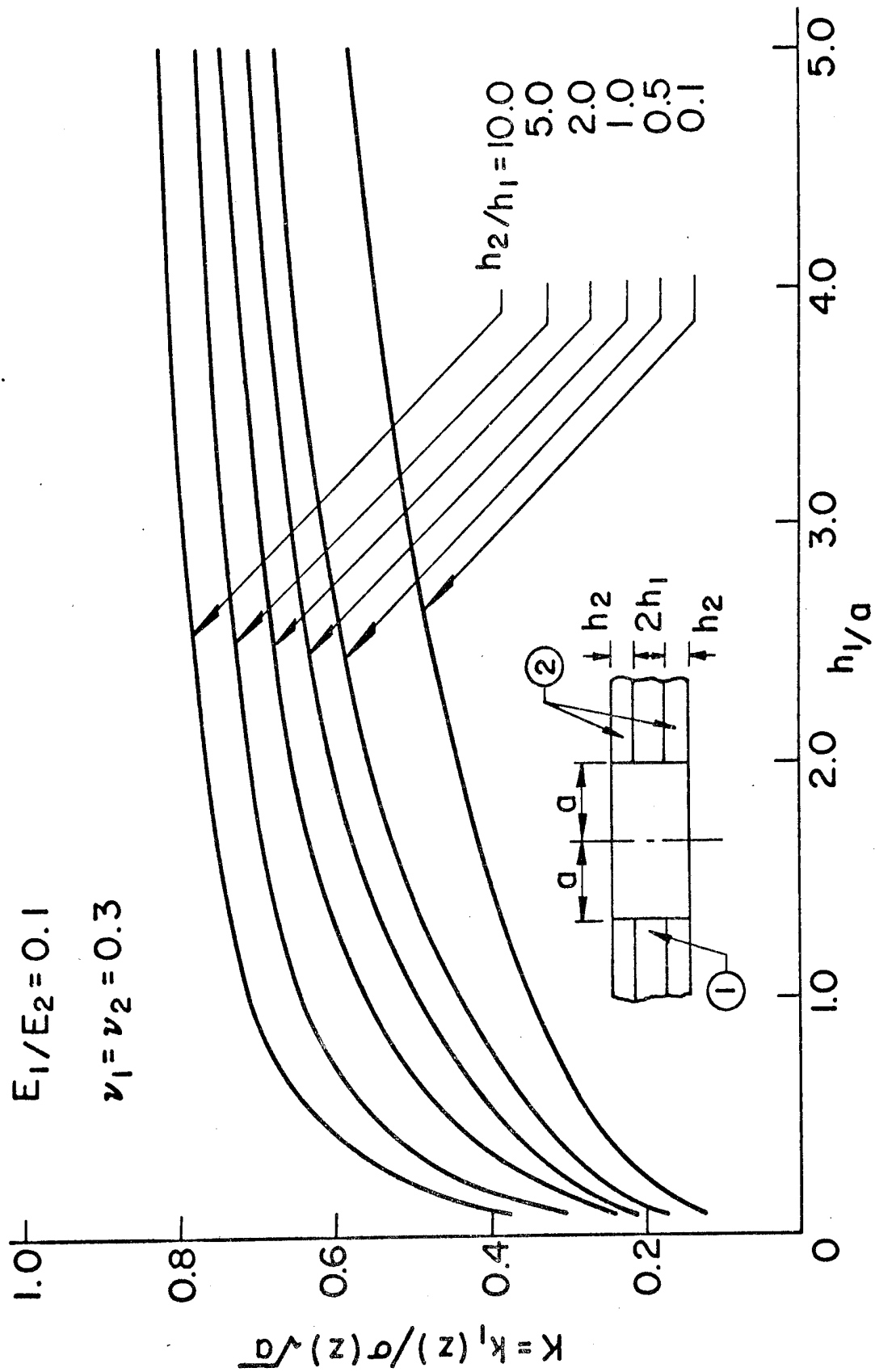
Figure 3.3.3.10 – Influence of Relative Layer Thickness on Normalized Stress Intensity Factor
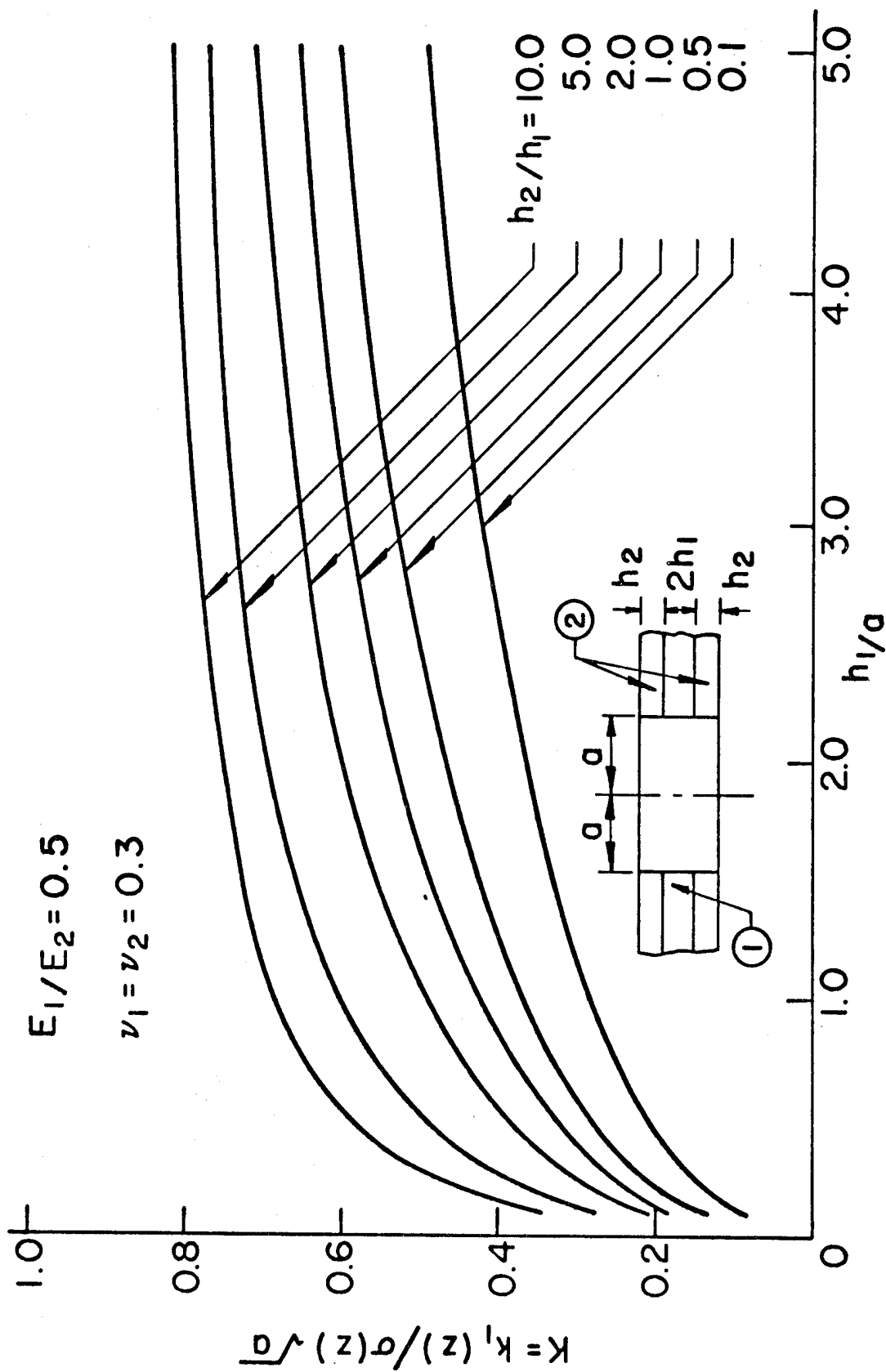
Figure 3.3.3.11 - Influence of Relative Layer Thickness on Normalized Stress Intensity Factor

$E_1/E_2 = 2.0$

$\nu_1 = \nu_2 = 0.3$

$h_2/h_1 = 10.0$
5.0
2.0
1.0
0.5
0.1

h_1/a

$K = k_1(z)/\sigma(z)\sqrt{a}$

h_2
$2h_1$
h_2
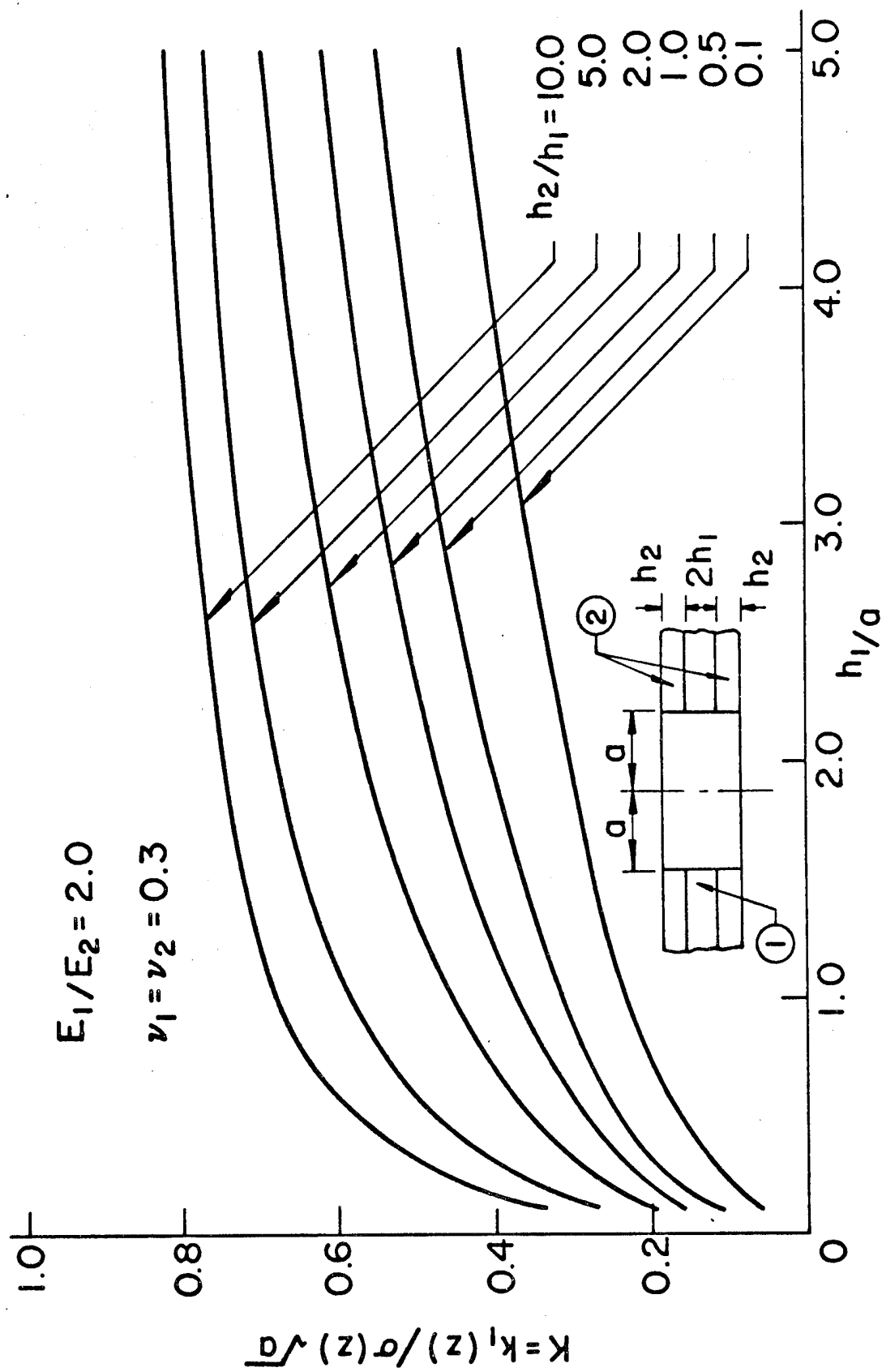
Figure 3.3.3.12 - Influence of Relative Layer Thickness on Normalized Stress Intensity Factor
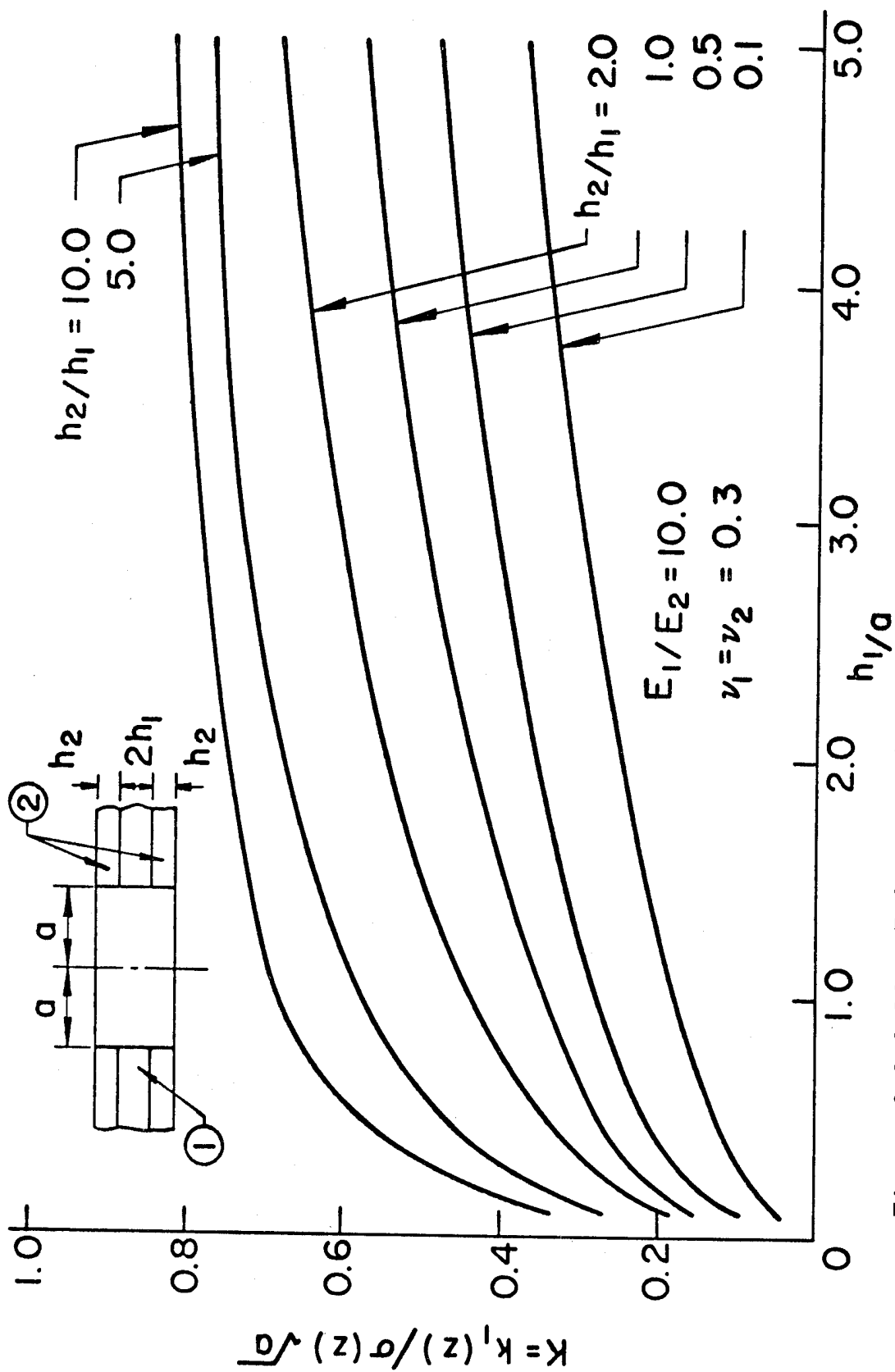
Figure 3.3.3.13 - Influence of Relative Layer Thickness on Normalized Stress Intensity Factor
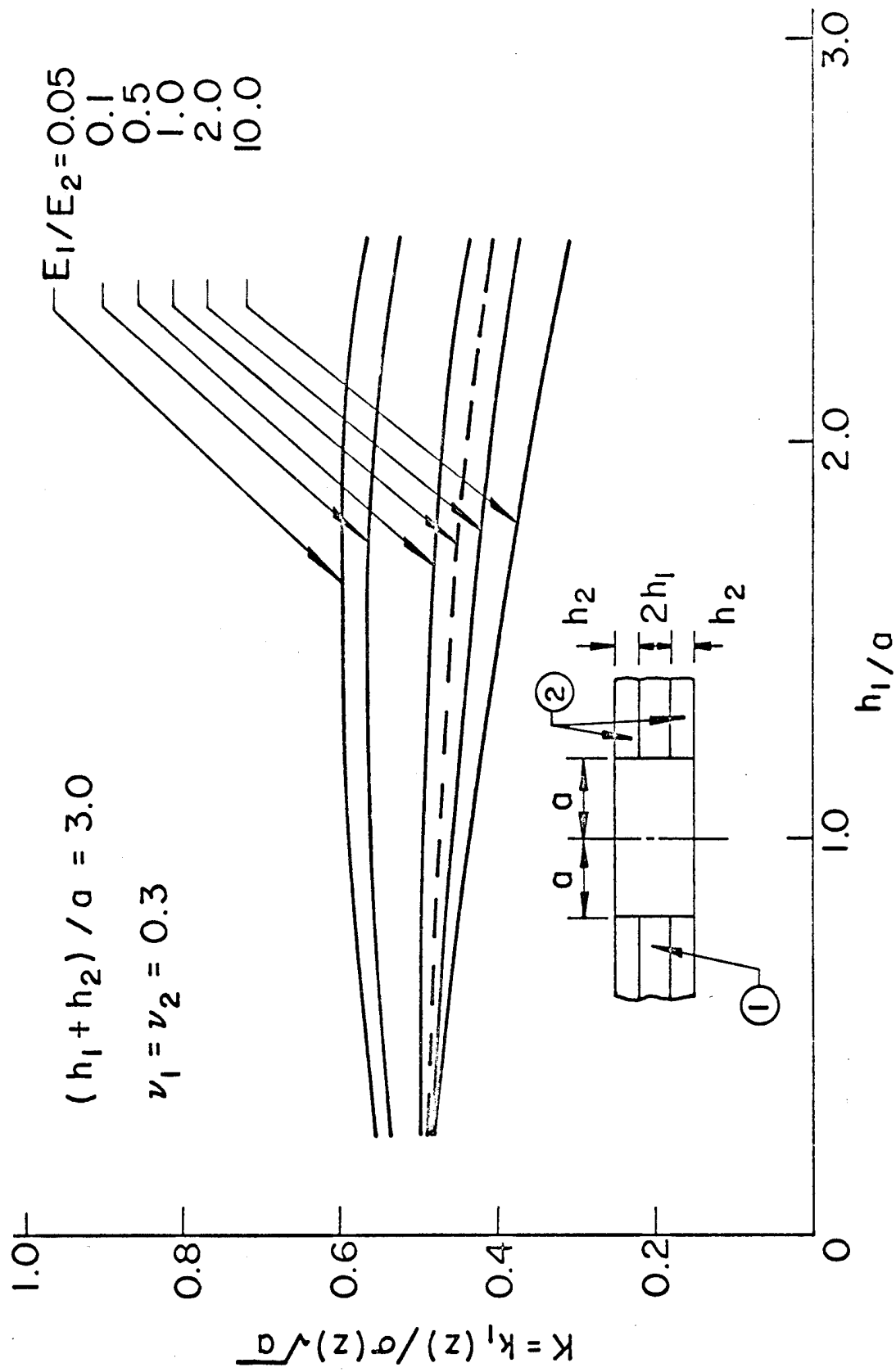
Figure 3.3.3.14 – Influence of Relative Layer Stiffness and Thickness on Stress Intensity Factor for Constant Normalized Plate Thickness
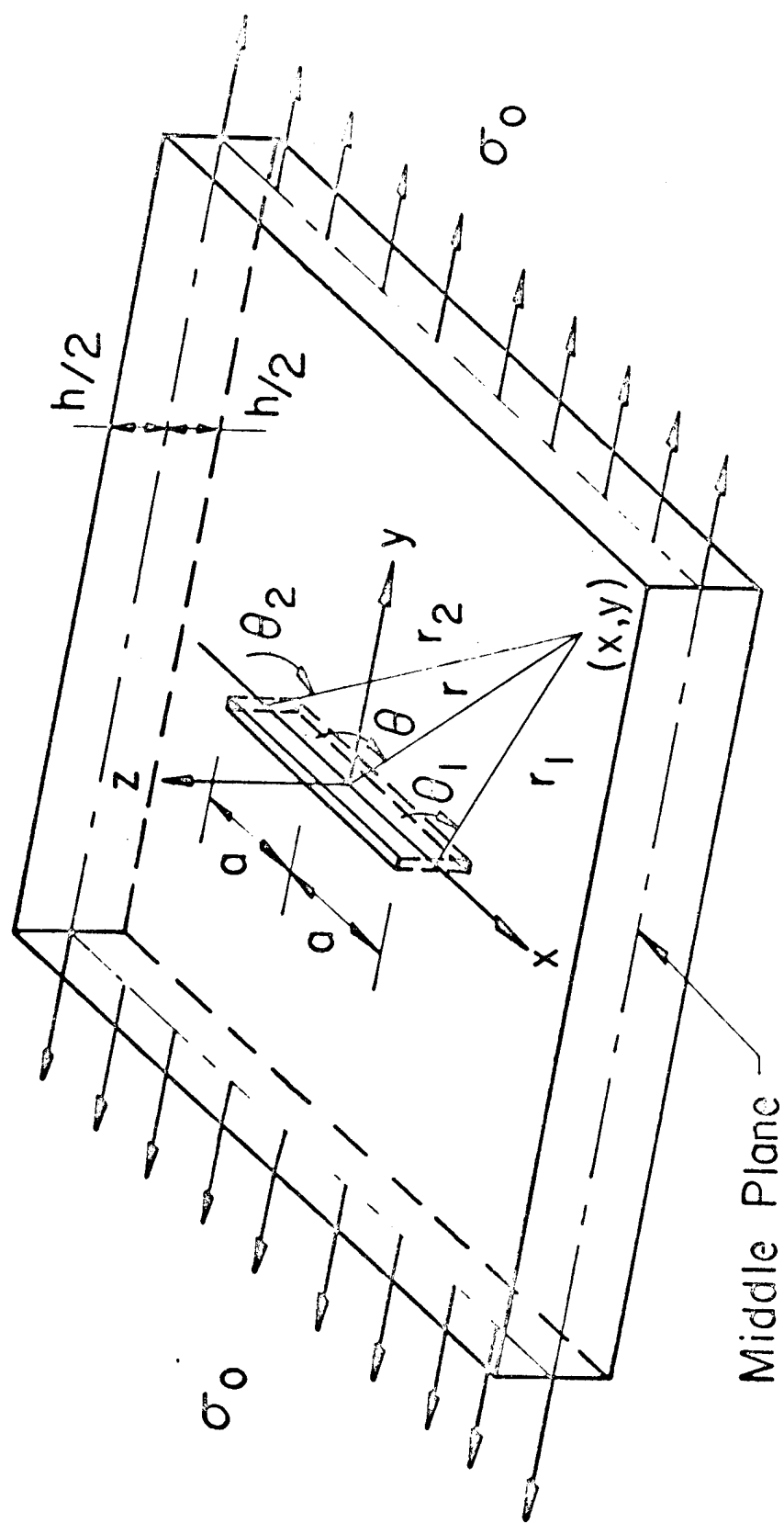
Figure 4.1 – A Central Crack in an Infinite Plate
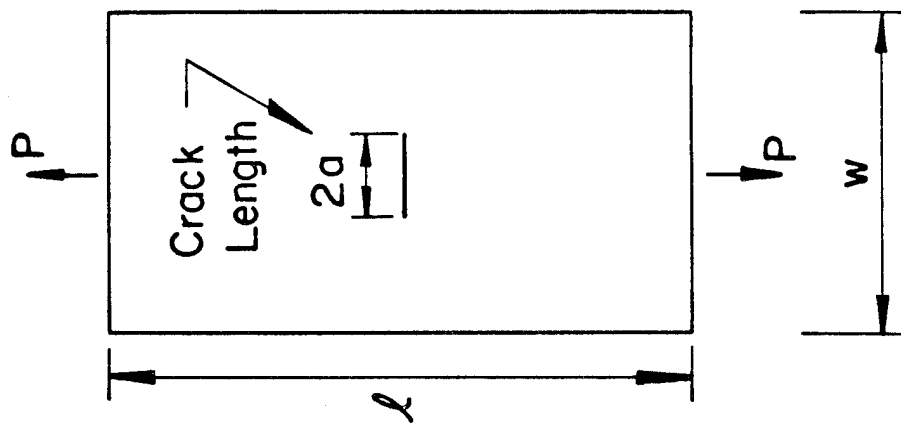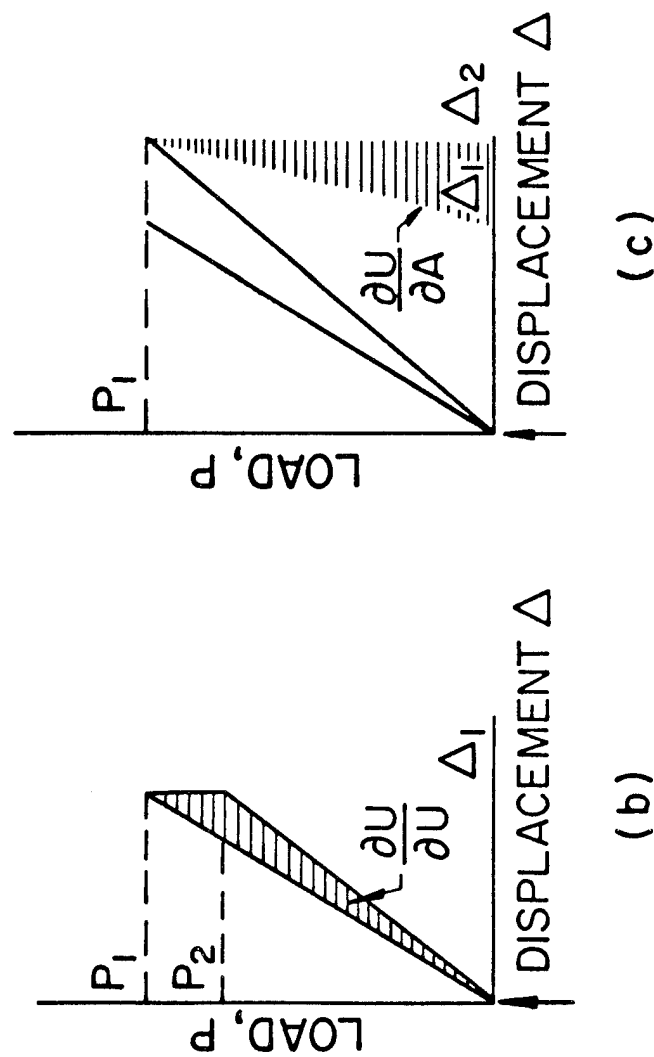
Figure 4.2a – Plate Containing a Central Crack

Figure 4.2b – Load-Displacement Curve for Constant Displacement During Crack Extension

Figure 4.2c – Load-Displacement Curve for Constant Load During Crack Extension
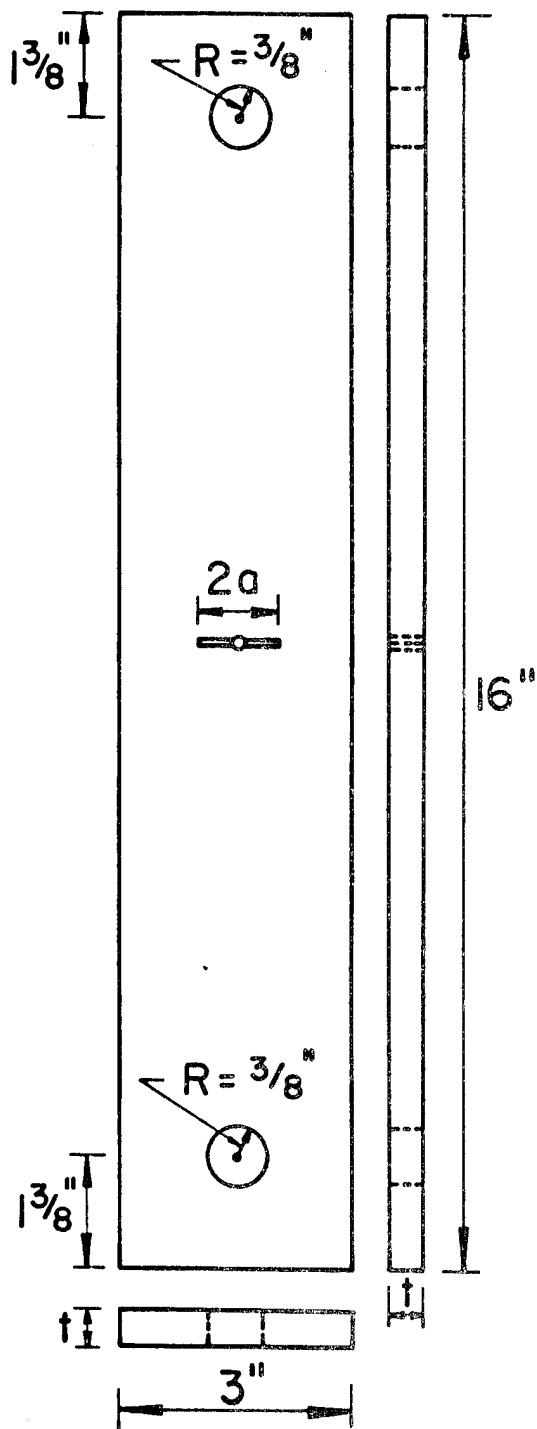
This specimen was designed for

$t = \frac{1}{16}", \frac{1}{8}", \frac{1}{4}", \frac{3}{8}", \frac{1}{2}", \frac{5}{8}", \frac{3}{4}"$

and

$2a = \frac{1}{4}", \frac{1}{2}", \frac{3}{4}", 1", 1\frac{1}{4}", 1\frac{1}{2}"$

Figure 4.3 – Specimen Geometry
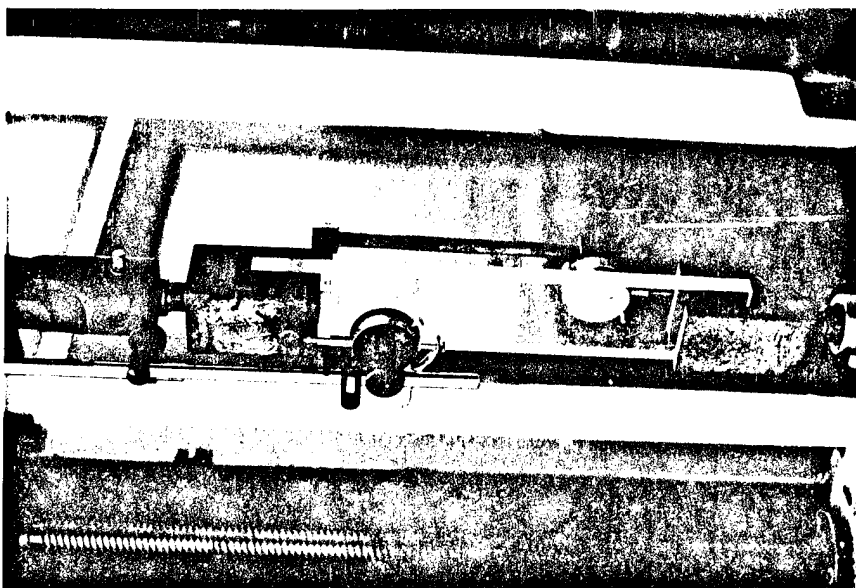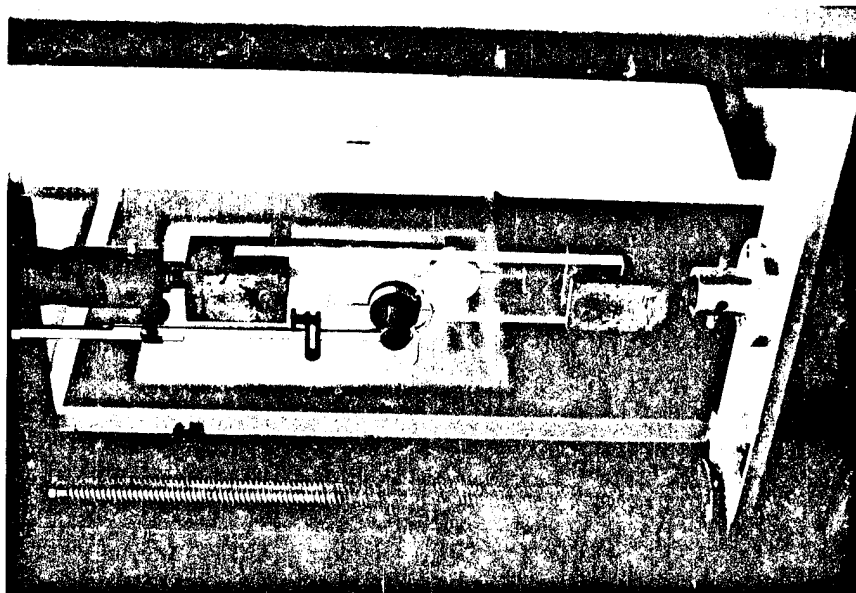
Figure 4.4 - Testing Details
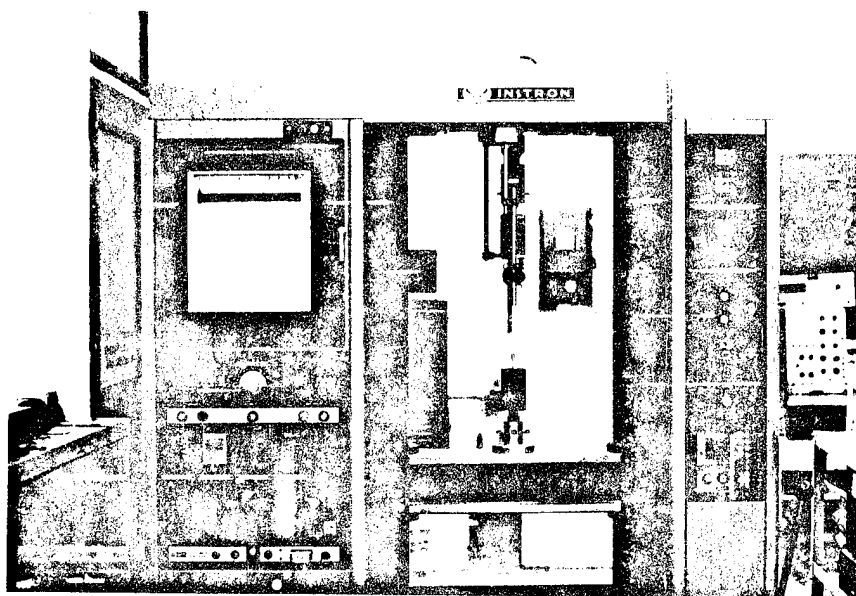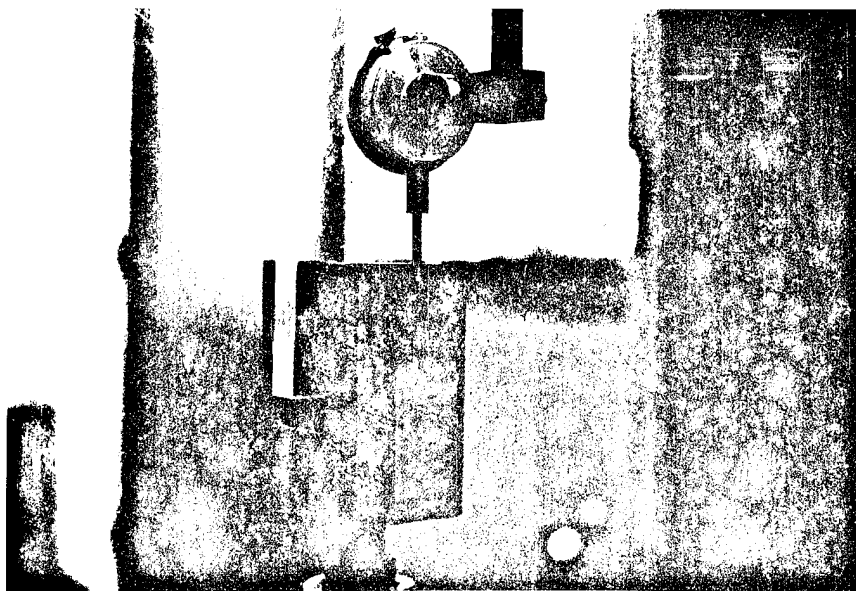
Figure 4.5 - Testing Details
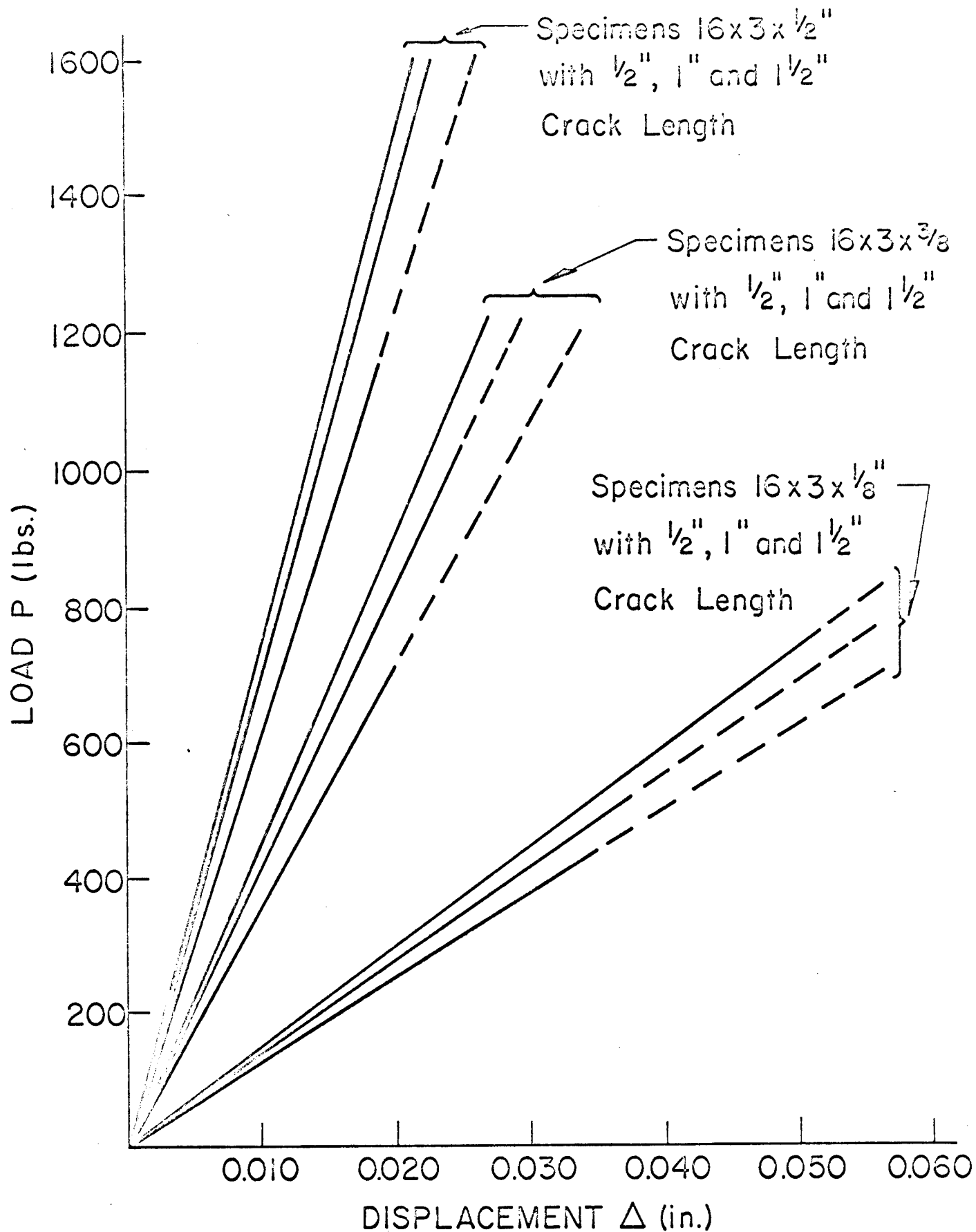
Figure 4.6 - Load-Displacement Curves
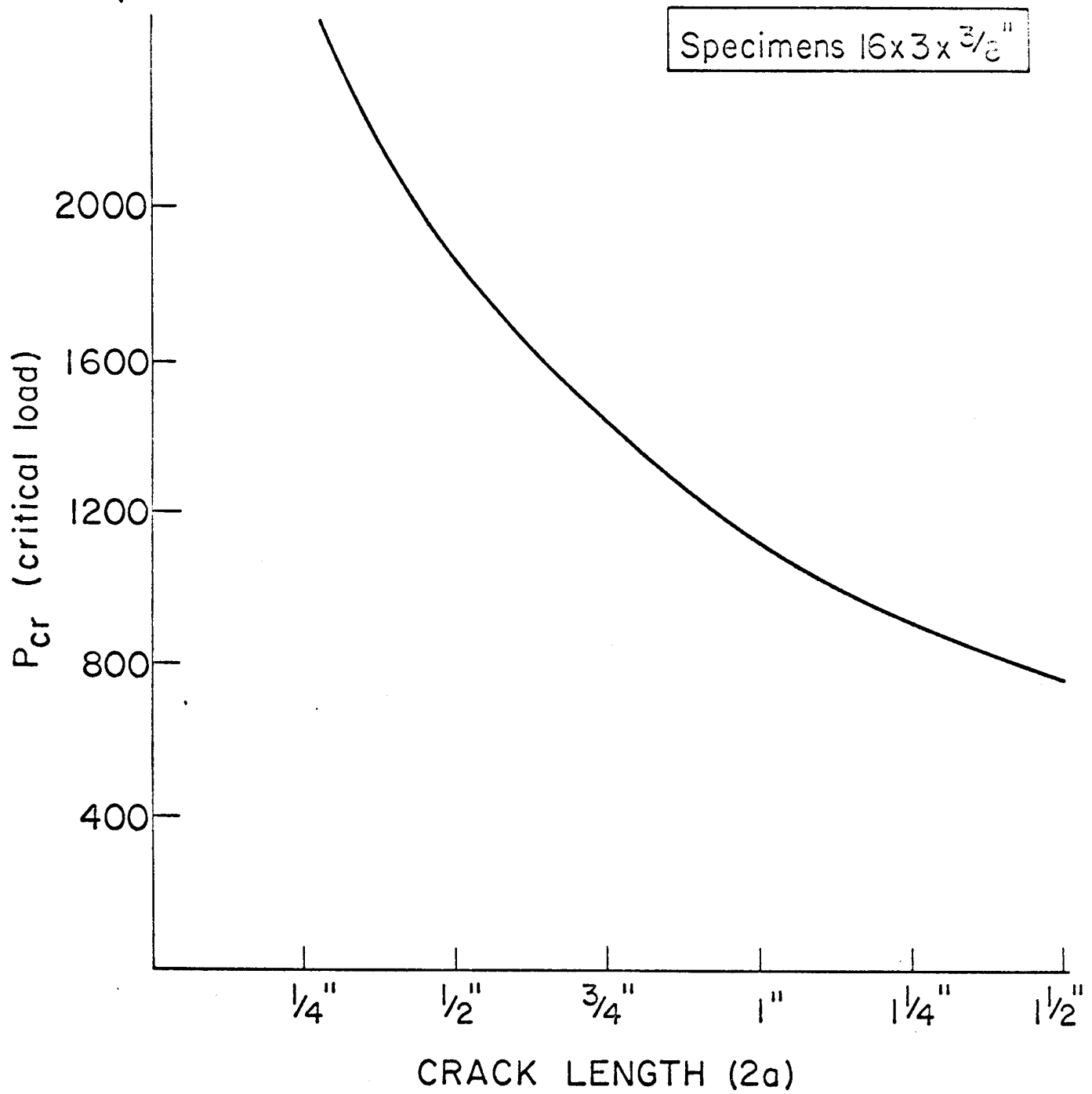
Figure 4.7 - Critical Load as a Function of Crack Length
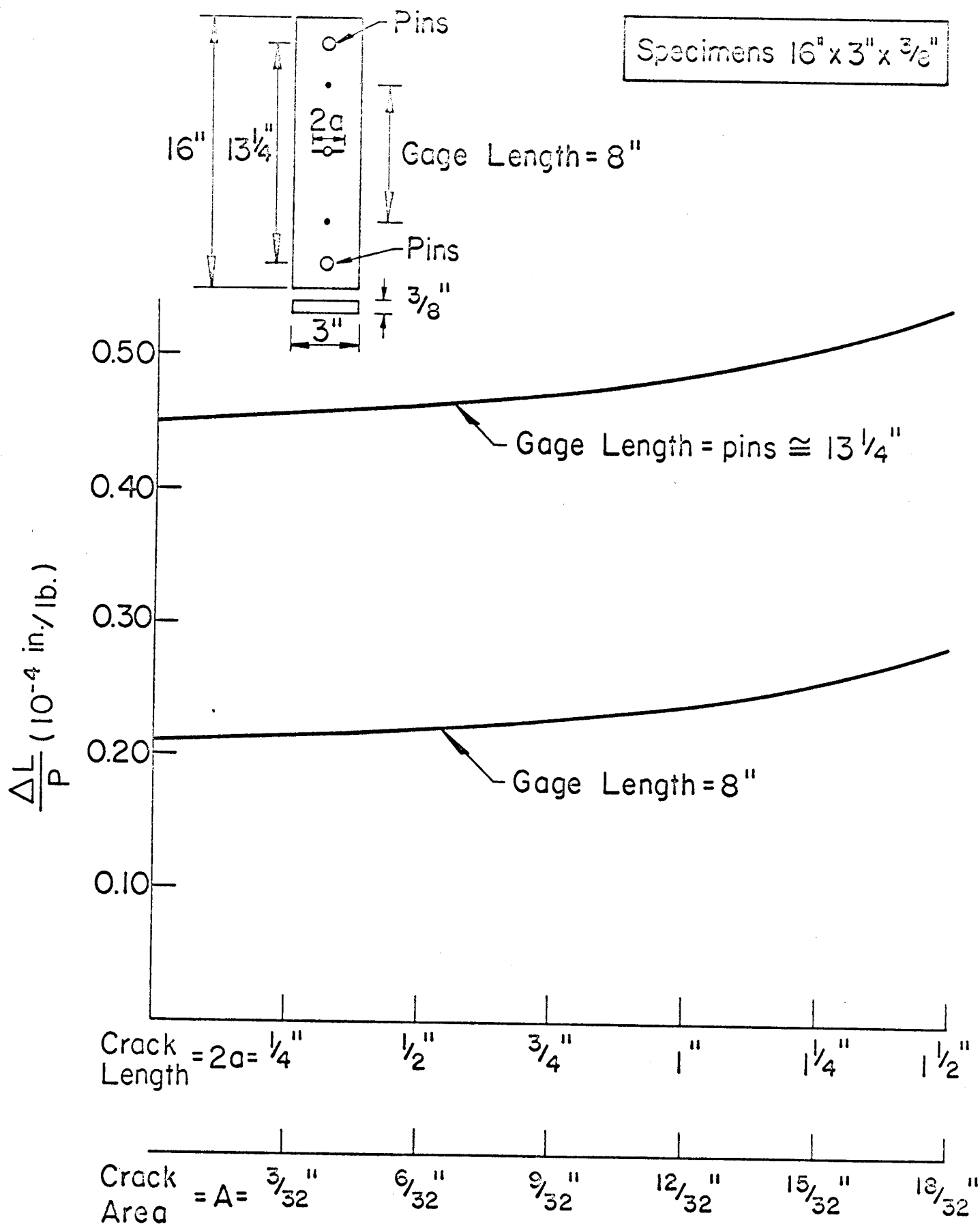
Figure 4.8 - Compliance Curves for 3/8" Specimens

Plexiglas G (Acrylic Sheet)

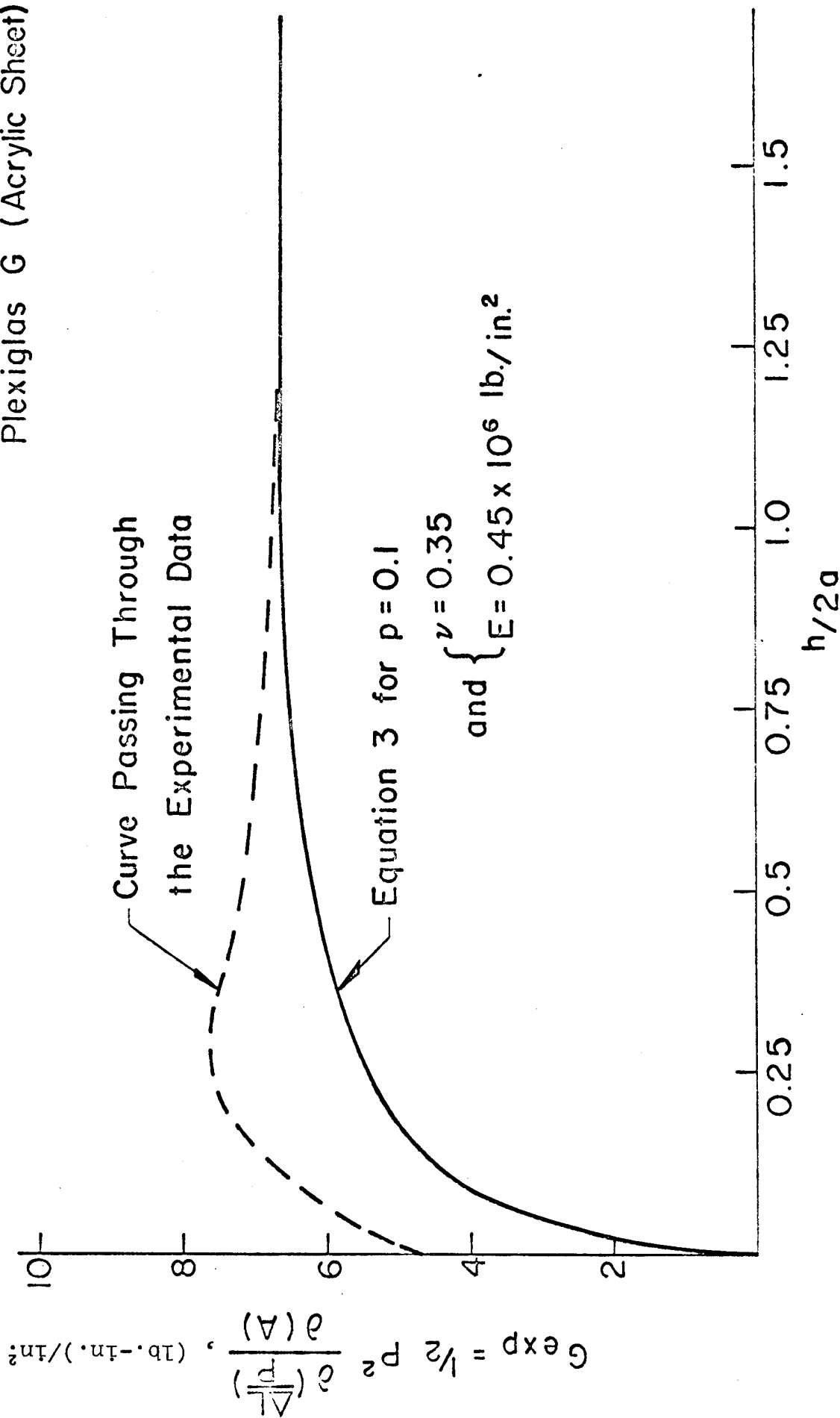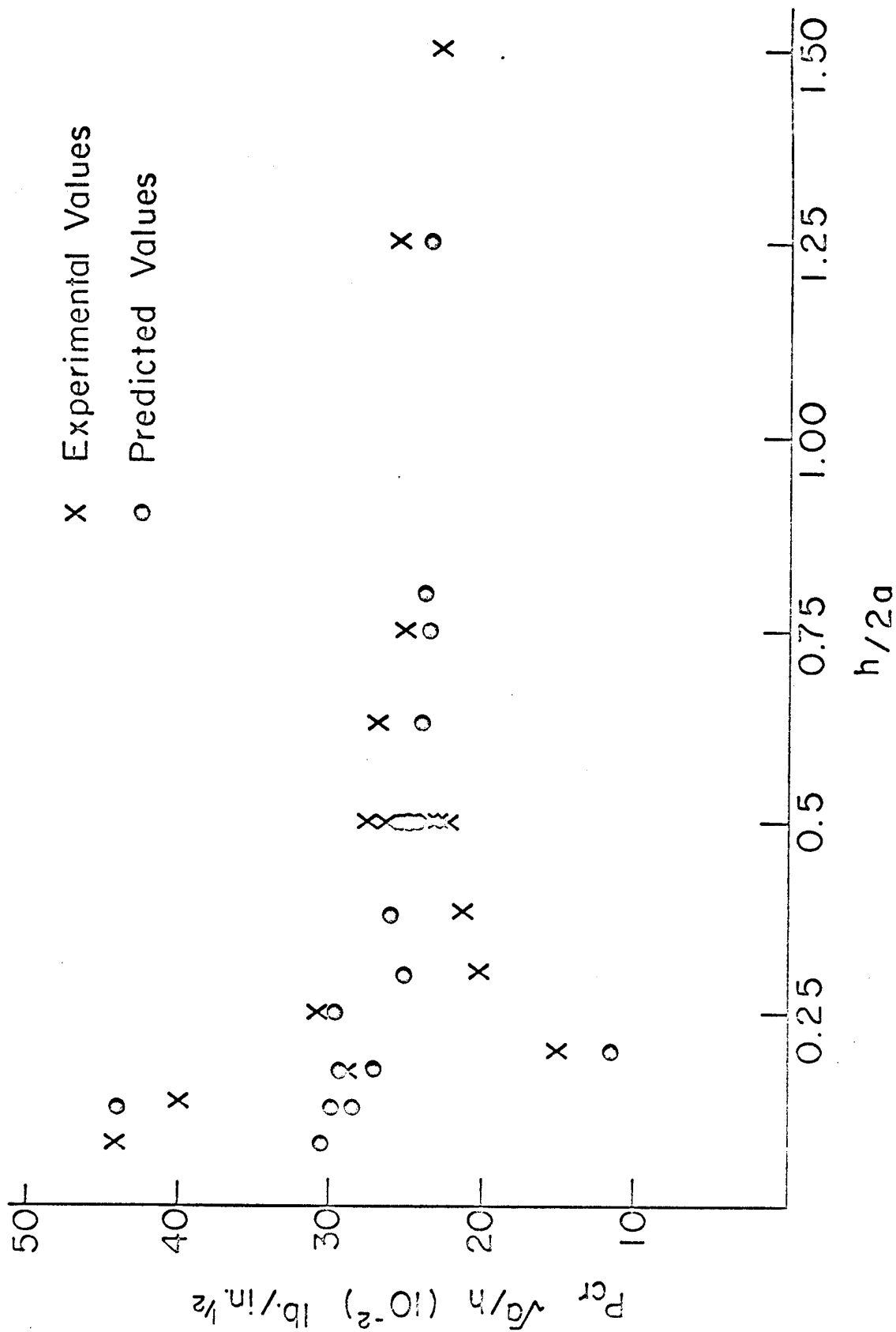$$G_{exp} = \frac{1}{2} P^2 \frac{\partial \left(\frac{\Delta L}{P}\right)}{\partial (A)}, \quad (lb.-in.)/in.^2$$

Curve Passing Through
the Experimental Data

Equation 3 for p = 0.1

$\nu = 0.35$
and $\left\{ E = 0.45 \times 10^6 \ lb./in.^2 \right.$

h/2a

Figure 4.9 – Strain Energy Release Rate as a Function of Normalized
Plate Thickness

4.10 - Comparison of Predicted and Observed Critical Loads at Various Ratios of Plate
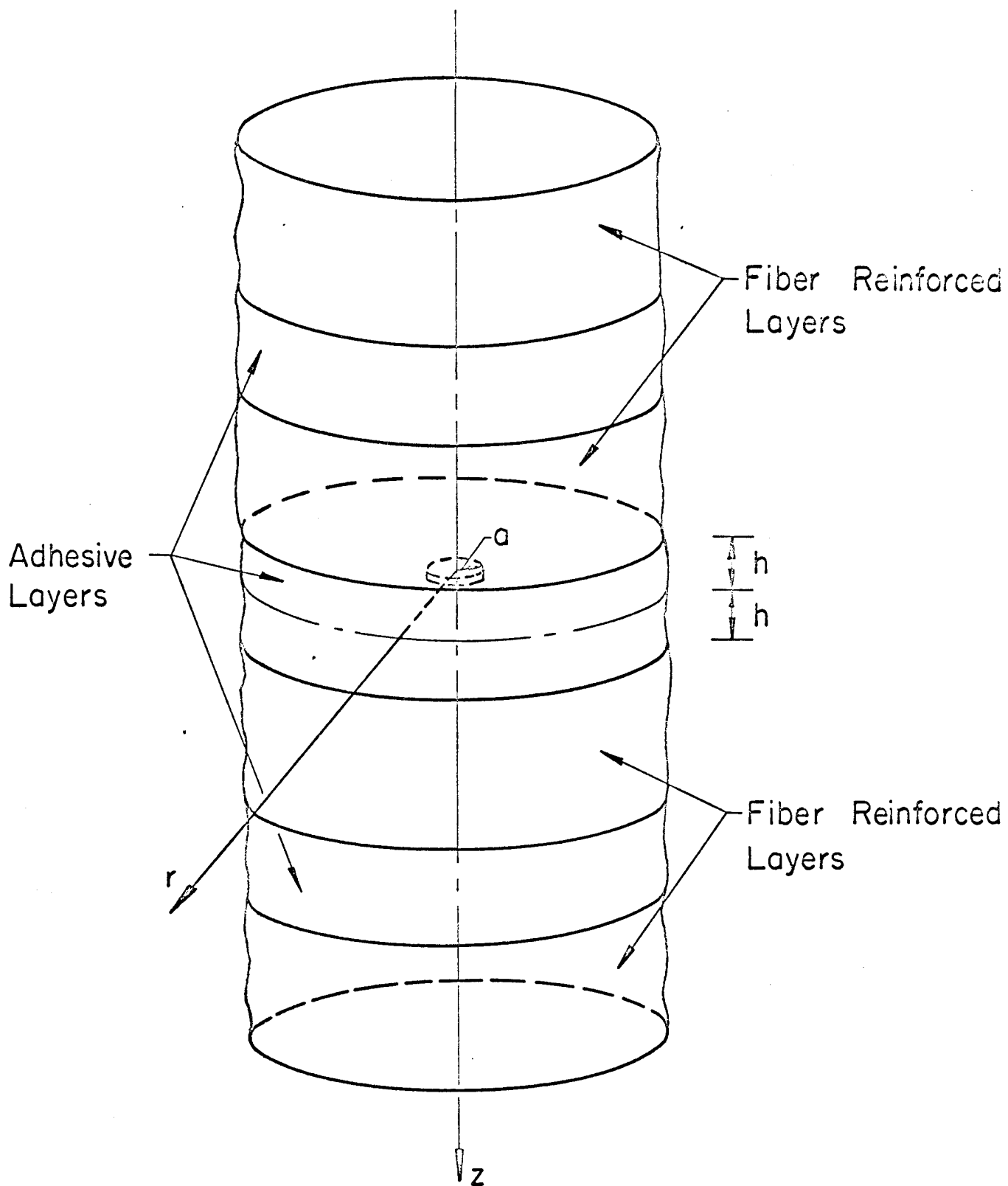   Thickness to Crack Length

Figure 5.1 - A Penny-Shaped Crack in an Adhesive Layer
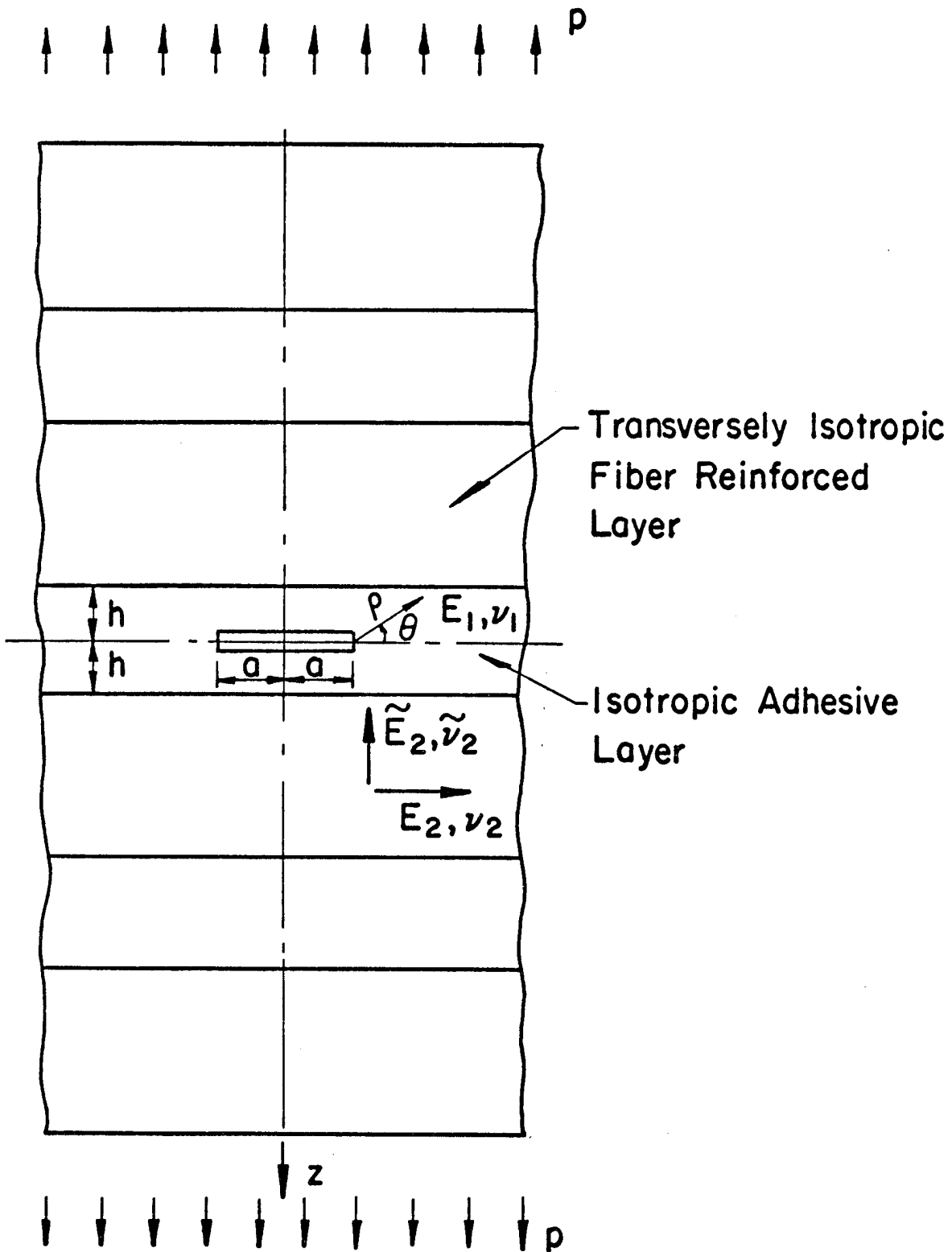Between Fiber Reinforced Layers

Figure 5.2 – Remote Loading for the Composite Cylinder
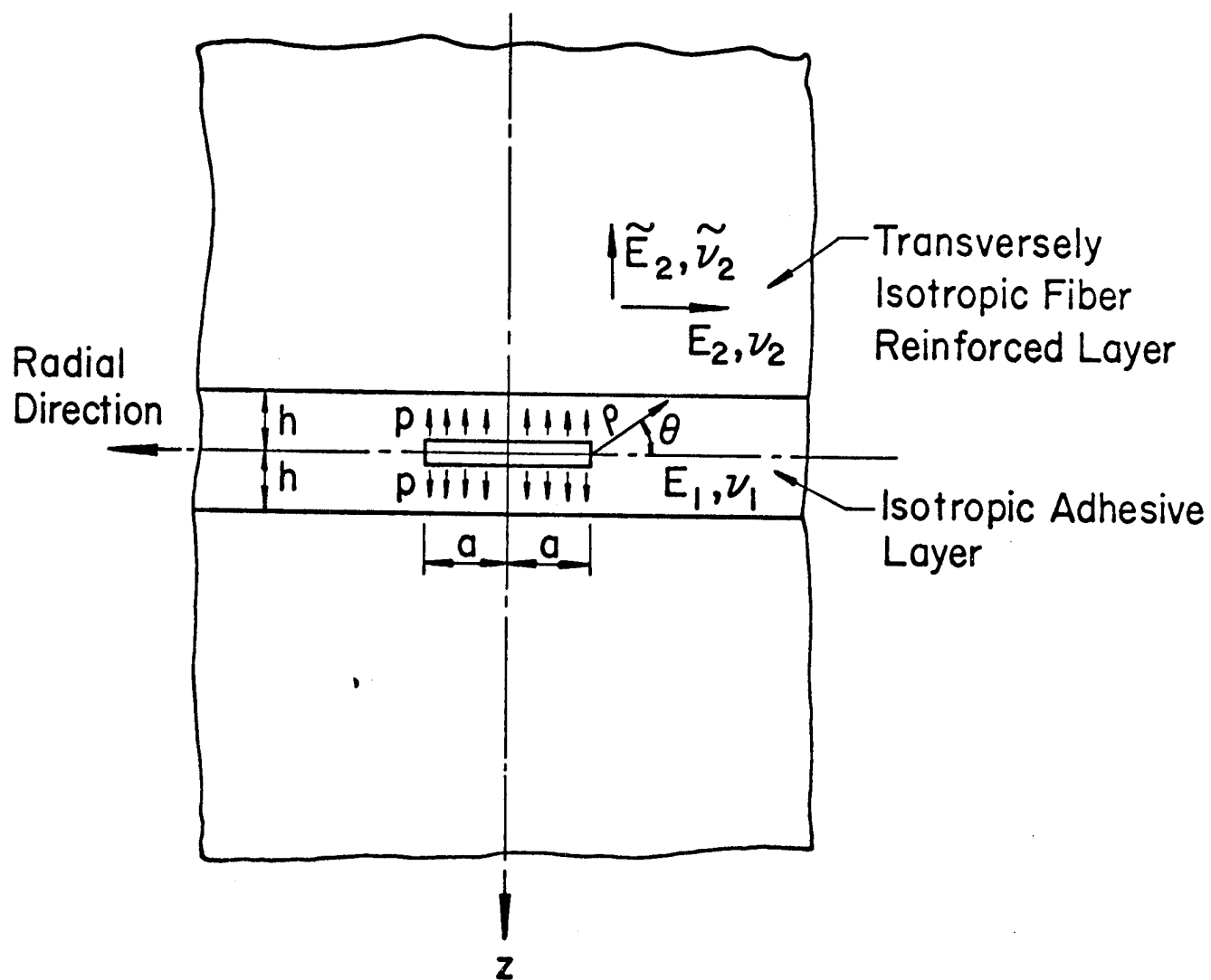Containing a Penny-Shaped Crack in the
Adhesive Layer

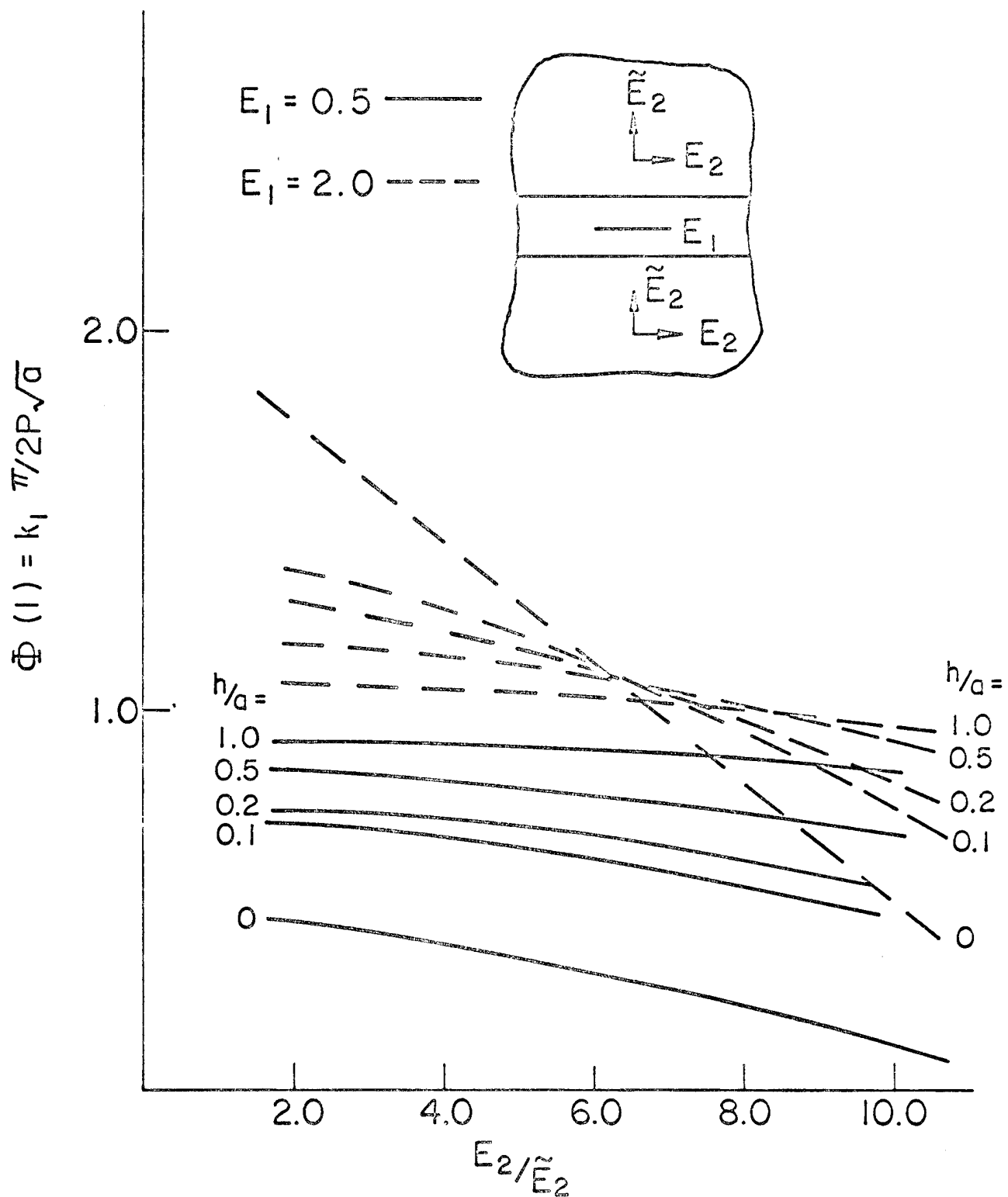Figure 5.3 – Idealized Model for the Composite Containing
a Penny-Shaped Crack

Figure 5.4 – Variation of the Normalized Stress Intensity
Factor with Material Properties and Relative
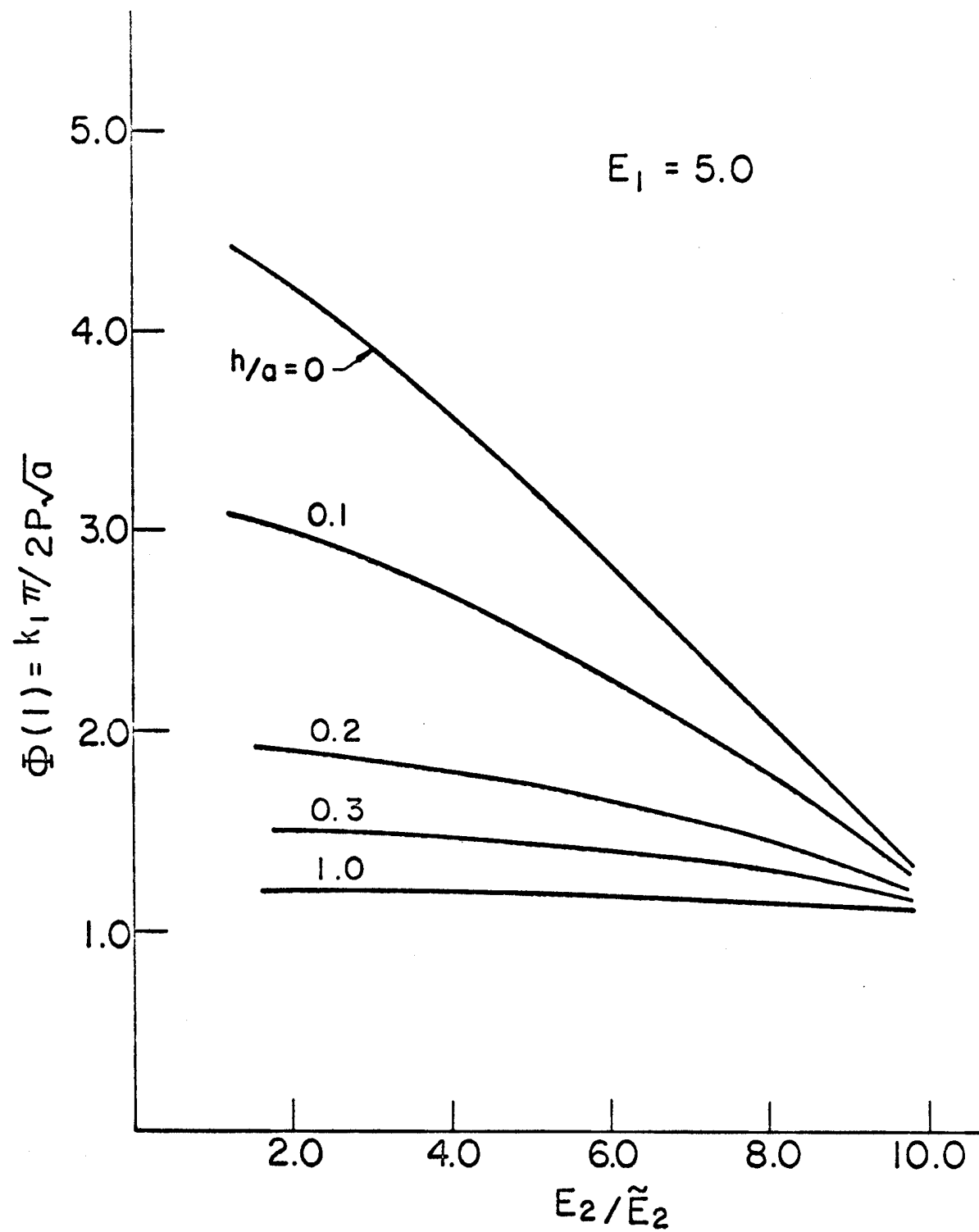Layer Thickness

Figure 5.5 – Variation of the Normalized Stress Intensity
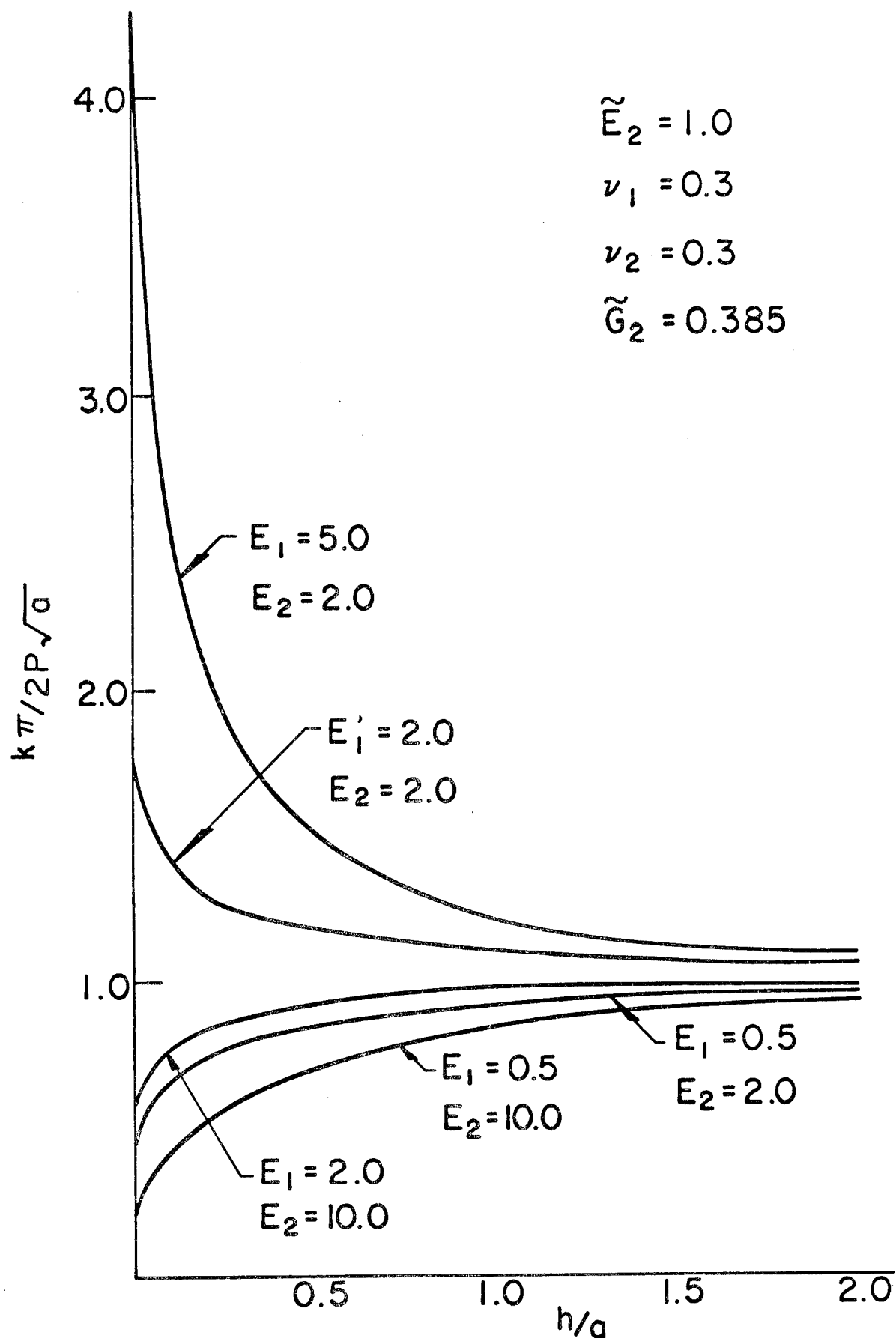Factor with Material Properties and Relative
Layer Thickness

Figure 5.6 – Normalized Stress Intensity Factor as a
Function of Relative Layer Height

DOCUMENT CONTROL DATA - R & D

(Security classification of title, body of abstract and indexing annotation must be entered when the overall report is classified)

1. ORIGINATING ACTIVITY *(Corporate author)*	2a. REPORT SECURITY CLASSIFICATION
Institute of Fracture and Solid Mechanics Lehigh University Bethlehem, Pennsylvania 18015	Unclassified
	2b. GROUP

3. REPORT TITLE

Exploratory Development of Fracture Mechanics of Composite Systems

4. DESCRIPTIVE NOTES *(Type of report and inclusive dates)*

Third Annual Report – July 1971 to June 1972

5. AUTHOR(S) *(First name, middle initial, last name)*

G. C. Sih, P. D. Hilton, R. Badaliance and G. Villarreal

6. REPORT DATE	7a. TOTAL NO. OF PAGES	7b. NO. OF REFS
January 1973	166	34

8a. CONTRACT OR GRANT NO.	9a. ORIGINATOR'S REPORT NUMBER(S)
F33615-71-C-1429	
b. PROJECT NO.	
c.	9b. OTHER REPORT NO(S) *(Any other numbers that may be assigned this report)*
d.	

10. DISTRIBUTION STATEMENT

This document has been approved for public release and sale; its distribution is unlimited.

11. SUPPLEMENTARY NOTES	12. SPONSORING MILITARY ACTIVITY
	Air Force Materials Laboratory Wright-Patterson Air Force Base Dayton, Ohio 45433

13. ABSTRACT

Analyses for laminar plates are reviewed in this report. It is observed that while approximate global stress analyses have been performed for laminates, little has been accomplished in the area of strength analysis. The work presented here is concentrated in that area, i.e., mathematical models to consider the influence of flaws on failure loads associated with crack propagation and/or delamination. In particular, an approximate three-dimensional formulation for laminates based on the variational principle of minimum complementary potential energy is presented and applied to the problem of a three layer composite plate containing a through crack. This model is employed to study the influences of the geometric and material characteristics of the composite on the local stress field in the vicinity of the flaw.

Results of an experimental program to determine the influence of plate thickness on critical load for a centrally cracked tensile specimen are reported. Extension of the experimental program to consideration of laminated specimens is currently in progress.

A stress analysis has been carried out for another problem of particular interest in the study of failure for composite systems. The effect of voids in adhesive layers on the behavior of multi-layer fibrous composites is modeled by the problem of a penny shaped flaw contained in an isotropic layer joining two orthotropic half spaces. Stresses in the vicinity of the crack edge are calculated in terms of the loading and the properties of the components for this composite system.

DD FORM 1 NOV 65 **1473** (PAGE 1)

S/N 0101-807-6801

14. KEY WORDS	LINK A		LINK B		LINK C	
	ROLE	WT	ROLE	WT	ROLE	WT
Composite						
Laminate						
Three-Dimensional Plate Theory						
Through Crack						
Thickness Variation						
Energy Release Rate						
Interface Crack						
Penny-Shaped Crack						
Fiber Reinforcement						